Paleozoic Paleogeography of the South Western Part of the Central Asian Orogenic Belt - Paleomagnetic Constraints

Uwe Kirscher

München 2014

Paleozoic Paleogeography of the South Western Part of the Central Asian Orogenic Belt - Paleomagnetic Constraints

Uwe Kirscher

Dissertation
zur Erlangung des Doktorgrades
an der Fakultät für Geowissenschaften der
Ludwig–Maximilians–Universität München

vorgelegt von
Uwe Kirscher
aus Neustadt/Aisch

München, den 30.10.2014

1. Gutachter: Prof. Dr. Valerian Bachtadse
2. Gutachter: Prof. Dr. Helmut Echtler
Tag der mündlichen Prüfung: 29. April 2015

Preambel

This thesis is generally written in American English (AE). However, in three chapters the according publisher requires British English (BE). The thesis consists of two papers published in 'Journal of Geophysical Research: Solid Earth' and 'Geophysical Journal International':

U. Kirscher, A. Zwing, D.V. Alexeiev, H.P. Echtler and V. Bachtadse. Paleomagnetism of Paleozoic sedimentary rocks from the Karatau Range, Southern Kazakhstan: Multiple remagnetization events correlate with phases of deformation. *Journal of Geophysical Research: Solid Earth*, 2013, doi:10.1002/jgrb.50253. (written in AE)

U. Kirscher, D. Bilardello, A. Mikolaichuk and V. Bachtadse. Correcting for inclination shallowing of early Carboniferous sedimentary rocks from Kyrgyzstan-indication of stable subtropical position of the North Tianshan Zone in the mid-late Palaeozoic. *Geophysical Journal International*, 2014, doi:10.1093/gji/ggu177. (written in BE)

one paper, which is submitted for publication in 'Gondwana Research':

U. Kirscher, V. Bachtadse, A. Mikolaichuk, and A. Kröner. Early to middle Paleozoic evolution and terrane accretion in Central Asia - Paleomagnetic confirmation for a collision event in the Ordovician. *Gondwana Research*, Manuscript number: GR-D-14-00306. (written in BE)

and a book chapter, which is accepted for publication within the book on composition and evolution of Central Asian Orogenic Belt:

U. Kirscher and V. Bachtadse. Palaeozoic Palaeomagnetism of the South-Western Segment of the Central Asian Orogenic Belt – A Critical Review. *E. Schweizerbart'sche Verlagsbuchhandlung (Publisher)*, Kroener, A.(ed). (written BE)

Additionally, unpublished and preliminary results are presented.

Abstract

The Central Asian Orogenic Belt (CAOB) is one of the world's largest accretionary orogens, which was active during most of the Paleozoic. In recent years it has again moved into focus of the geological community debating how the acrreted lithospheric elements were geographical arranged and interacting prior and/or during the final amalgamation of Kazakhstania. In principal two families of competing models exist. One possible geodynmaic setting is based on geological evidence that a more or less continuous giant arc connecting Baltica and Siberia in the early Paleozoic was subsequently dissected and buckled. Alternatively an archipelago setting, similar to the present day south west Pacific was proposed.

This thesis collates three studies on the paleogeography of the south western part of the CAOB from the early Paleozoic until the latest Paleozoic to earliest Mesozoic. It is shown how fragments of Precambrian to early Paleozoic age are likely to have originated from Gondwana at high southerly paleolatitudes ($\sim$ 500 Ma), which got then accreted during the Ordovician ($\sim$ 460 Ma), before this newly created terrane agglomerate (Kazakhstania) migrated northwards crossing the paleo-equator. During the Devonian and the latest Early Carboniferous ($\sim$ 330 Ma) Kazakhstania occupied a stable position at about $\sim 30°$N. At least since this time the area underwent several stages of counterclockwise rotational movements accompanying the final amalgamation of Eurasia ($\sim 320 - 270$ Myr). This overall pattern of roughly up to 90° counterclockwise bending was replaced by internal relative rotational movements in the latest Paleozoic, which continued probably until the early Mesozoic or even the Cenozoic.

In Chapter 2 a comparison of declination data acquired by a remagnetization process during folding in the Carboniferous and coeval data from Baltica and Siberia lead to a documentation and quantification of rotational movements within the Karatau Mountain Range. Based on this results it is very likely that the rotational reorganization started in the Carboniferous and was active until at least the early Mesozoic. Additionally, the data

shows that maximal declination deviation increases going from the Karatau towards the Tianshan Mountains (i.e. from North to South). This observation supports models claiming that Ural mountains, Karatau and Tianshan once formed a straight orogen subsequently bent into a orocline. The hinge of this orocline is probably hidden under the sediments of the Caspian basin.

In chapter 3 we show that inclination shallowing has affected the red terrigenous sediments of Carboniferous age from the North Tianshan. The corrected inclination values put this part of the Tianshan in a paleolatitude of around 30°N during Carboniferous times. These results contradict previously published paleopositions of the area and suggest a stable latitudinal position between the Devonian and the Carboniferous.

Chapter 4 presents paleomagnetic data from early Paleozoic rocks from within the North Tianshan. They imply a second collisional accretion event of individual terranes in the Ordovician.

To further constrain the dimensions of these early Paleozoic terranes, chapter 5 presents a compilation of all available paleomagnetic data from the extended study region of southern Kazakhstan and Kyrgyzstan. Apart from a broad coherence of paleolatitudes of all studies at least since the Ordovician and the exclusive occurrence of counterclockwise declination deviations, no areas with the same rotational history can be detected. Also a clear trend caused by oroclinal bending can not be observed. We conclude that first order counterclockwise oroclinal bending, shown in chapter 2, resulted in brittle deformation within the mountain belt and local block rotations.

In order to improve our understanding of intra-continental deformation a study combining the monitoring of recent deformation (Global Positioning System, GPS) with a paleomagnetic study of Cenozoic age in the greater vicinity of the Talas-Ferghana fault has been undertaken in chapter 6. The major task was to distinguish between continuous versus brittle deformation. As it turned out the GPS signal indicates rather continuous and consistent counterclockwise rotational movements of the order of $\sim 2^\circ$ per Myr. This is in contrast to our paleomagnetic results, where even within fault bounded areas the error intervals of the rotations do always overlap. This indicates that a pure block model seems not appropriate even to explain Cenozoic paleomagnetic data. If this means that also Paleozoic rocks have been affected by complex recent deformation, and that the Paleozoic rotational pattern has been obscured by this, can not be decided based on the present data set. It means, however, that interpreting Paleozoic rotational data from this area has to be done with great caution.

Contents

1 Introduction

The Central Asian Orogenic Belt (CAOB, Yanshin, 1965) is one of the world's largest accretionary orogens. It was active during the Neoproterozoic and the entire Paleozoic until its growth ceased, and the newly formed continental crust finally became trapped between Siberia, Baltica and the Tarim and Turan microplates. The region has attracted the interest of many geological studies, not only concerning paleogeographic reconstructions (e.g., Windley *et al.*, 2007, and references therein), but also attempting to decipher the mechanisms controlling the growth of continental crust in general (e.g. Kröner *et al.*, 2014).

The interpretations and models published can generally be categorized into two groups and their derivates. Şengör *et al.* (1993) propose a giant arc model, where the individual arc components were subsequently welded together whereas several authors (e.g., Windley *et al.*, 2007, and references therein) suggest an archipelago type nucleus for the paleo-Asian domain, which is comparable to the plate tectonic situation in the present-day South West Pacific (e.g. Hall, 2009).

The south-western segment of the CAOB, situated mostly in Russia, Kazakhstan and Kyrgyzstan, is characterized by markedly curved geologic structures (Şengör *et al.*, 1993). Lithostratigraphic terranes are arcs striking north-south along the Ural mountains, north/west-south/east along the Karatau Range and east-west along the Tianshan Mountains at the outer

western and southern rims of the CAOB (see figure 6 in Windley *et al.*, 2007). This suggests a major orocline with the hinge situated under the Caspian basin. Geological evidence, such as collisional or oriented subduction features (e.g., Samygin and Burtman, 2009), seem to support the hypothesis that the Ural Mountains, the Karatau Range, and the Tianshan Mountains are structurally linked (Samygin and Burtman, 2009). However, this oroclinal bending feature has not been clearly identified by paleomagnetic data (Van der Voo *et al.*, 2006).

The degrees of freedom in paleogeographic reconstructions reflect patchy information on a) the early Paleozoic drift history of individual terranes prior to amalgamation of the Kazakhstan microcontinent, b) motion of the Kazakhstan microcontinent during the middle and late Paleozoic and the mechanisms of its incorporation into Eurasia, and c) the overall kinematics of late Palaeozoic Kazakhstania and the relative role of rotations, bending, and wrenching prior to- and during the process of multiple collisions during the late Carboniferous and Permian.

This thesis presents paleomagnetic results from the Kazakh and Kyrgyzs parts of the Northern Tianshan and Karatau Mountain Ranges. It adds constraints to the origin and evolution of potential terranes, which form the south-western part of the CAOB. Additionally, the paleogeography of Kazakhstania during the middle to late Paleozoic and the bending during the final amalgamation are tackled. Finally, a review of all available paleomagnetic data for the Paleozoic period from the region and a comparison of active to recent deformation is presented. The latter outlining future approaches to better understand the Paleozoic evolution of this complex area where more or less continuous deformation took place between the late Paleozoic and the Cenozoic.

2

Paleomagnetism of Paleozoic Sedimentary Rocks from the Karatau Range, Southern Kazakhstan: Multiple Remagnetization Events Correlate with Phases of Deformation

by ***U. Kirscher, A. Zwing, D.V. Alexeiev, H.P. Echtler, and V. Bachtadse***
Published in Journal of Geophysical Research, *2013,* ***118****(B50253)*

Abstract

The paleogeography of the Altaids and its kinematic and tectonic evolution during the final collision and amalgamation of Eurasia is still poorly known. Addressing this problem, a paleomagnetic study has been undertaken on Paleozoic sedimentary rocks from the Karatau, southern Kaza-

khstan. Stepwise thermal demagnetization reveals the presence of a high-temperature component of magnetization in most samples. Fold tests indicate a syn-folding age of magnetic remanence acquisition at three of the five areas studied. Directional data of Devonian and Permian rocks yield a positive fold-test, implying a primary magnetization. Resulting pre-folding paleolatitudes for Permian and Devonian rocks show the proximity of the Karatau to Baltica during those periods in time. Syn- and post-folding magnetzations result in paleolatitudes for Karatau, which intersect the paleolatitude curve based on the Baltica apparent polar wander path (APWP), at times, which can be correlated to major deformational events at $\sim$ 280Ma, $\sim$ 260Ma and $\sim$ 230Ma, respectively.

We interpret this with a complicated pattern of remagnetization events accompanying deformation, which can include syn-folding remagnetization events and areas of primary magnetic signals. Additionally, the differences between reference declinations based on the APWP for Baltica and observed declination values suggest successive counterclockwise rotational reorganization of the Karatau during the late Paleozoic to Early Mesozoic, with maximal rotation values of $\sim 65^\circ$ with respect to the Baltica APWP. The remagnetization events are correlated with the latest intracontinental stages of the orogenic evolution in the Ural mountains and thus the Paleozoic amalgamation of the Eurasian continent, and suggest a synchronous and coherent tectonic evolution in the Urals and Karatau mountains.

2.1 Introduction

The Central Asian Orogenic Belt (CAOB) or Altaids (Fig. 2.1) represents one of the largest accretionary orogens and one of the places, where formation of Phanerozoic continental crust was most excessive, on the Earth (Mossakovsky *et al.*, 1993; Windley *et al.*, 2007). It consists of heterogeneous domains integrating Precambrian microcontinents, island arcs and oceanic domains, ophiolite complexes, subduction- and collision-related metamorphic complexes, and ancient accretionary wedges, which were welded together from Neoproterozoic to Permian times. A variety of tectonic models consider the CAOB as a result of interaction of numerous short-living arcs separated by diachronous sutures and general reconstructions resemble present-day setting of the west Pacific- Indonesia region (Zonenshain *et al.*, 1990; Mossakovsky *et al.*, 1993; Berzin and Dobretsov, 1994; Yakubchuk *et al.*, 2001; Buslov *et al.*, 2002; Windley *et al.*, 2007; Xiao *et al.*, 2008,

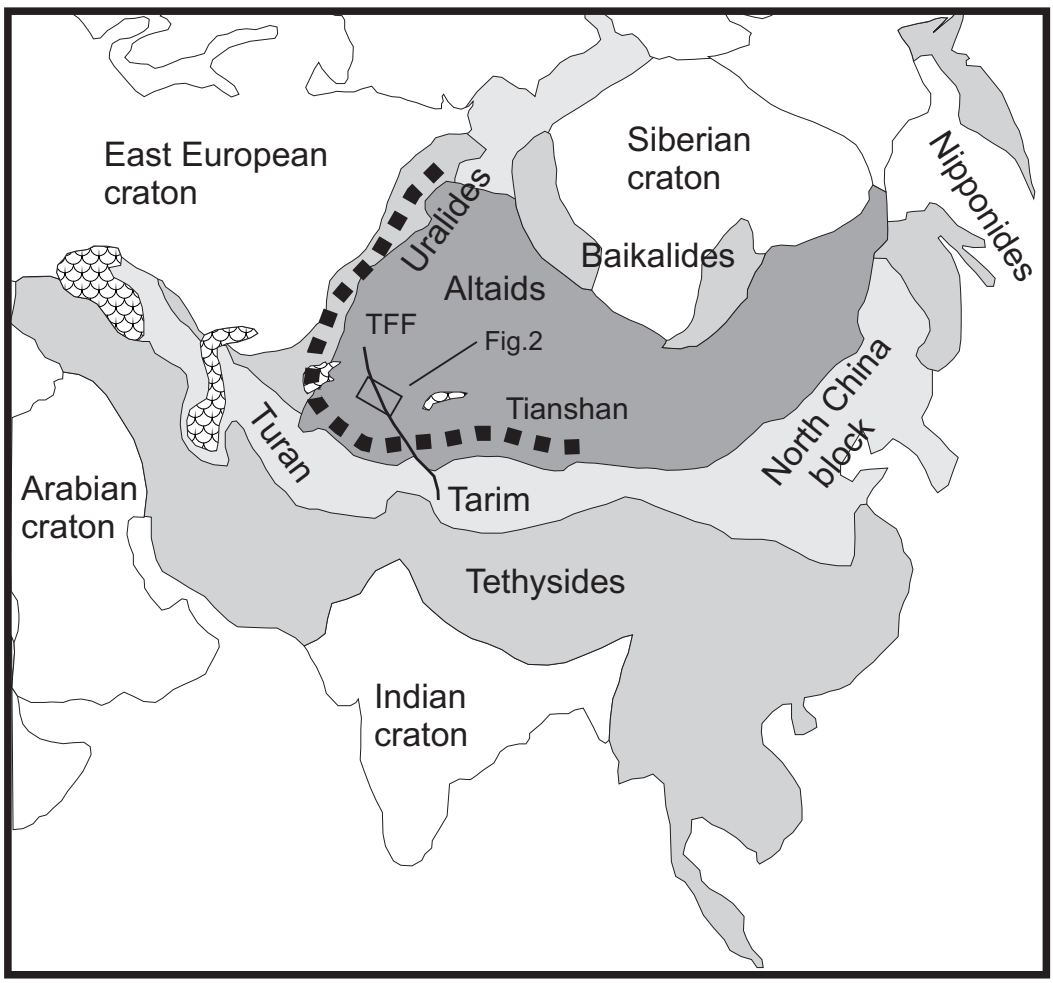

Figure 2.1: Simplified tectonic map of Eurasia. Thick dashed line shows Ural-Tianshan belt. TFF - Talas-Ferghana Fault. Outline of figure 2.2 is marked with black rectangle.

2010). An alternative model argues in favor of a primarily continuous single arc which was deformed by giant strike-slip faults (Şengör *et al.*, 1993) though in many cases this model does not explain the diversity of tectonic environments and the nature of various structural episodes known in different parts of the CAOB (Windley *et al.*, 2007).

It was already assumed in the earliest models based on geological evidence that the western part of CAOB within Kazakhstan represents a

major orocline (Zonenshain *et al.*, 1990) in the southern prolongation of the Uralides. Oroclinal bending was recently confirmed by paleomagnetic data between North Tianshan and Chingiz Range (Levashova *et al.*, 2007; Abrajevitch *et al.*, 2007, 2008). Extensive paleomagnetic studies during last decade had also significantly promoted the understanding of the general paleogeographic evolution of the western CAOB (Bazhenov *et al.*, 1999, 2003; Alexyutin *et al.*, 2005; Van der Voo *et al.*, 2006; Levashova *et al.*, 2007; Abrajevitch *et al.*, 2007, 2008) although a number of questions are still far from solved. The principal uncertainties are connected with a) the early Paleozoic histories of individual terranes and their travel paths prior to formation of the Kazakhstan continent, b) the motion of the Kazakhstan continent during middle and late Paleozoic time and mechanisms of its incorporation in Eurasia, and c) the overall kinematics of the Late Paleozoic Kazakhstan and relative role of rotations, bending and wrenching prior to- and during a process of multiple collisions of Kazakhstan with Siberia, Baltica and Tarim in the late Carboniferous and Permian, synchronous with the Uralian orogen.

Our current paleomagnetic study is devoted to Devonian, Carboniferous and Permian sedimentary rocks in Karatau Range of Southern Kazakhstan. This area is located at a junction of two Paleozoic collisional thrust and fold belts of the Urals and the pre-Cenozoic Tianshan, which delineate western and southern boundaries of the CAOB. It provides important hints for a better understanding of above two belts as well as for a reconstruction of the entire CAOB, but remains so far significantly less studied in comparison to adjacent regions. The results of our study reveal major rotations due to syn-collisional strike slip motions and allow us to establish a link between remagnetization and tectonic events.

2.2 Geological Setting and Tectonic History

The Karatau ('Black mountains') of South Kazakhstan is a mountain range up to a height of 2 km, which trends NW-SE between the Syr-Dar'ya and Chu-Sarysu basins (Inset in Fig. 2.2) and consists mainly of Neoproterozoic and Paleozoic rocks (Fig. 2.2). Structurally it is subdivided into the Greater (Bolshoi) and Lesser (Malyi) Karatau, separated from each other by the Main Karatau Fault (MKF), which represents a Northern segment of the Talas-Ferghana Fault (TFF) (Abdulin *et al.*, 1986; Allen *et al.*, 2001; Rolland *et al.*, 2013). Its geological and structural setting has been described by a

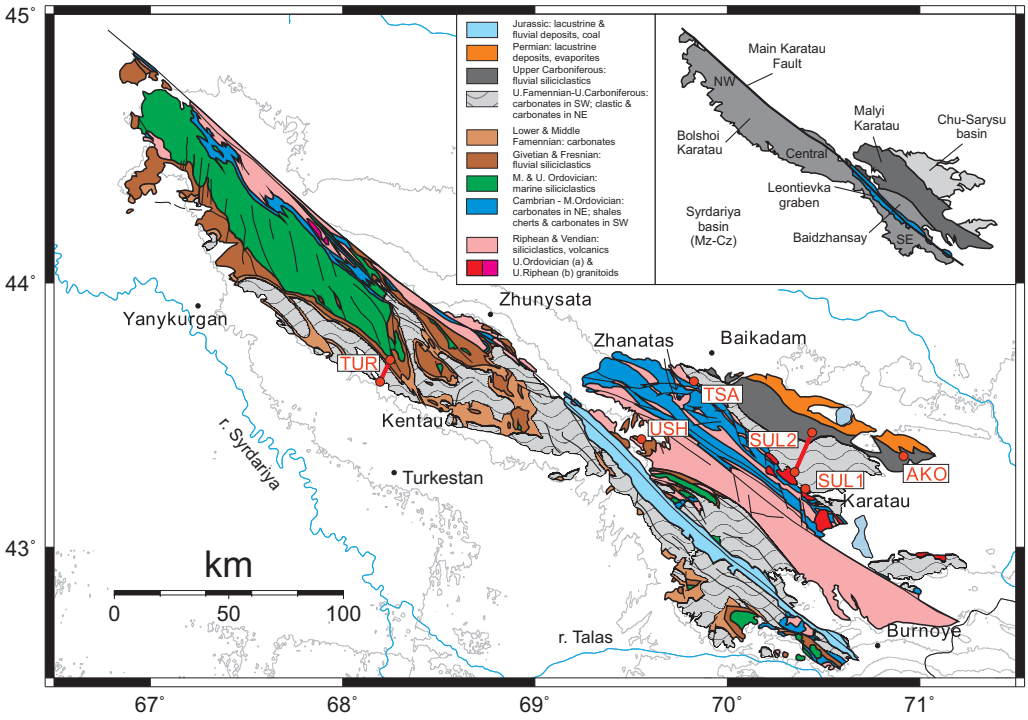

Figure 2.2: Geologic map of the Karatau Range (modified after Alexeiev *et al.* (2009)). Small: tectonic setting of the Karatau Range. Red dots indicate sampled areas.

number of authors (Abdulin *et al.*, 1986; Cook *et al.*, 1991, 1995; Allen *et al.*, 2001; Cook *et al.*, 2002; Alexeiev *et al.*, 2009). After Neoproterozoic rifting in the Karatau, several carbonate seamounts developed due to thermal subsidence of the newly formed crust. This sedimentation was terminated by late Ordovician compressional deformation, related to amalgamation of several terranes in the Kazakhstan continent. Extensive transgression in the Middle Devonian was followed by formation of a major passive margin carbonate platform during the Famennian to early Pennsylvanian within Bolshoi Karatau. During the same time shallow marine epi-continental basins with mixed carbonate and clastic facies evolved in the NE within the Chu-Sarysu basin (Cook *et al.*, 2002). Carbonate sedimentation in the Bolshoi Karatau ceased in middle Bashkirian (early Pennsylvanian) as a result of the collision of Kazakhstan with Baltica (East European craton) and orogenic

uplift in the Karatau and Tianshan isolated the Chu-Sarysu basin from the ocean. Since middle Bashkirian to late Permian this terrane evolved as an intracontinental basin with fluvial and lacustrine deposits (Abdulin *et al.*, 1986; Allen *et al.*, 2001).

Recent structural studies in the Karatau have revealed three distinct

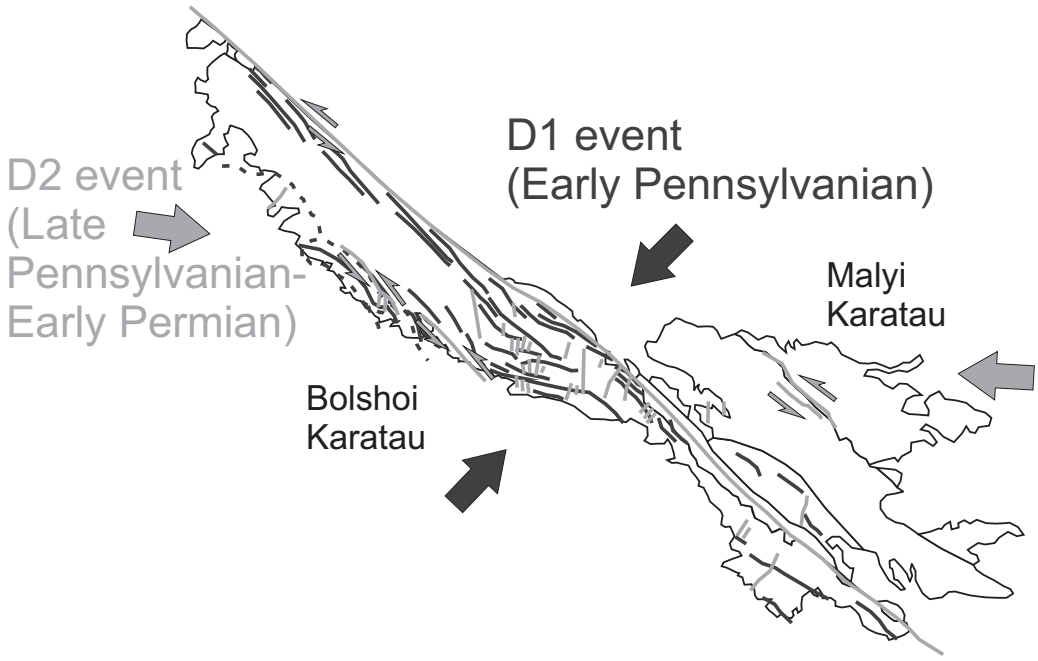

Figure 2.3: Distribution of characteristic structures and shortening directions of two principal deformation events. Dark grey - early Pennsylvanian event at $\sim$ 315 Ma. Light grey - late Pennsylvanian to early Permian event, around $\sim$ 300 Ma. Solid lines show fold axes, lines with arrows - strike slip faults (modified after Alexeiev *et al.* (2009)).

phases of deformation during the Pennsylvanian to early Mesozoic (Alexeiev *et al.*, 2009). The first episode (D1) in the early Pennsylvanian is characterized by NW-trending folds and thrusts with a general direction of motion towards NE (Fig. 2.3). The second episode (D2), which took place presumably during the late Pennsylvanian to early Permian, reflects shortening in east-west direction, evidenced by N-S trending folds and NW trending sinistral strike slip faults (Fig. 2.3). The third episode (D3) was dominated by

shortening in a N-S direction connected with the initiation of dextral motion along the Talas Ferghana Fault (Alexeiev *et al.*, 2009). The age of the latter can be constrained within late Permian to early Mesozoic, based on recent Ar-Ar age data obtained for Talas-Ferghana fault (Rolland *et al.*, 2013). All three phases of deformation can be correlated with synchronous orogenic increments in the Uralian belt following amalgamation of Baltica, Siberia and Kazakhstan paleocontinents in Eurasia (Echtler *et al.*, 1996, 1997; Brown *et al.*, 2008).

2.3 Local Geologic Setting and Sampling

During the field campaign 434 oriented samples were drilled from 71 sites in six areas within Malyi and Bolshoi Karatau (Fig. 2.2) covering Devonian, Carboniferous and Permian sedimentary rocks. Orientation of samples and bedding planes were measured using a standard magnetic compass as well as sun compass techniques. All samples were treated with thermal demagnetization techniques using a Schoenstedt oven with peak temperatures of ~ 700°C. Magnetization directions were measured with a 2-G squid magnetometer in three components in a magnetically shielded room. Sample mean directions were calculated using at least four consecutive demagnetization steps applying the least squares method proposed by Kirschvink (1980) on linear portions of the demagnetization paths. Rock magnetic parameters of representative samples were obtained using a variable field translation balance (VFTB, Krasa *et al.* (2007)) and the Lowrie method (Lowrie, 1990), to get information about the magnetic carriers of the remanent magnetization of the sampled material.

2.3.1 Bolshoi Karatau

Along the Zhankurgan river in the SW Bolshoi Karatau (Fig. 2.2) one of the most complete sections in the area with rocks ranging in age from Middle Devonian (Givetian) to Pennsylvanian, early Bashkirian (Abdulin *et al.*, 1986; Cook *et al.*, 2002) is exposed. Here, Devonian and Carboniferous rocks are folded in major NW- trending synclines and anticlines, which were formed during the main deformation episode (D1) in the early Pennsylvanian (Allen *et al.*, 2001; Alexeiev *et al.*, 2009). In the Zhankurgan valley (section TUR) 133 drill cores were obtained at 22 sites, covering Upper Devonian (Frasnian) red sandstones and Uppermost Devonian (Frasnian and

Famennian) to lower Carboniferous (Tournaisian and Visean) carbonates, (see Cook *et al.* (2002) for detailed stratigraphic descriptions).

2.3.2 Malyi Karatau

Five spatially separated locations were studied in the Malyi Karatau (Fig. 2.2) including four sections of Devonian and Carboniferous rocks (TSA, USH, SUL1 and SUL2) and one section with Permian rocks (AKO).
Devonian rocks sampled in the Ushbas area (section USH) in the NW Malyi Karatau (Fig. 2.2) are part of the same sedimentary formations as in the adjacent Bolshoi Karatau including Givetian and Frasnian red beds and Famennian limestones. Similar structural patterns in both the Zhankurgan and Ushbas areas suggest that the rocks were deformed during the same episode and thus a late Carboniferous age of deformation can be inferred in the Ushbas area as well. In the southern part of the Ushbas syncline 11 sites with 67 samples were studied in middle and Upper Devonian red sandstones of the Tyul'kubash formation.

The section TSA is located on the road between Zhanatas and Baikadam (Fig. 2.2) at the SW edge of Chu-Sarysu basin. The rocks comprise uppermost Devonian to lower Carboniferous red sandstones and conglomerates of the Suleimansay formation, which are deformed in a narrow NW- trending syncline (Abdulin *et al.*, 1986). Two sites, each with 6 samples, were collected in fine-grained red sandstones from both limbs of the fold.

Two sections were also studied in the SE Malyi Karatau on the SW flank of the Chu-Sarysu basin. In total 14 sites with 84 samples were drilled from the section SUL-1 near the Suleimansay mine (Fig. 2.2) from the same formation as at TSA. The sequence is dominated by brown sandstones with interlayers of light dolomites and grey limestones. The latter contain rare brachiopoda and foraminifera fossils, which constrain the age of the Suleimansay formation and the overlying sediments as latest Devonian to earliest Carboniferous (Abdulin *et al.*, 1986; Cook *et al.*, 2002). At this location 14 sites with a total of 84 samples were drilled.

Section SUL-2 is exposed along the river Koktal and includes Visean, Serpukhovian, and lower Pennsylvanian rocks. The lower Carboniferous sequence is generally dominated by light-colored shallow marine limestones and fossiliferous limestones, which contain subordinate evaporites in the lower Visean, argillaceous limestones and marls in the middle Visean and sandy limestones and limy sandstones in the upper Visean and Serpukhovian. The lower Bashkirian consists mainly of shallow marine carbonate

sandstones and sandy limestones with conglomerate layers. They are overlain with erosional contact by fluvial conglomerates and sandstones of the Kyzylkanat Formation, which has a Pennsylvanian age. Lower and upper Carboniferous rocks from the SUL-2 section are deformed in relatively low-angle linear folds, trending NW-SE (Abdulin *et al.*, 1986; Allen *et al.*, 2001; Cook *et al.*, 2002). 14 sites were investigated along the Koktal river with a total of 91 samples.

The section AKO includes several sites within Permian sedimentary succession, which were sampled in the area around the town of Akkol (Fig. 2.2) in the very east of Malyi Karatau, within in southwestern part of the Chu-Sarysu basin. Permian rocks are represented by lacustrine facies and consist of red and grey fine-grained sandstones and siltstones with subordinate interlayers of carbonates and evaporites (Abdulin *et al.*, 1986; Bazhenov *et al.*, 1995). Eight localities have been sampled with a total of 47 samples.

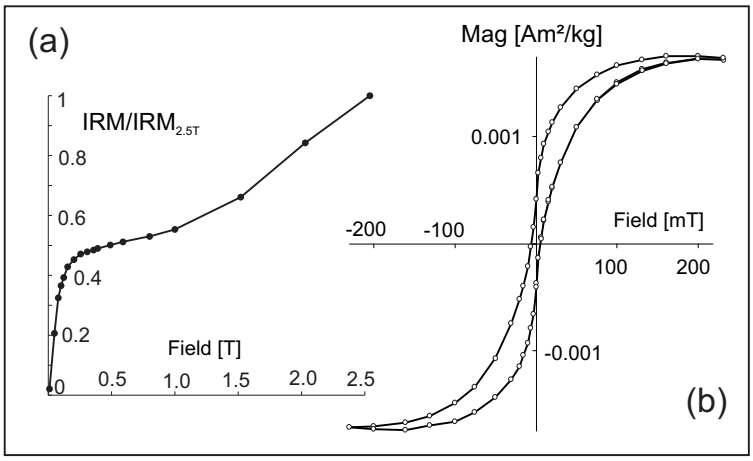

Figure 2.4: Exemplary plot of measured hysteresis loop (left) of a representative sample and acquisition curve (right) of isothermal remanent magnetization (IRM).

2.4 Rockmagnetic Results

In order to obtain information on the magnetic inventory, representative samples from all different areas were studied rockmagnetically using a

Variable Field Translation Balance (VFTB, Krasa *et al.* (2007)) to obtain magnetic hysteresis data, isothermal remanent magnetization (IRM), thermomagnetic curves and thermal demagnetization of a 3-axis composite IRM. In general, none of the samples subjected to IRM experiments saturates at 2.5 T and the IRM acquisition curves indicate the presence of at least two magnetic phases with different coercivity spectra (Fig. 2.4a). Furthermore, hysteresis loops are either characterized by pot-bellied or wasp-waisted shape (Tauxe *et al.*, 1996), which is also an argument for the existence of more than one prominent magnetic mineral (or a mixture of different grain sizes) in these rocks (Fig. 2.4b).

Additional information was acquired using thermal demagnetization of composite 3-axis IRMs (Lowrie, 1990) in combination with in-field ($\sim$ 100 mT) thermomagnetic curves in (insets in figure 2.5). The orthogonal IRMs were imparted sequentially using d.c. fields of 2.5, 0.4 and 0.12 T.

The Permian red sandstones (AKO) are characterized by unblocking temperatures of the natural remanent magnetization (NRM) of $\sim 680 - 700$°C. Furthermore, there are indications for additional magnetic phases, which is on one hand a low temperature phase up to $\sim$ 200°C, visible both in thermomagnetic curves and when demagnetizing the low coercivity IRM. Additionally, the IRM demagnetization shows distinct unblocking temperatures of $\sim$ 580°C and $\sim$ 680°C for all rocks, independent of coercivity (Fig. 2.5).

Rocks from Suleimansay (SUL-1 and SUL-2) and Zhankurgan (TUR) show prominent unblocking temperatures at $\sim 550 - 580$°C in thermomagnetic curves and in the low coercivity IRM (Fig. 2.5). SUL-1 shows an additional high temperature phase at the (in-field) thermomagnetic curve, which drops to zero at $\sim$ 680°C.

Samples from Ushbas and Zhanatas indicate two unblocking temperatures at $\sim$ 580°C and $\sim$ 680°C, respectively, at both thermomagnetic curves and at demagnetization of orthogonal IRMs (Fig. 2.5).

In conclusion, these results suggest the predominance of magnetite together with differing amounts of hematite within all the samples. In conclusion, the magnetomineralogy of all sampled lithologies is dominated by magnetite. The magnetic properties of samples from AKO, USH, TSA and - to a lesser degree - from SUL1 show a significant contribution of hematite.

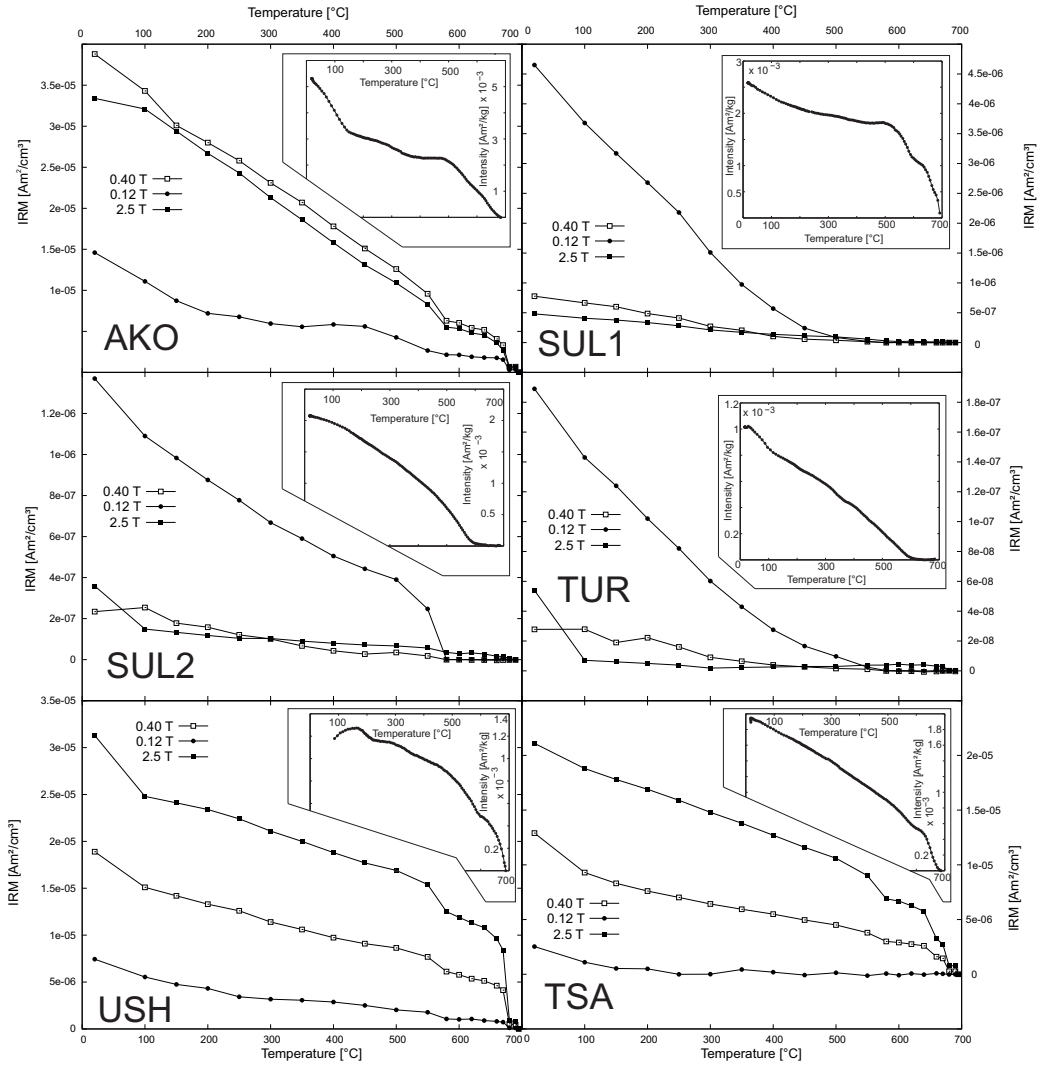

Figure 2.5: Thermal demagnetization of a 3-axis composite IRM for one representative sample from all areas. Orthogonal d.c. fields of 2.5, 0.4 and 0.12 T were applied sequentially to all samples prior to heating. Also shown are representative thermomagnetic curves (with d.c. bias field of ~ 100 mT) of rocks of the particular area (small).

2.5 Demagnetization Results

In accord with our rockmagnetic results, detailed thermal demagnetization experiments reveal the presence of at least two magnetic components, with different paleomagnetic directions. An initial low temperature component (LTC) was identified during thermal stepwise demagnetization between 100°C and up to 300°C. LTC is broadly pointing to the North and down and yields an overall mean direction which is consistent with the present day magnetic field in the sampling area. Only in samples from Ushbas the LTC is present up to ~ 600°C.

A high temperature component (HTC) of reversed polarity in tilt corrected coordinates was identified as linear segments from $\sim 300 - 350$°C up to $\sim 600 - 680$°C. The samples with unblocking temperatures larger than 600°C carry two high temperature components, which are, however, not distinguishable within error limits (Fig. 6.2, (a,d)).

2.5.1 Bolshoi Karatau

Table 2.1: Site mean directions for Zhankurgan section (Givetian - Visean).

Site	Bed.	N	In situ				Bedding-corrected			
			D[°]	I[°]	k	α_{95} [°]	D[°]	I[°]	k	α_{95} [°]
Zhankurgan (TUR)										
Tur-1*	210/42	6/6	224.0	-33.6	3.1	45.7	246.5	-72.3	3.1	45.7
Tur-2*	233/30	6/6	181.3	-11.0	6.4	28.9	172.4	-25.8	6.4	28.9
Tur-3*	213/40	7/7	197.8	-5.3	4.5	35.8	190.4	-42.2	4.5	35.8
Tur-4	223/44	6/6	200.1	-15.5	21.8	14.9	181.4	-51.6	21.8	14.9
Tur-5	233/45	6/5	203.4	-28.5	140.8	6.5	167.3	-58.1	140.8	6.5
Tur-6	230/47	6/6	206.2	-29.8	302.2	3.9	165.3	-63.5	302.2	3.9
Tur-7	244/45	6/6	211.8	-26.4	135.6	5.3	178.3	-55.0	135.6	5.3
Tur-8*	201/39	7/7	55.9	-53.6	3.0	42.3	44.1	-17.6	3.0	42.3
Tur-9•	227/43	6/5	14.4	49.7	49.3	11.0	301.8	65.1	49.3	11.0
Tur-10	245/20	6/5	199.1	-34.0	77.4	8.8	186.8	-43.6	77.7	8.7
Tur-11	004/07	6/3	195.3	-39.2	68.2	15.0	194.8	-32.2	68.2	15.0
Tur-12	225/55	6/4	206.9	-7.3	35.9	15.5	187.0	-54.9	35.4	15.7
Tur-13	233/49	6/6	212.8	-11.6	15.6	18.1	193.8	-53.2	15.6	18.1
Tur-14	243/50	6/6	205.6	-9.6	146.6	5.6	187.2	-42.0	160.5	5.3
Tur-15	223/43	6/6	196.7	-34.1	57.4	9.1	155.5	-63.2	57.4	9.1
Tur-16	047/54	6/6	153.4	-56.9	67.7	8.3	196.2	-23.9	67.7	8.3
Tur-17	214/66	6/4	204.4	11.6	167.3	7.1	195.5	-51.6	167.3	7.1
Tur-18	215/25	5/5	200.9	-18.8	67.6	9.4	195.3	-42.1	67.6	9.4
Tur-19	215/75	5/5	202.1	12.0	120.3	7.0	185.7	-57.7	120.3	7.0
Tur-20	052/37	7/6	187.4	-34.2	181.9	5.0	197.9	-9.2	181.3	5.0
Tur-21	205/48	6/6	204.8	-10.5	129.9	5.9	200.3	-58.3	131.7	5.9
Tur-22	196/42	6/5	201.0	-5.5	176.9	5.8	209.1	-47.5	176.9	5.8
MEAN	–	22/18**	201.1	-20.2	15.6	9.3	188.4	-48.2	24.5	7.3

Site: sampling site, Bed.: bedding orientation, dip direction/plunge (ss), N: number of measured samples/number of samples used for calculating site mean directions. Declination (D) and Inclination (I) in degrees, Fisher radius (α_{95}) of 95% confidence, Fisher precision parameter k (Fisher, 1953), in geographic (*in situ*) and bedding corrected coordinates, respectively.
(*) site mean direction not included in calculating area mean direction, because of α_{95} values larger than 20°. • rejected site because of proximity of *in situ* direction to present day field. ** For area mean directions: N: number of obtained site mean directions/number of used site mean directions for calculating area mean.

Zhankurgan The LTC of Zhankurgan area (TUR) yields a mean direction of $D = 1.9°$, $I = 61.7°$, $k = 31.5$ and $\alpha_{95} = 2.6°$ (*in situ*) based on 92

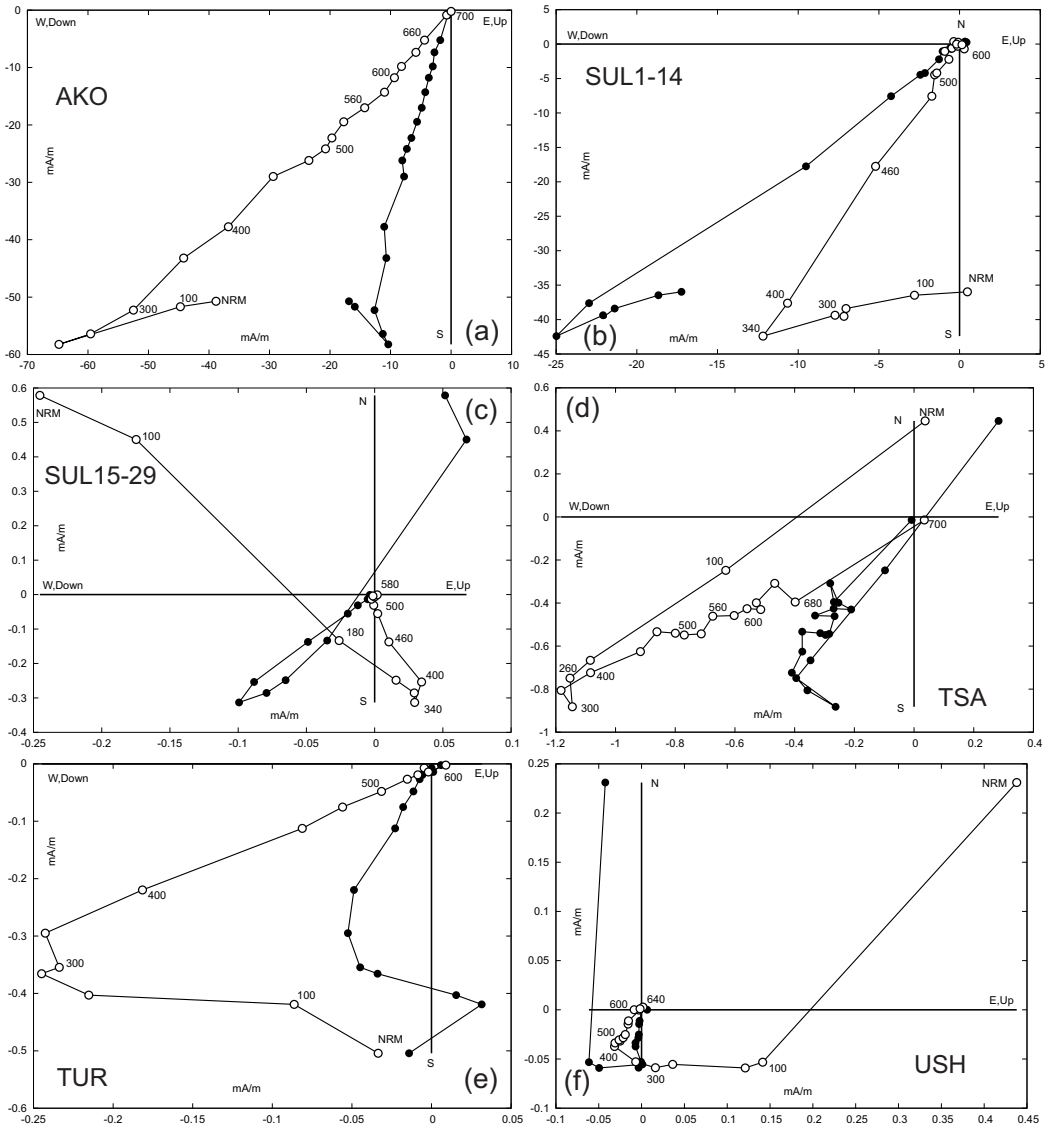

Figure 2.6: Results of thermal demagnetization experiments plotted as orthogonal vector diagrams (Zijderveld, 1967) in stratigraphic coordinates. Solid and open dots represent vector endpoints projected onto the horizontal and vertical planes, respectively. Positive values represent projection in north, east and up direction, respectively. Temperature steps in °C are indicated.

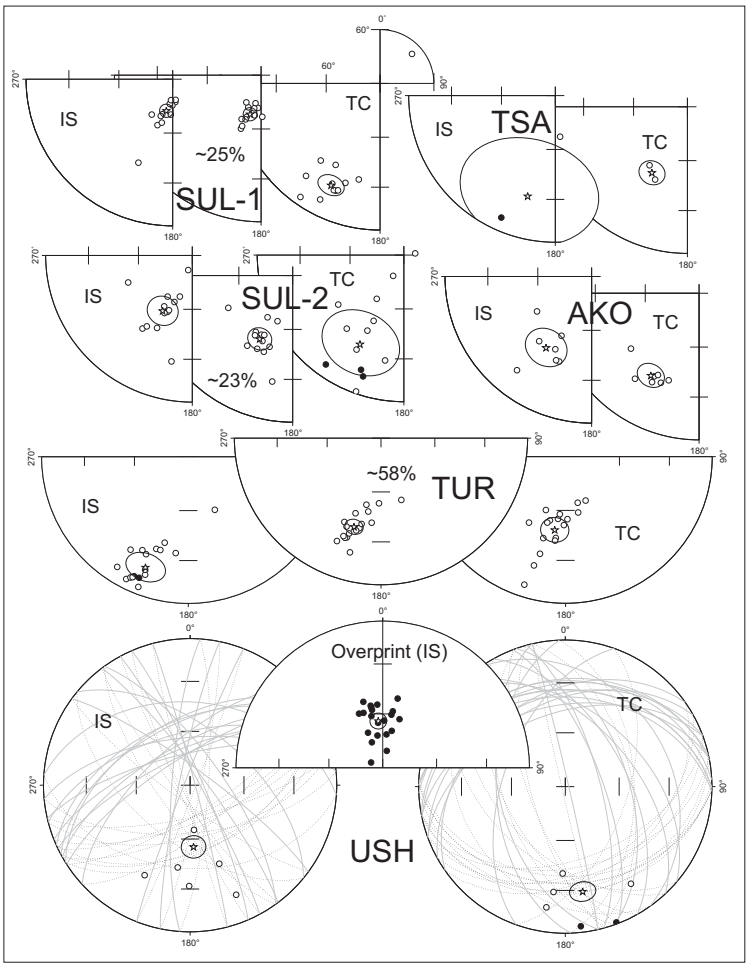

Figure 2.7: Stereographic projections of site mean directions for all sampled areas, loacted in the Bolshoi and Malyi Karatau. IS refers to *in situ* data, and TC refers to tilt-corrected data. The stars indicate the area mean direction with 95% confidence circles. Solid and open dots represent projection on the upper and lower hemispheres, respectively. Central plot shows mean directions after % of unfolding for maximal k value (Watson and Enkin, 1993). USH: overprinted component of representative samples is also shown in *in situ* coordinates.

samples. Furthermore a high temperature component (HTC) is identified in 91% (121 specimens) of all treated specimens with unblocking temperatures

of up to ~ 600°C. Based on sample mean directions of the HTC site mean directions were calculated (Tab. 2.1). Five of the 22 site mean directions are rejected because of α_{95} values higher than 20° for further analysis. The remaining 17 site mean directions were subjected to the fold test of Watson and Enkin (1993). Stepwise unfolding results in a maximum k-value at $\sim 58\%$ untilting with a confidence interval of 5.2° (Fig. 2.8), indicating an acquisition age of the characteristic remanence during folding. The resulting syn-folding area mean direction is $D = 196.9°$, $I = 37.0°$, $k = 60.4$ and $\alpha_{95} = 4.6°$ (Fig. 2.7).

2.5.2 Malyi Karatau

Table 2.2: Site mean directions for Zhanatas (Famennian) and Akkol (Permian) sections.

Site	Bed.	N	In situ				Bedding-corrected			
			D[°]	I[°]	k	α_{95} [°]	D[°]	I[°]	k	α_{95} [°]
Zhanatas (TSA)										
Tsa-1	064/28	6/4	173.3	-67.1	612.2	3.7	212.9	-50.9	612.2	3.7
Tsa-2	196/55	6/4	203.9	10.0	36.7	15.4	203.9	-45.0	36.7	15.4
MEAN	–	2/2**	195.3	-29.7	3.6	34.1	208.2	-47.7	66.3	6.9
Akkol (AKO)										
Ako-1	258/25	6/6	218.5	-19.5	28.1	12.9	208.4	-35.9	28.1	12.9
Ako-2	055/05	5/5	200.9	-38.1	270.1	4.7	203.1	-34.1	270.1	4.7
Ako-3*	030/04	6/6	149.0	-71.0	3.9	39.0	158.1	-68.8	3.9	39.0
Ako-4	300/05	6/6	203.0	-38.1	152.1	5.4	199.2	-37.3	152.1	5.4
Ako-5	025/15	6/4	206.9	-52.7	65.8	11.4	206.7	-37.7	61.7	11.8
Ako-6	025/15	7/7	237.5	-53.7	28.4	11.5	230.9	-40.0	28.4	11.5
Ako-7	025/15	5/3	219.0	-42.8	71.4	14.7	216.9	-28.1	65.8	15.3
Ako-8	035/12	6/6	206.5	-44.0	1193.2	1.9	207.9	-32.1	1156.3	2.0
MEAN	–	8/7**	212.6	-41.9	31.1	11.0	210.4	-35.3	74.9	7.0

(*) site mean direction not included in calculating area mean direction, because of large α_{95} values. See Tabel 2.1 for more information.

Zhanatas A LTC is identified in 11 samples from Zhanatas area and yield a mean direction of $D = 14.4°$, $I = 58.1°$, $k = 34.7$ and $\alpha_{95} = 7.9°$ in *in situ* coordinates. Averaging the HTC from twelve samples of the two sites results in $D = 190.8°$, $I = -39.5°$, $k = 3.6$ and $\alpha_{95} = 30.0$ before and $D = 207.1°$, $I = -48.0°$, $k = 11.9$ and $\alpha_{95} = 14.6$ after tilt correction (Fig. 2.7, Tab. 4.3). Stepwise unfolding indicates a maximum k-value at 100% unfolding (Fig. 2.8), which suggests a pre-folding age of this magnetization. Calculating mean directions and performing fold-tests on only two site mean directions would not yield statistically sufficient results. Therefore all statistic procedures where carried out on sample level. All treatments are conducted with sample mean directions. Unfortunately, outcrop conditions in this area have not allowed a more detailed sampling.

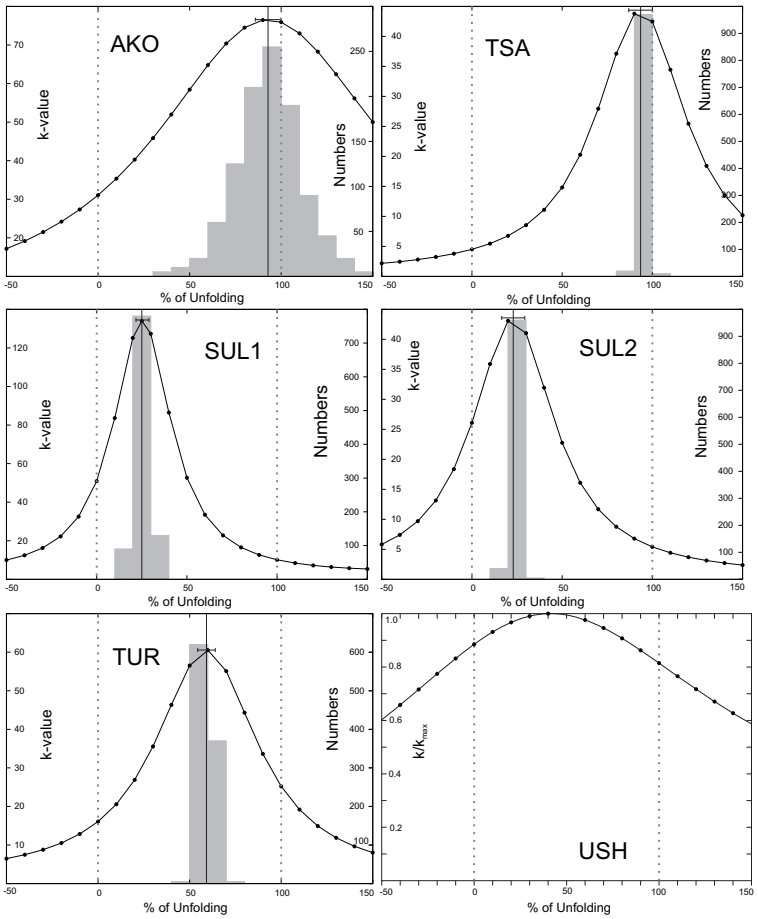

Figure 2.8: Plots of precision parameter k for stepwise unfolding of site mean directions for every area. Dotted lines indicate 100% and 0% unfolding, respectively. Black line shows maximum k-value with error limit, which is obtained from 1000 parametric simulations Watson and Enkin (1993). The results of these simulations are shown in grey histograms. Area USH shows k-values for stepwise unfolding including remagnetization great circles (McFadden and McElhinny, 1990).

Suleimansay Thermal demagnetization experiments of samples from area SUL-1 indicate a LTC component below 300°C (Fig. 6.2) which yields a sample mean direction of $D = 9.1°$, $I = 59.8°$, $k = 34.9$ and $\alpha_{95} = 3.0°$ (*in situ*) based on 66 samples. Above 300°C, a high temperature component

Table 2.3: Site mean directions for Suleimansay-1 section (Famennian - Visean).

Site	Bed.	N	In situ				Bedding-corrected			
			D[°]	I[°]	k	α_{95} [°]	D[°]	I[°]	k	α_{95} [°]
Suleimansay-1 (SUL-1)										
Sul-1	022/50	4/3	173.4	-77.3	191.2	8.9	199.2	-29.1	180.4	9.2
Sul-2*	025/45	4/4	10.0	-75.8	8.2	34.2	219.1	-58.0	8.2	34.2
Sul-3	026/45	6/6	196.5	-69.8	285.2	4.0	205.5	-25.3	285.2	4.0
Sul-4	025/55	6/6	180.6	-75.5	179.7	5.0	202.4	-22.1	179.7	5.0
Sul-5	030/52	6/6	198.2	-63.1	477.7	3.1	207.3	-12.0	477.7	3.1
Sul-6	022/47	6/6	197.9	-68.6	399.8	3.4	203.4	-21.8	399.8	3.4
Sul-7	040/37	5/4	182.9	-70.4	686.2	3.5	208.6	-37.0	686.3	3.5
Sul-8	200/75 215/75	6/5	202.3	-38.5	54.3	10.5	47.3	-65.9	26.3	15.2
Sul-9	033/74	8/7	194.0	-65.2	38.3	9.9	215.0	-6.1	38.3	9.9
Sul-10	055/55	6/5	171.8	-78.5	357.3	4.1	218.7	-20.4	357.3	4.1
Sul-11	040/45	8/8	186.7	-76.3	137.5	4.7	217.5	-34.2	136.4	4.8
Sul-12	010/45	6/6	167.4	-71.7	19.1	18.0	185.5	-28.3	19.1	18.0
Sul-13	010/45	6/6	210.6	-67.2	96.0	6.9	201.5	-22.8	96.0	6.9
Sul-14	010/45	7/7	184.4	-78.4	22.1	13.1	192.5	-33.5	22.1	13.1
MEAN	–	14/13**	191.3	-72.2	151.3	3.7	205.70	-24.0	51.3	6.4

See Tabel 2.1 for more information.

(HTC) is observed up to ~ 680°C (Fig. 6.2, Tab. 4.2). Stepwise unfolding of these site mean directions results in a maximum k value after $\sim 25\%$ unfolding (Fig. 2.8). Performing the fold test of Watson and Enkin (1993) leads to a maximum k-value at 25.4% with an error of $\pm 8.1\%$. The syn-folding direction with the maximum k-value is $D = 198.5°$, $I = -60.4°$, $k = 134.5$ and $\alpha_{95} = 3.6°$ (Fig. 2.7).

Table 2.4: Site mean directions for Suleimansay-2 section (Serpukhovian - Moscovian).

Site	Bed.	N	In situ				Bedding-corrected			
			D[°]	I[°]	k	α_{95} [°]	D[°]	I[°]	k	α_{95} [°]
Suleimansay-2 (SUL-2)										
Sul-15	030/26	6/6	203.7	-55.6	181.4	5.0	206.6	-28.8	181.4	5.0
Sul-16	215/55	7/7	214.3	-39.6	37.1	10.7	81.7	-83.7	37.1	10.7
Sul-18	038/68	6/6	208.9	-57.6	701.9	2.5	215.5	9.3	701.9	2.5
Sul-19	060/24	5/5	203.0	-56.8	149.2	6.3	217.8	-36.8	149.2	6.3
Sul-20	355/15	6/4	247.2	-51.0	125.7	8.7	233.0	-43.4	125.7	8.7
Sul-21*	227/48	6/5	214.3	-54.8	11.7	20.7	91.7	-68.5	11.7	20.7
Sul-22	253/02	6/6	191.1	-27.3	63.4	8.5	190.1	-28.0	63.4	8.5
Sul-23	210/35	8/8	212.7	-42.2	211.1	3.8	207.3	-77.1	211.1	3.8
Sul-24	040/02	6/6	210.9	-63.4	172.8	5.1	211.8	-61.4	172.8	5.1
Sul-25	015/80	5/5	195.4	-81.7	29.9	14.2	199.3	-1.7	29.9	14.2
Sul-26	015/80	6/5	201.0	-62.3	150.2	6.3	200.5	17.7	150.2	6.3
Sul-27	015/80	7/6	196.7	-66.2	163.7	5.3	198.6	13.8	163.7	5.3
Sul-28	010/05	9/8	205.8	-54.2	109.1	5.3	204.7	-49.3	109.1	5.3
Sul-29	013/02	8/8	205.9	-44.4	183.9	4.1	205.7	-42.4	183.3	4.1
MEAN	–	14/13**	208.1	-54.8	26.1	8.3	206.2	-32.8	19.7	5.4

See Tabel 2.1 for more information.

At SUL-2 85 of the 91 samples show stable demagnetization behavior, revealing the presence of both a LTC and a HTC. Stepwise heating up to ~ 300°C completely removes the LTC. The sample mean direction for LTC is $D = 2.6°$, $I = 61.6°$, $k = 82.8$ and $\alpha_{95} = 1.9°$ based on 85 samples. Between ~ 300°C and ~ 600°C a HTC is present. Site mean directions of 14 sites yield

a mean directions of $D = 208.1°$, $I = -54.8°$, $k = 26.1$ and $\alpha_{95} = 8.3$ *in-situ* and $D = 206.2°$, $I = -32.8°$, $k = 5.4$ and $\alpha_{95} = 19.7°$ after tilt correction (Fig. 2.7, Tab. 4.4). We note, however, that a maximum k-value is reached at $\sim 23\%$ unfolding (Fig. 2.8), which indicates a syn-folding age of remanence acquisition and results in a mean direction of $D = 207.5°$, $I = -49.8°$, $k = 43.6$ and $\alpha_{95} = 6.4°$ (Fig. 2.7). The statistical fold test of Watson and Enkin (1993) yields a narrow interval of unfolding percentages ($\pm 3.5\%$). This confirms a robust syn-folding age of the magnetization acquisition.

Ushbas The LTC of Ushbas area (USH) results in a mean direction of $D = 5.5°$, $I = 66.0°$, $k = 14$ and $\alpha_{95} = 4.0$ based on 67 samples. The HTC shows ambiguous behavior. Above 300°C and up to 700°C stepwise demagnetization experiments yield curved demagnetization trajectories, failing to reach the origin of the projection. Using the McFadden and McElhinny (1988a) algorithm to analyze great circle data, including at least six stable endpoints, with mean directions of six exceptional high quality samples (Fig. 2.7) yield a characteristic mean direction of $D = 176.8°$, $I = -55.4°$, $k = 19.0$ and $\alpha_{95} = 6.5$ in *in situ* coordinates and $D = 170.6°$, $I = -28.3°$, $k = 19.9$ and $\alpha_{95} = 6.3$ after tilt correction. Stepwise unfolding of combined directional and great circle data (McFadden and McElhinny, 1990) results in a maximum of the Fisher (1953) k value at $\sim 50\%$ unfolding (Fig. 2.8) suggesting that the resulting mean direction $D = 173.0°$, $I = -41.5°$, $k = 23.5$ and α_{95} of 5.8 is of syn-folding age.

Since a large number of samples from all sites at Ushbas show only LTCs during demagnetization, no site mean directions for HTC could be obtained here. Our procedure of computing an area mean direction out of samples from different sites certainly enlarges the error, which is not sufficiently represented by the α_{95} value.

Akkol The LTC holds a mean direction of $D = 358.1°$, $I = 64.2°$, $k = 31.5$ and $\alpha_{95} = 4.2°$ in *in situ* coordinates, using data of 38 samples. Between 300°C and $\sim$ 700°C there is a HTC present. Based on mean directions of individual sites, an area mean direction is calculated. The other seven sites yield a mean direction of $D = 212.6°$, $I = -41.9°$, $k = 31.1$ and $\alpha_{95} = 11.0°$ before and $D = 210.4°$, $I = -35.3°$, $k = 74.9$ and $\alpha_{95} = 7.0°$ after tilt correction (Fig. 2.7, Tab. 4.3). Stepwise unfolding shows a maximum k-value at 100% unfolding (Fig. 2.8), which suggests a pre-folding age of the magnetization acquisition.

2.5.3 Folding Symmetry

Fold tests using stepwise unfolding techniques are usually based on the assumption, that the rotation of bedding planes occurred about an horizontal axis (fold axis). In cases, were deformation occurred by rotation about inclined or multiple axes, the true direction of syntectonic (or even pretectonic) magnetizations cannot be restored by these algorithms. In order to control these effects, the geological structures of all sampled areas were investigated in more detail.

The deformation pattern in sections Akkol (AKO), Suleimansay 1+2 (SUL1+2), Zhanatas (TSA) and Zhankurgan is characterized by upright symmetrical folds with NW-SE trending horizontal fold axes and vertical axial planes as shown by stereoplots of normal vectors to bedding planes (Fig. 2.9). This is taken as a strong argument, that fold formation took place in a symmetrical way. Consequently, we infer, that for these sections the directions of remagnetization acquired during deformation can be correctly restored by symmetrical stepwise unfolding as applied by the fold tests used in this study (McFadden and McElhinny, 1990; Watson and Enkin, 1993). At Ushbas, the axial planes of folds are equally vertical, however the fold axes dip with $\sim 30^\circ$ towards SE (Fig. 2.9). This indicates, that at Ushbas area, which is located in the vicinity of the TTF, deformation was more complex and challenges the reliability of the results of the fold test analysis.

2.5.4 Data Summary

Table 2.5: Area mean directions after refolding procedure at maximal k values with resulting paleopoles.

Area	N	D [°]	I[°]	k	α_{95} [°]	[%] unf.	λ[°]	Plat	Plon	dp	dm	Inf. Age of Magn.
SUL-1	13	198.5	-60.4	134.5	3.6	25.4 ± 8.1	41.4	-76.2	341.8	5.5	4.2	∼190-215
SUL-2	13	207.5	-49.8	43.6	6.4	22.8 ± 3.5	30.6	-64.8	1.5	8.5	5.7	255-260
TSA	12	207.1	-48.0	11.9	14.6	100	29.0	-64.0	4.5	19.1	12.5	355-360$^\bullet$
AKO	7	210.4	-35.3	74.9	7.0	100	19.5	-55.1	14.4	4.7	8.1	∼255-290$^\bullet$
TUR	18	196.9	-37.0	60.4	4.6	58.4 ± 5.2	20.6	-63.0	31.5	3.2	5.4	275-280
USH	22,6*	173.0	-41.5	23.5	5.8	51	23.9	–	–	–	–	–

N: number of mean directions, used for performing fold-tests (McFadden and McElhinny, 1990; Watson and Enkin, 1993) and calculating area mean directions, mean Declination (D), mean Inclination (I) and Fisher (Fisher, 1953) radius of 95% confidence (α_{95}) after [%] unfolding of the directional data. λ_P degrees north latitude of paleopole. Error limits of unfolding degree is obtained using monte carlo simulations (Watson and Enkin, 1993). λ is the paleolatitude. Resulting paleopole (pole latitude (Plat) and longitude (Plong)) with error ellipse dp and dm. * at Ushbas (USH) 22 demagnetization great circles were combined with linear segments of 6 samples (McFadden and McElhinny, 1988a) to get a regional mean direction. Inf. Age of Magn.: Inferred age of acquisition of the magnetization (primary ($^\bullet$) or due to remagnetization).

After removal of a LTC, which is generally aligned with the present day field, a HTC is identified in most of the thermally demagnetized material

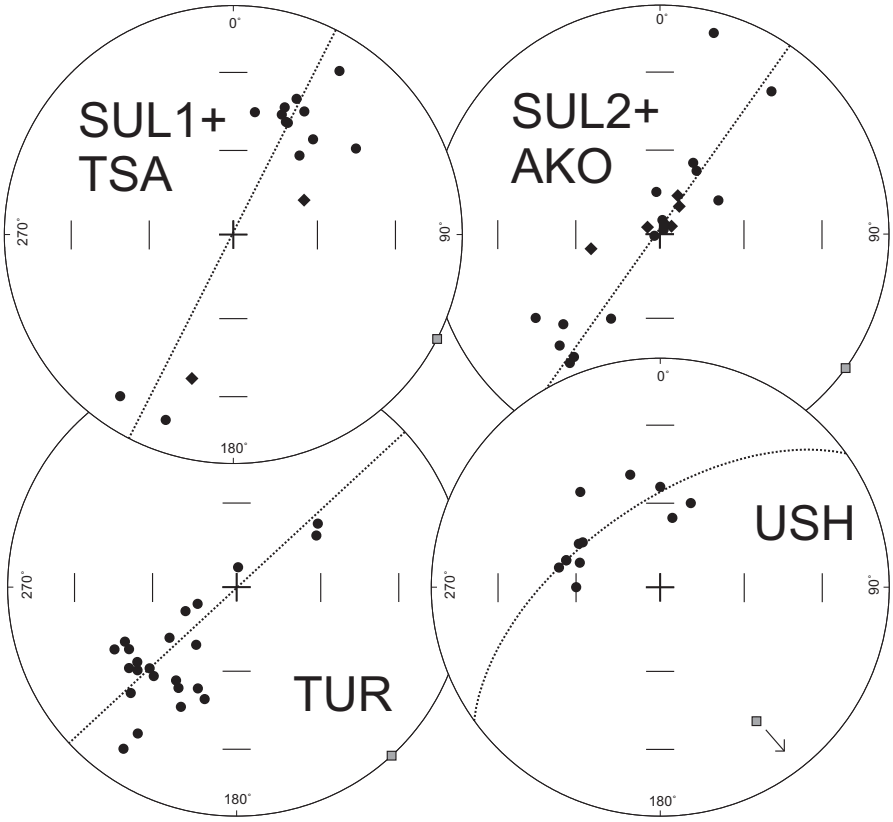

Figure 2.9: Stereographic projection of normal vectors of all bedding planes for respective areas. Dotted line indicate fitted great circle. Solid dots represent projection on the upper hemisphere. Grey square indicate resulting fold axis, arrow shows supposed direction of correction for tilted fold axis. Bedding planes of TSA and AKO are indicated as diamonds.

from Bolshoi- and Malyi-Karatau (Tabs.2.1,4.3,4.2,4.4). Site mean directions with α_{95} greater than (20°) were rejected and not used for further analysis. The HTC directions isolated in the sections at SUL-1, SUL-2, TUR and USH (Fig. 2.7+2.8) indicate a syn-folding age of acquisition of the magnetic signal (Tab. 2.5), which suggests, that the magnetization was acquired during a process of folding (Bachtadse *et al.*, 1987; McFadden and McElhinny, 1990). Two area mean directions show a maximum k (Fisher, 1953) (AKO: 43.8 and TSA: 62.7) after tilt correction (Fig. 2.8), indicating a pre-folding age of magnetization.

The area of Ushbas (USH) shows a plunging fold axis (Fig. 2.9). The result of the syn-tilt direction is therefore questionable, and might be biased by unknown amounts of rotation about inclined axes. Because of this, and also due to the poor quality of the demagnetization results we omit this area from further analysis.

The directional mean data was transformed into five paleopole positions (Tab. 2.5). The paleopoles are not consistently grouped within α_{95} error limits, nor do they fall onto any part of the Paleozoic apparent polar wander path (APWP) of Baltica (Smethurst *et al.*, 1998). All poles are, however, rotated counterclockwise (ccw) with respect to their expected locations in vicinity to the Baltic APWP.

2.6 Age of Magnetization

Foldtests (Fig. 2.7 and 2.8) indicate that four of the six Paleozoic areas studied have been subjected to remagnetization. The sampled rocks at AKO span most of the Permian period. The positive fold test at 100% of unfolding suggests that the primary magnetization was acquired prior to Mesozoic deformation. The slight underestimation of the paleolatitude compared to expected values from the APWP of Baltica can be explained by inclination shallowing, which has been proposed for Permian red beds from South Kazakhstan (Bazhenov *et al.*, 1995) and red beds in general (e.g. Tauxe and Kent (2004)). However, the syn-folding acquisition of magnetization observed in rocks from the other areas studied makes inclination shallowing rather unlikely.

It is now widely accepted that remagnetization of unmetamorphosed sedimentary rocks is related to orogenically triggered fluid flow from the orogen into the foreland (Oliver, 1986) and the associated new formation of magnetite and to a smaller extend hematite (McCabe and Elmore, 1989). Expanding the orogenic fluid flow concept, Zegers *et al.* (2003) stress the importance of elevated temperatures within deformation zones. They show that a complex pattern can accompany orogenesis, involving different mechanism, which can lead to remagnetization, like formation of TVRM (thermo-viscous remanent magnetization) or CRM (chemical remanent magnetization) during smectite to illite conversion.

It seems, that in the Karatau Mountains, at least two phases of remagnetiztion can be identified. An early event of deformation, leading to a syn-folding signal in the Bolshoi Karatau and maybe westernmost Malyi Karatau

(TUR and USH). Localities SUL-1 and SUL-2, in the Malyi Karatau, were also remagnetized during a folding period. However, here the degree of unfolding, which is necessary to obtain ideal clustering of magnetic directions is lower, and the resulting syn-folding inclinations are higher. Therefore, it might reflect a different phase of remagnetization.

In contrast, areas of TSA and AKO do not show any sign of remagnetization. It seems, that remagnetization events are, as proposed by Zegers *et al.* (2003) a complex superposition of different mechanisms, depending crucially on the temperature(s) of migrating fluids and deformation geometry at the specific area. Therefore, remagnetization behavior can have quite different appearance in a single orogenic.

2.7 Implications for the Geotectonic History

In summary all paleopoles, derived from Paleozoic rocks from the Karatau Range, which yield pre- or syn-folding magnetization ages, feature two characteristics in comparison with the East European apparent polar wander path (Smethurst *et al.*, 1998) as a reference:
(1) A deviation in polar longitude (ΔPlong) of $25^\circ - 65^\circ$ counterclockwise with respect to the Baltic APWP, present in all studied rocks (Fig. 2.10). Thus rotational reorganization took place at least until the early Mesozoic.
(2) Analysis of the expected paleolatitudes (or inclinations) of the area in a Baltic reference frame leads to the following implications: (a) the paleolatitude of rocks from TSA are in agreement with a primary Devonian acquisition age of magnetization, (b) rocks from AKO show a slightly lower paleolatitude than expected, which can be explained by inclination shallowing, (c) rocks from TUR, since they hold a syn-folding magnetic signal, can be correlated with a remagnetization event at $\sim 275 - 280$ Myrs ago (probably during the D1 or D2 event of Alexeiev *et al.* (2009)), (d) rocks from SUL-1 and from SUL-2 areas yield a paleolatitude, which fits the expected value at $\sim 220 - 225$ and $\sim 255 - 260$ Myrs ago, respectively, (probably at different times during phase D3 of Alexeiev *et al.* (2009)) (Fig. 2.11). Errors of the paleolatitudes reflect corresponding value of inclination of syn-tilt direction at $\pm 10\%$ of the optimal untilting percentage. This amount includes all uncertainties from the Watson and Enkin (1993) fold test.

In this respect, we correlate the first remagnetization event with the D1 and D2 events of Alexeiev *et al.* (2009), which accompanied the initial collision of Kazakhstan and Baltica. In these phases most of the folding amount

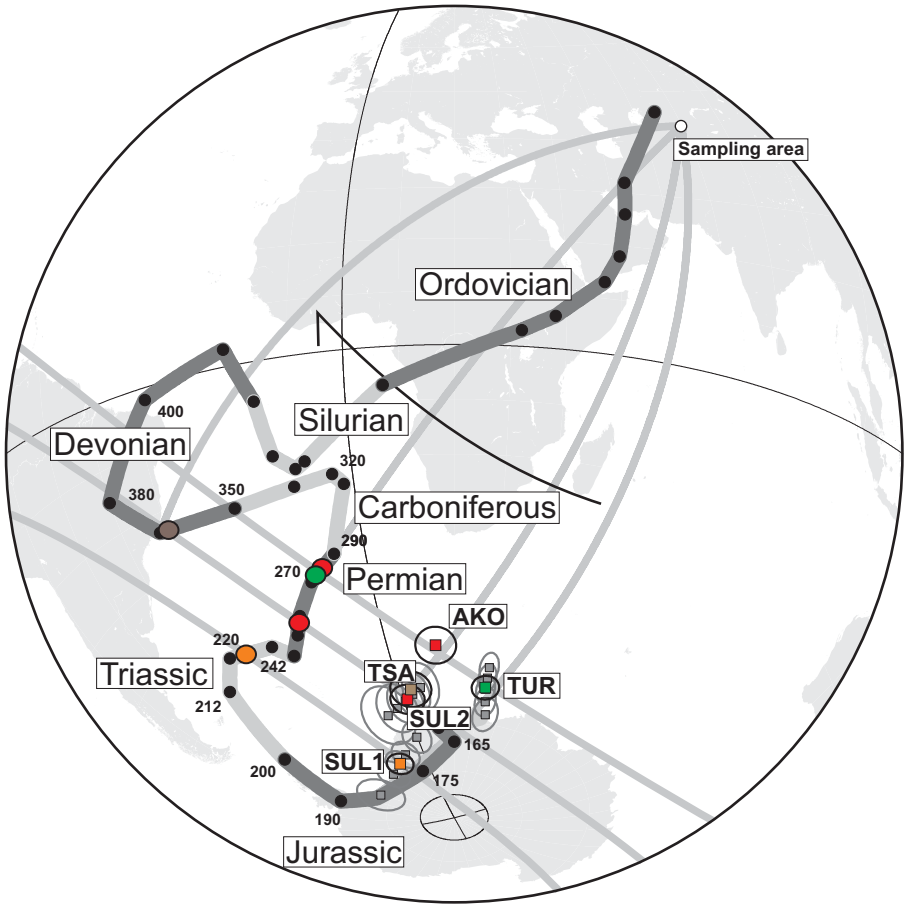

Figure 2.10: Paleopoles calculated from the characteristic area mean directions. Shown are the proposed deviations compared to the apparent polar wander path (APWP) of the East European Craton (Smethurst *et al.*, 1998) (with ages in Myrs). Wedges about the sampling area illustrate the rotational reorganization about a vertical axis. Colored ellipses indicate intersections of particular small circles with the associated part of the APWP. Grey squares at TUR, SUL1 and SUL2 show paleopoles calculated from directions for a bandwidth of ±20% around the optimal (maximum k) unfolding percentage.

took place. Subsequently, folding in the Chu-Sarysu basin, which took place from late-Permian to early Mesozoic times (Abdulin *et al.*, 1986; Allen *et al.*, 2001; Alexeiev *et al.*, 2009), is accompanied by remagnetization in the SUL

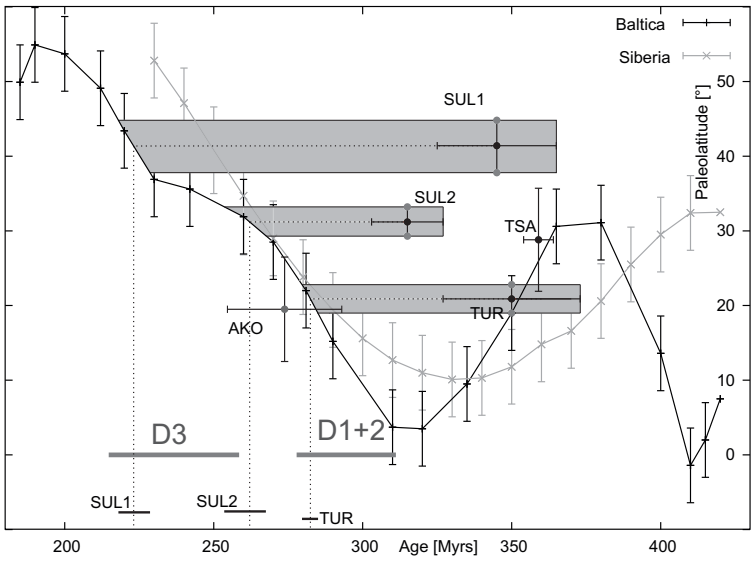

Figure 2.11: Plot of paleolatitudes versus age, calculated with respect to the apparent polar wander paths of Baltica (Smethurst *et al.*, 1998) and Siberia (B solution, according to Cocks and Torsvik (2007)) for a reference site in the Karatau mountains with a mean error of 5°. Also plotted are paleolatitudes, calculated from the regional mean directions (Tab. 2.5). Horizontal errorbars define the age uncertainty. Vertical errorbars are associated with a paleolatitude based on the direction at +10 and -10% untilting about the optimal untilting value (Tab. 2.5). TSA and AKO are plotted with the α_{95} confidence error. Grey boxes indicate intersection of paleolatitudes based on syn- or post-folding magnetizations from Karatau with the expected value based on the APWP of Baltica. Grey lines at the bottom (D1, D2 and D2 after Alexeiev *et al.* (2009)) mark the timing of the deformational phases in the Karatau.

areas. Folding in the area could have proceeded until early Mesozoic times, because of a lack of unconformities in the Devonian to Upper Permian sequences.

The amounts of counterclockwise rotation with respect to (wrt) the APWP of Baltica decrease as a function of time of acquisition of magnetization. Devonian rocks carrying a primary magnetization are rotated away by $\sim 65°$ (TSA), whereas rocks re-magnetized during phase I of folding (~ 280 Ma) are only rotated by $\sim 40°$ whereas rocks magnetized during the

youngest pahse (II) only show roations in the order of $\sim 30-20°$ (Fig. 2.10). This observation is strengthening our interpretation.

The robustness of the declination deviations (ΔDec) is shown by calculating paleopoles of syn-folding directions at $\pm 20\%$ of the optimal untilting value (Fig. 2.10). Small differences of vertical axis rotations, between SUL1 and SUL2, and between TUR and AKO, respectively, might be explained by minor local variations of the deformational history.

The amount of rotation in Karatau does not exceed $\sim 65°$, and is significantly less than maximum rotation values in the Tianshan, which can reach $\sim 90°$ (Van der Voo *et al.*, 2006). The latter can be interpreted as evidence for an increase of maximal rotation values while following a transect from the Urals via the Karatau towards the Tianshan. Correcting for the maximal amount of rotation in the Karatau mountains suggests, that the Karatau Range was originally a N-S striking fold-belt, which got subsequently bent into an 'orocline' s.l. as the collision evolved through time. It might therefore represent a continuation of the Ural mountains.

2.8 Conclusions

Primary and syn-folding magnetizations were isolated for Devonian, Carboniferous and Permian rocks in three areas of the Karatau mountain range, based on the outcome of fold tests (Watson and Enkin, 1993). The magnetizations identified in rocks of Permian and Devonian age in the Zhanatas and Akkol areas pass the fold test and are therefore interpreted to be of primary origin. The resulting mean direction after full tilt correction is $D = 210.4°$, $I = -35.3°$, $k = 74.9$ and $\alpha_{95} = 7.0°$ for the Permian rocks (AKO) and $D = 208.2°$, $I = -47.7°$, $k = 66.3$ and $\alpha_{95} = 6.9$ for the Devonian rocks (TSA). The obtained paleolatitudes of TSA are in agreement with corresponding values of a reference site within the Karatau mountains based on the Baltica APWP (Smethurst *et al.*, 1998). AKO yield a slightly underestimated paleolatitude compared to the APWP, which might reflect inclination shallowing.

Magnetic directions of rocks from the area TUR of Bolshoi Karatau and SUL-1, SUL-2 of Malyi Karatau indicate a syn-folding age of acquisition of the magnetic signal, at $\sim 58\%$ (for TUR), and $\sim 23\%$, $\sim 25\%$ (for SUL-1 and SUL-2) of untilting, respectively. The syn-folding magnetic mean directions are $D = 196.9°$, $I = 37.0°$, $k = 60.4$ and $\alpha_{95} = 4.6°$ for TUR, $D = 198.5°$, $I = -60.4°$, $k = 134.5$ and $\alpha_{95} = 3.6°$ for SUL-1 and

$D = 207.5°$, $I = -49.8°$, $k = 43.6$ and $\alpha_{95} = 6.4°$ for SUL-2. Because the major folding in this area started at ~ 315 Myrs ago (Alexeiev *et al.*, 2009), the resulting paleolatitudes of these areas intersect the paleolatitude curve of a reference site within Karatau Mountains of the Baltica APWP at ~ 280 Myrs (TUR), at ~ 260 (SUL-2) and at ~ 230 Myrs (SUL-1).
These observations are in agreement with major phases of deformation (D1,D2 and D3 after Alexeiev *et al.* (2009); Rolland *et al.* (2013)) in this area and the Eastern Urals - Transuralian Fault system (Echtler and Hetzel, 1998). They indicate a series of distinct remagnetization events, which form a complex pattern within this orogenic environment.

The whole region was, during all that time (middle Bashkirian early Mesozoic), exposed to rotational reorganization connected with the appearance of major strike slip fault systems. The Karatau mountain range shows vertical axis rotations reflected in ΔDec compared to expected values in a counterclockwise sense with amounts in a range between 20° to 60°. The amounts of observed vertical axis rotation decrease with decreasing magnetization age. The Devonian rocks from Zhanatas (TSA) show the largest amount of declination deviation ($\sim 60°$), whereas ΔDec observed at SUL-1, SUL-2 and AKO are in the order of about 20°.

By comparing the new results with studies from the Tianshan and South Kazakhstan, a similar tectonic evolution is noticeable. The maximal amount of observed rotations, however, increases from the Karatau towards the Tianshan, where ΔDec reach values more than 90° (Van der Voo *et al.*, 2006). In the Tianshan the rotational history seems, however, much more complicated than in the Karatau mountains.

Our data identify the Karatau Range as the structural linkage between the Ural mountains and the CAOB basement of the Tianshan mountains relative to their Late Paleozoic to Early Mesozoic evolution. Though the Main Karatau Fault was reactivated during Neogene Tianshan orogeny, the Paleozoic sedimentary record shows the character of a major discontinuity already since Early Paleozoic. Late Carboniferous onset of contractional tectonics is shown by syn-deformational remagnetization followed by more remagnetization events during Late Permian and maybe Triassic, respectively.

Acknowledgements

We thank the Editor André Revil, C. Mac Niocaill and one anonymous reviewer for their critical and very constructive comments on the manuscript. Their comments lead to a significant improvement of the paper. The study was funded by research grants (Ba1210/13) of the German Research funding agency (DFG) to V. Bachtadse and grant 13-05-91151 from the Russian Foundation for Basic Researches (RFBR) to D. Alexeiev. We are thankful for logistical support and hospitality by the Research Station of Russian Academy of Sciences, Bishkek, Kirghiyzia. Support during field work from Alexander Mikolaichuk is greatly appreciated. Large amounts of measurements were carried out by Rosi Weindl.

3

Correcting for inclination shallowing of early Carboniferous sedimentary rocks from Kyrgyzstan – indication of stable subtropical position of the North Tianshan Zone in the mid-late Palaeozoic

by ***U. Kirscher, D. Bilardello, A. Mikolaichuk, and V. Bachtadse***
Published in Geophysical Journal International, *2014,* ***198****(1000-1015)*

Abstract

High-quality palaeomagnetic data for the early Carboniferous of Central Asia are scarce and the palaeogeographic evolution of this area prior to final

amalgamation of the region east of the Ural mountains is still rather obscure. Here, we present palaeomagnetic data for early Carboniferous deposits from two areas in the Kyrgyz North Tianshan (NTS). Detailed rock-magnetic analysis indicates the presence of magnetite and haematite as magnetic carriers in these red sediments. In the Kazakh basin section (KEL), we identify a high-temperature component (HTC) of magnetization during stepwise thermal demagnetization at temperatures of up to ~ 680°C yielding a site mean direction of $D = 176.2°$, $I = -36.4°$, $k = 57.4$ and $\alpha_{95} = 8.9°$ after tilt correction. Two HTCs of magnetization were identified in samples from the Sonkul Basin (DUN) with maximum blocking temperatures of ~ 600°C (magnetite) and ~ 680°C (haematite). The magnetite component was also identified with alternating field demagnetization. The resulting site mean directions for these two components identified in 16 and 14 sites, respectively, are $D = 149.3°$, $I = -50.3°$, $k = 73.6$ and $\alpha_{95} = 4.3°$ for the magnetite and $D = 139.6°$, $I = -35.1°$, $k = 71.6$ and $\alpha_{95} = 4.7°$ for the haematite component. All three mean directions show a significant increase of the precision parameter k after tilt correction indicating acquisition of the high-temperature magnetization prior to the main folding event in the Jurassic. We explain the difference of the two components of DUN by a process of inclination bias due to compaction to which the platy haematite particles are more susceptible. Applying the elongation-inclination (E/I) method to directional data from over 100 individual samples from location DUN results in a negligible correction for the magnetite component ($< 5°$), whereas the inclination of the haematite component corrects from $-35.0°$ to $-50.3°$ ($f = 0.6$, error interval $-41.4°$ to $-57.9°$), which is then equal to the uncorrected magnetite inclination. The small number of samples from section KEL does not allow application of the E/I technique and inclination correction based on high field anisotropy of isothermal remanent magnetization was applied, yielding a corrected inclination of $-75.2° \pm 4°$. Assuming comparable degrees of compaction for both study areas and applying the flattening factor obtained in DUN on samples from KEL, however, would result in comparable inclinations. The identification of inclination shallowing at both sections indicates that the age of magnetization is close to the deposition age.

Assuming a reversed polarity of the directions from both areas results in palaeolatitudes of ~ 30°N for section DUN and ~ 60°N for the anisotropy-based correction of section KEL. The large difference, however, is geologically very unlikely. The inclination of the magnetite component of DUN (unaffected by inclination shallowing) favours a palaeoposition of ~ 30°N.

This is supported by the inclination shallowing corrected haematite component of DUN yielding a comparable inclination. Therefore, our results indicate that the NTS domain was situated at $\sim 30°$N in the early Carboniferous. Furthermore, the NTS zone was probably not connected to Baltica or Siberia prior to the late Palaeozoic.

3.1 Introduction

Despite the fact that the Central Asian Orogenic Belt (CAOB, Fig. 3.1) is probably one of the largest accretionary structures on planet Earth, it was only in rather recent times that it attracted the attention of the Earth sciences community [see thorough review by Windley *et al.* (2007)] and a series of competing models have been brought forward since the early 1990s (Windley *et al.*, 2007; Xiao *et al.*, 2010) which can be grouped as modifications of (a) the 'multiple island arc' or (b) the 'single arc' model. The multiple island arc model (a) is based on similarities in the structural evolution of the CAOB or Altaids (sensu Şengör *et al.*, 1993) between 1.0 Ga to 250 Ma and the south western Pacific (Hall, 2009; Xiao *et al.*, 2010) where crustal growth is basically characterized by the interaction of islands arcs, oceanic islands, sea-mounts, accretionary wedges and continental blocks. In this model, originally proposed by Zonenshain *et al.* (1990) and later been taken up by mostly Russian authors (e.g. Mossakovsky *et al.*, 1993; Berzin and Dobretsov, 1994; Yakubchuk *et al.*, 2001; Buslov *et al.*, 2002; Xiao *et al.*, 2008), Precambrian fragments, now integrated into the Altaids show affinities either to Gondwana or to Siberia. In the single arc model (b) Şengör *et al.* (1993) postulate the existence of an originally continuous island arc (Kipchak-Tuva-Mongol arc) about 7000 km in length. In this model early Palaeozoic roll-back of the subducted crust triggers the formation of the Khanty-Mansi back-arc ocean (Xiao *et al.*, 2010). Subsequent differential rotation of Siberia and Baltica caused segmentation and duplication of the arc by strike-slip shuffling and oroclinal bending associated with the final closure of the Khanty-Mansi ocean by late Carboniferous times.

By this time the general amalgamation and large scale tectonic organization of all the blocks and arc-related structures was completed. Subsequently, oblique northward directed subduction of the Palaeotethys lead to a transpressional stress field (Samygin and Burtman, 2009) including the formation of large strike-slip fault systems (Buslov, 2011).

Uncertainties remain concerning the overall kinematics of the late Palaeozoic incorporation of the early Palaeozoic terranes into Eurasia. Additionally, there is still a lack of knowledge about the precise palaeogeographic configuration of the two major blocks Baltica and Siberia relative to the Kazakh terranes throughout the middle–late Palaeozoic, especially in the early Carboniferous. High-quality studies from Kazakhstan and the Tianshan mountains are sparse between Middle Devonian and Permian times. On the other hand, the apparent polar wander paths (APWPs) of Siberia and

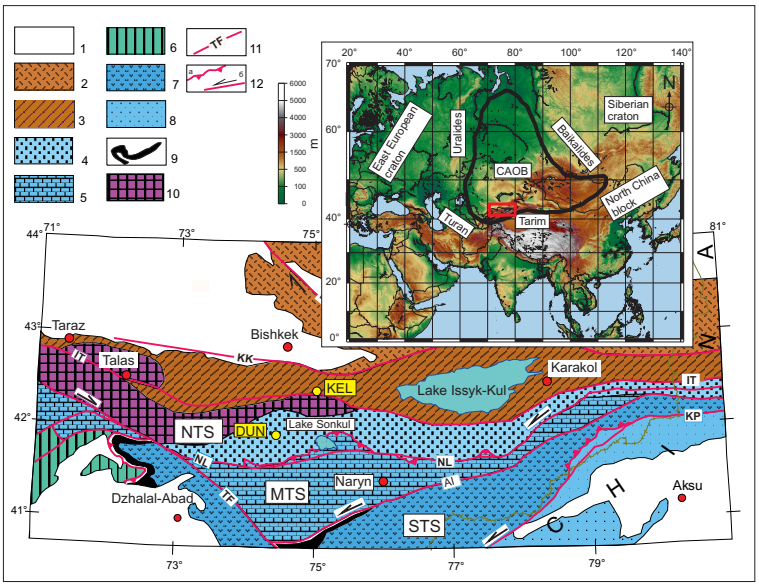

Figure 3.1: Small panel: Topographic map of Eurasia [created using GMT of Wessel and Smith (1998) and topographic dataset ETOPO1 (Amante and Eakins, 2009)] showing important geologic features for this study including East European craton (Baltica), Siberian craton, collisional orogens of Uralides and Baikalides, continental blocks Turan, Tarim and North China. Main part of the CAOB is outlined in black. Outline of enlarged geologic map in red. Large panel: Map of Central Tianshan Late Palaeozoic (D_3-C_1) complex distribution. 1 – Mesozoic-Cenozoic sediments of foreland basins, 2-3 – Kazakh palaeobasin complexes: 2 – early Carboniferous volcanic belt, 3 – marine and deltaic sediments; 4-9 – Turkestan palaeoocean complexes: 4-5 – northern passive margin: 4 – deltaic, lagoonal and flysch complexes of the Sonkul-Turuk depression, 5 – Middle Tianshan carbonate platforms; 6 – Chatkal-Kurama volcanic belt of West Tianshan, 7 – South Tianshan collisional belt (volcanogenic-siliceous and carbonate-volcanogenic complexes), 8 – southern passive margin (shelf and continental slope sediments of Tarim continental block), 9 – South Tianshan ophiolite complex; 10 – inferred land of Late Devonian - Early Carboniferous. 11 – main Late Palaeozoic faults: DN – Jalair-Naiman, KK – Kyrgyz-Kungei, IT – Ichkeletau-Terskei, NL – Nikolaev Line, AI – Atbashi-Inylchek, KP – Kipchak, TF – Talas-Fergana; 12a – frontal Hercynian thrusts, 12b – Late Palaeozoic strike-slip faults. NTS, MTS and STS indicate North, Middle and South Tianshan provinces, which are divided by the AI and NL.

Baltica itself are also not as well constrained in this time interval as during other time periods (Torsvik *et al.*, 1996; Cocks and Torsvik, 2007; Torsvik *et al.*, 2012). In addition, some of the palaeolatitudinal scatter observed in the Palaeozoic of the European platform might be related to inclination shallowing unaccounted for (Iosifidi *et al.*, 2010). As far as Kazakhstan is concerned, its palaeogeographic position is rather well constrained for Devonian and Permian times, but poorly or even undefined for the remaining Palaeozoic period (Bazhenov *et al.*, 1999; Abrajevitch *et al.*, 2007). A recent study of red beds of Carboniferous age (Bazhenov *et al.*, 2003) yielded a palaeolatitude for the NTS at $\sim 15°$N. If these results are taken at face value, they imply a Carboniferous palaeolatiutude for the Kazakh-NTS zone in the tropics, in contrast to geological observations (Didenko *et al.*, 1994; Şengör and Natal'in, 1996; Filippova *et al.*, 2001) arguing in favour of a rather subtropical position at $\sim 30°$N.

However, no corrections for inclination shallowing were applied in this study (Bazhenov *et al.*, 2003) and it can be suspected that the inclination in these rocks has been affected by this phenomena like in other parts of Asia (e.g. Gilder *et al.*, 2001; Tauxe and Kent, 2004).

To constrain early Palaeozoic terranes of Central Asia and reconstruct their palaeogeography better defined palaeomagnetic pole positions for the Middle to Late Palaeozoic of this area are needed. We present palaeomagnetic results for early Carboniferous sediments from 22 sites covering two geographically distinct areas of the North Tianshan (NTS; Fig. 3.1).

3.2 Tectonic Setting and Global Geodynamic Evolution

The Tianshan mountain belt within the borders of Kyrgyzstan can be subdivided into the Southern Tianshan (STS), the Middle Tianshan (MTS) and the NTS zones (Fig. 3.1). Precambrian continental fragments and Neoproterozoic to early Palaeozoic palaeooceanic and island arc complexes are overlain in the MTS and NTS mountains by Ordovician island arc related lithologies. Late Ordovician S-type granites indicate then collisional conditions (Burtman, 2006), which have been related to the amalgamation of Kazakhstania (Kheraskova *et al.*, 2003). Silurian active continental margin and backarc complexes are the first indications for the closure of the Turkestan ocean (Bakirov and Mikolaichuk, 2009; Biske and Seltmann, 2010). Upper Carboniferous terrigenous sediments are transgressively

thrusting upon Devonian to early Carboniferous sediments (Jenchuraeva, 1997, Fig. 3.1). These are the geological markers demonstrating that by the earliest late Carboniferous Kazakhstania had collided with Baltica (Puchkov, 1997, 2000). Subsequently, the area underwent several stages of intra continental deformation within non-orthogonal stress regime (e.g. Natal'in and Şengör, 2005; Cogné *et al.*, 2013), including folding and faulting until the early Mesozoic (Bazhenov *et al.*, 1999; Alexeiev *et al.*, 2009).

The two areas, which were studied, are situated in the Kazakh and Sonkul basins (Bakirov and Mikolaichuk, 2009) of the NTZ, north of the Nikolaev line (Fig. 3.1). The early Carboniferous sequence of the Sonkul basin has been interpreted to have been deposited on the northern (modern coordinates) passive margin of the Turkestan palaeoocean (Bakirov and Mikolaichuk, 2009, Fig. 3.1). The Kazakh basin was separated from the Turkestan ocean basin by a Devonian terrigenous sequence (Mikolaichuk and Djenchuraeva, 2000; Bakirov and Mikolaichuk, 2009, Fig. 3.1). It has been proposed that the Kazakh basin was even connected to the Junggar-Balkhash oceanic basin (Filippova *et al.*, 2001). The early Carboniferous sediments in this region are represented mainly by red sand-, siltstones and conglomerates. They rest on Late Devonian rocks (Kazakh basin) or unconformably on Cambrian to Ordovician rocks of different composition (Sonkul Basin), respectively.

3.3 Local Geological Setting and Sampling

Sonkul basin

Within the Sonkul basin the early Carboniferous sedimentary sequence is subdivided from old to young into the **Dungurme**, the **Jamanechke** and the minor **Jumgal Formations** (Fig. 3.2). The approximate thickness of these formations are ~ 350, $\sim 1000 - 1200$ and ~ 120m, respectively.

The **Dungurme Formation** is dominated in the lower part by red-coloured conglomerates, grits and sandstones, which are overlain by interbedded sandstones, siltstones, mudstones and limestones. The fossil complex indicate an age of the Dungurme Formation within the Late Visean–Early Serpukhovian (Khristov, 1970, 1971; Neyevin, 2008).

The **Jamanechke Formation** consists of red-coloured conglomerates, sandstones, shales and limestones (Galitskaya and Korolev, 1961; Khristov, 1970, 1971).

The Jamanechke formation is subdivided into three parts (Fig. 3.2). At

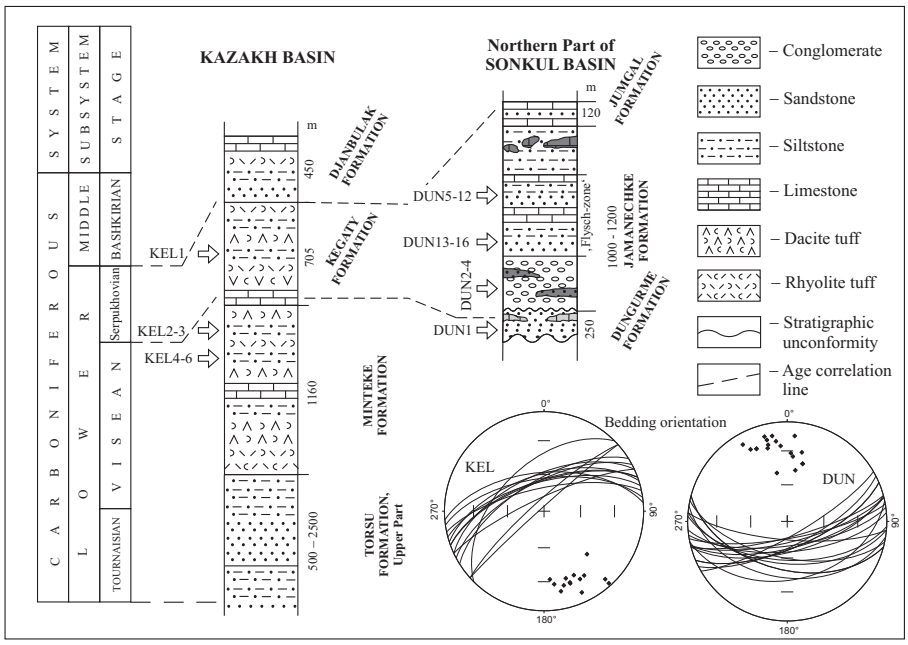

Figure 3.2: Stratigraphic columns of Late Palaeozoic sediments in the Kazakh and Sonkul Basins [redrawn after Khristov (1970, 1971); Burg *et al.* (2004)]. Approximate sampling locations are indicated together with all taken bedding orientations of the two areas.

the base, 250 – 300m brown-red polymictic poorly sorted conglomerates with layers and lenses of coarse-grained sandstones and gritstones. On top of these, up to 500m of rhythmic sequences of cross-bedded polymictic gritstones underlie thinly bedded sandstones and siltstones.

The top consists of up to 300 m of siltstones and shales, among which are subordinate fine-grained quartz-feldspar sandstones, cherts and limestones. This unit is characterized by variegated (red, maroon, brown, grey, green) coloured rocks. At the top of the last member appear lenses and layers of white gypsum (thicknesses from 0.5 to 10 m). The formation age is established by a brachiopod collection, which indicate Serpukhovian age (Galitskaya and Korolev, 1961; Khristov, 1970, 1971).

On top of the studied section red arkosic sandstones and limestones of the **Jumgal Formations** are present. A rich Late Serpukhovian–Early Bashkirian fossil complex has been described there (Khristov, 1970, 1971). Within the Sonkul Basin, a total of 160 oriented drill cores were obtained

Table 3.1: Position and age of sampled sections.

Site	Lat. ($^\circ N$)	Long. ($^\circ E$)	Age	Formation
Dungurme				
DUN-1	41.6585	74.3414	Visean	Dungurme
DUN-2↦4	41.6557	74.3376	Serp.	Jamanechke
DUN-5↦12	41.6869	74.3148	Serp.	Jamanechke
DUN-13↦16	41.6783	74.3366	Serp.	Jamanechke
Kegaty				
KEL-1	42.5242	75.0932	Serp.	Kegaty
KEL-2	42.5255	75.0908	Visean	Minteke
KEL-3	42.5260	75.0892	Visean	Minteke
KEL-4	42.5361	75.1049	Visean	Minteke
KEL-5	42.5340	75.1058	Visean	Minteke
KEL-6	42.5305	75.1026	Visean	Minteke

Site, sampling site; Lat. and Long., coordinates in ° north (N) and east (E); age, proposed age of sedimentation; Serp., Serpukhovian; formation, formation name.

at 15 sites, from the Jamanechke formation (DUN2-16) and one site from the Dungurme formation (DUN1, Table 4.1). Whereas most of the sites are separated outcrops which can only qualitatively be arranged in a chronological order (Fig. 3.2), sites DUN5-12 represent a continuous section, which is subdivided into these sites. Sample spacing ranges between tens of centimetres up to several metres depending on the outcrop conditions. The total length of the section is $\sim$ 58m, with very uniform bedding conditions of $\sim 342^\circ$ dip direction and $\sim 74^\circ$ dip (Fig. 3.2). Site DUN1 is located within a light, fine grained, red sandstone layer. Sites DUN 2-4 were sampled from poorly sorted, moderately rounded conglomerates with different amounts of fine grained matrix. Also the colour of the matrix of these samples varies from more greyish (DUN3) to more reddish (DUN2). As expected from the lithologic position of DUN5-16 (Fig. 3.2), the grain size varies repeatedly, gradually from pelitic to arenitic with slight colour changes from light to dark red. The fossils from the overlying formation (Jumgal) constrain the age of our samples to late Visean to Serpukhovian ($\sim 335 - 323.2$Ma). One site (DUN1) is located close to site CB of the study by Bazhenov *et al.* (2003).

Kazakh basin

Within the Kazakh basin the Devonian to Carboniferous sedimentary sequence from old to young consists of the **Torsu Formation**, the **Minteke Formation** and the **Kegaty Formation** (Fig. 3.2). The thicknesses of these formations are highly variable reaching maximum values of $\sim$ 2500, $\sim$ 1160 and $\sim$ 705m, respectively.

The **Torsu Formation** is characterized by polymictic conglomerates and red-coloured fine-grained sandstones, siltstones and claystones. Cross bedding, ripple marks and intraclastic breccias indicate upper shelf and deltaic environments.

The **Minteke Formation** conformably covers the Torsu Formation (Fig. 3.2) and is represented at the base by brownish-cherry and green polymictic and volcanoclastic sandstones alternating with siltstones (Djenchuraeva, 1997; Burg *et al.*, 2004). They are replaced upwards by cherry-brown siltstones and tuffs of rhyolitic composition with thin interlayers of tuff-sandstones and lenses of gritstones and conglomerates. The middle section is characterized by 5-10 m thick layers of grey-green, fine-pebbled conglomerates laterally replaced by gritstones and tuff-gritstones. Upsection a bed of red and green siltstones alternates with similarly coloured tuff-sandstones and acid, intermediate tuffs containing rare rhyolitic flows and associated clastites. This sequence is overlain by a bed of limestone. Reworked tuff sandstones alternating with intermediate tuffs make the top of the formation. Tournaisian-Lower Visean foraminifera were found in this section (Grishchenko, 1967; Djenchuraeva, 1997; Burg *et al.*, 2004).

The **Kegaty Formation** conformably overlays the Minteke Formation (Fig. 3.2). It is composed at its base of variegated polymictic and volcanoclastic sandstones, andesitic-dacitic tuff- sandstones and tuffs. The formation contains abundant and up to 15-m-thick beds of sandy, bioclastic limestones and red-brown siltstones with calcareous nodular concretions. The upper part is composed of andesitic-dacitic tuffs and tuffites, cherry-brown siliceous siltstones, tuff rich siltstones and conglomerates. Brick-red tuff-siltstones containing single interbeds of tuff-sandstones, rhyolite lavas and tuffs become predominant towards the top.

Numerous Bashkirian foraminifers, corals and brachiopods were collected in the stratotype section (Djenchuraeva, 1997; Burg *et al.*, 2004). A rich Late Visean-Early Serpukhovian benthic fauna is also reported in this area (fauna catalogue, Burg *et al.*, 2004).

In this region, 57 oriented drill cores were taken from six sites, including

one site located in the Kegaty formation and five sites in the Minteke formation. All samples from this section, referred to as KEL (Table 4.1), were taken from cherry brown siltstone sites on the slope of the river Kegaty. All sites were spatial separated and the bedding conditions of them are quite uniform (Fig. 3.2). The age of the section ranges from early Visean to middle Serpukhovian ($\sim 340 - 328$Ma, Fig. 3.2).

3.4 Field and Laboratory Methods

All samples were cored in the field using a portable, water-cooled rock-drill. The orientation of the samples and their structural position were measured using a Brunton compass. After been formatted to standard palaeomagnetic specimens of $10cm^3$ in volume in the laboratory, all samples were stepwise demagnetized using thermal or alternating field (AF) techniques with peak temperatures of $\sim$ 700°C and peak fields of $\sim$ 200mT in zero field conditions. Measurements were performed in a magnetically shielded room at the Ludwig-Maximilians University, Munich. Magnetization directions were measured in three components with a vertical 2-G Enterprises squid magnetometre, Sand City, CA. Directions of the remanence components were identified as linear segments on the demagnetization diagrams, defined by at least five consecutive data points and subjected to principal compeonent analysis (PCA, Kirschvink, 1980). Only eigenvectors with a maximum angular deviation (MAD) of less than 10° were used to calculate the mean directions of the magnetic components identified.

In order to elucidate the coercivity spectrum of the material, an isothermal remanent magnetization (IRM) was imparted on selected specimens using a MMPM pulse magnetizer, Liverpool, UK, using peak fields of $\sim$ 6T. The IRM acquisition results were analysed by quantification of the magnetic coercivity components (Kruiver *et al.*, 2001; Heslop *et al.*, 2002). Thermomagnetic curves (in-field, $\sim$ 370mT) were obtained with a variable field translation balance, Petersen Instruments, Munich, Germany [VFTB, Krasa *et al.* (2007)]. Additionally, orthogonal three axes IRMs were imparted and subsequently thermally demagnetized following the procedure of Lowrie and Heller (1982) with peak temperatures of $\sim$ 700°C. For further analysis, these three-axes IRMs were also demagnetized using AFs up to $\sim$ 200mT. All rock-magnetic experiments were performed on representative samples from both localities. Samples from KEL are all rather uniform in colour and grain size. From section DUN samples from below (DUN1), within (DUN2-4) and

above the conglomerate (DUN5-16) were analysed. Additionally, samples of different grain size and colour were studied from the continuous section (DUN5-12) and from the remaining separated sites (DUN13-16).

The magnetic fabrics from both sections were studied using low field anisotropy of magnetic susceptibility (AMS) and anisotropy of isothermal remanence (AIR) in high fields.

Low field AMS was measured on an AGICO KLY-2 Kappabridge, Brno, Czech Republic, using the 15 position measurement scheme of Jelinek (1977).

For the AIR measurements, saturation IRMs (SIRMs) of 6.5 T were imparted on the specimens along x, y, z axes and along the $-x$, $-y$ and $-z$ axes. To reach such high fields in the pulse magnetizer, the coil with the smallest cavity was used. This did not allow magnetizing orientations that are off the specimens' principal coordinates (e.g. xy, xz, yz, ...) without drastically reducing the specimen dimensions. After each IRM was imparted, the specimens were thermally demagnetized at 120°C to eliminate possible contribution of goethite, a common alteration mineral in red beds. The specimens were also AF demagnetized in fields of 100 mT to minimize the contribution of magnetite, also present in the specimens. Each magnetization was successively measured on a 2-G Enterprises SQUID cryogenic magnetometre. For each positive and negative couple of measured specimen axes, the three components of each vector were averaged to obtain the three components of the magnetic vectors along the x, y and z field directions (Mxx, Mxy, Mxz for the IRMs applied along x, Myx, Myy, Myz for the IRMs applied along y and so on). Following Stephenson *et al.* (1986), six independent coefficients were obtained from these nine values, that is Mxx, Myy, Mzz, $(Mxy + Myx)/2$, $(Mxz + Mzx)/2$, $(Myz + Mzy)/2$ (theoretically $Mxy = Myx$ etc., but to minimize the experimental error an average value was taken). These six coefficients were used to compute the complete IRM ellipsoids by standard least-squares methods and principal axis orientations and lengths were calculated by iterative diagonalization (e.g., Press *et al.*, 1986; Tauxe, 1998; Borradaile and Jackson, 2004).

3.5 Results

3.5.1 Demagnetization Behaviour

Thermal demagnetization experiments show in general stable behaviour with unidirectional decay of intensity (Fig. 3.3). 80 per cent at section DUN

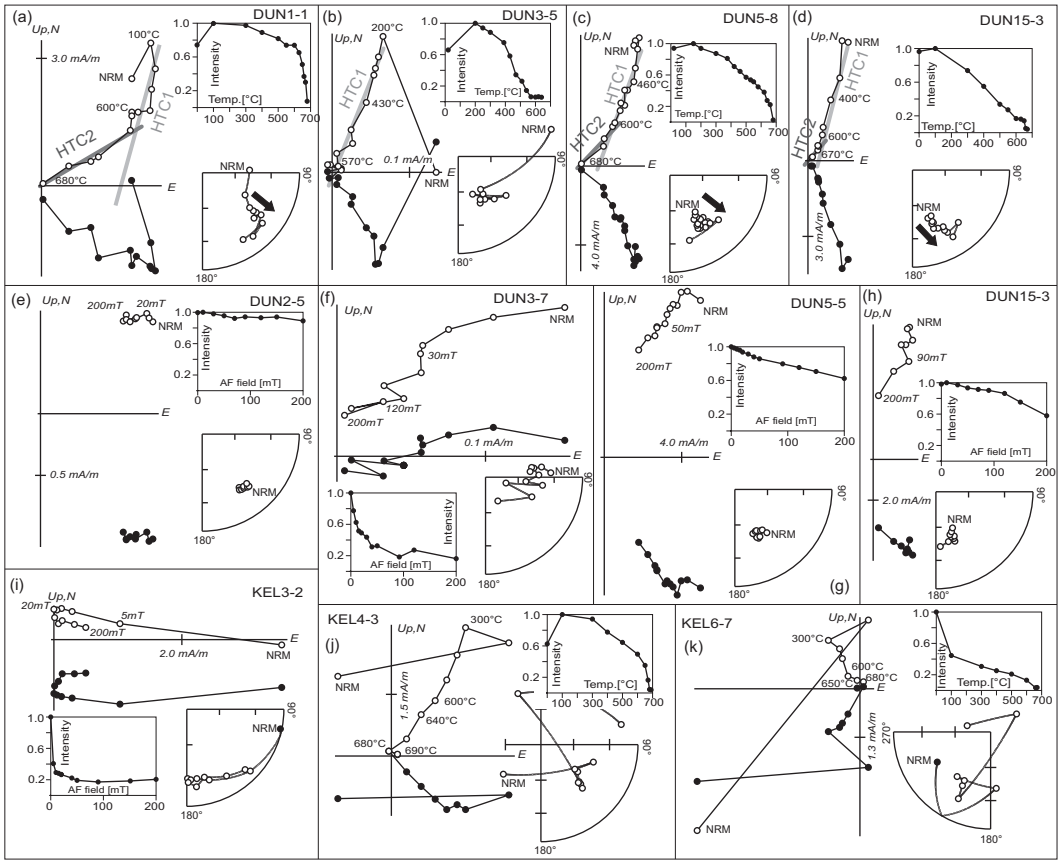

Figure 3.3: Results of thermal (a–d, j and k) and alternating field (e–i) demagnetization experiments plotted as orthogonal vector diagrams (Zijderveld, 1967) in stratigraphic coordinates. Solid and open dots represent vector endpoints projected onto the horizontal and vertical planes, respectively. Temperature and alternating field steps in °C and mT are indicated. Light grey and dark grey lines indicate proposed least square fits of the HTC1 and HTC2, respectively, of section DUN. Also shown are decay plots of normalized intensity and stereographic projection of the demagnetization data.

and 57 per cent at section KEL of the samples measured yield directions of magnetization fulfilling our requirement of at least five consecutive demagnetization steps defining linear segments. The remaining samples did not show any stable demagnetization behaviour.

Table 3.2: Palaeomagnetic site mean directions and overall mean directions of the ChRM.

Site	h (cm)	N	*In situ*				Bedding-corrected			
			$D(°)$	$I(°)$	k	α_{95} (°)	$D(°)$	$I(°)$	k	α_{95} (°)
Dungurme section – DUN, HTC1 (uncorrected)										
DUN-1	–	6/8	58.7	-76.7	93.8	7.0	134.8	-48.7	93.8	7.0
DUN-2	–	4/6	41.8	-63.3	106.1	9.0	152.4	-47.0	106.1	9.0
DUN-3	–	6/7	37.9	-62.5	22.4	14.5	139.8	-47.1	22.4	14.5
DUN-4	–	10/21	34.8	-62.2	23.8	10.1	137.4	-59.5	20.0	11.1
DUN-5	260	16/16	336.0	-55.1	91.9	3.9	149.3	-48.2	95.9	3.8
DUN-6	360	5/9	338.8	-65.5	279.2	4.6	148.4	-37.3	279.1	4.6
DUN-7	230	5/6	334.3	-59.3	103.6	7.6	150.4	-43.7	103.6	7.6
DUN-8	325	7/9	338.7	-56.3	45.6	9.0	146.7	-46.4	45.6	9.0
DUN-9	873	9/13	335.4	-55.9	70.7	6.2	150.1	-49.2	71.5	6.1
DUN-10	475	3/5	327.6	-52.2	146.5	10.2	139.6	-59.7	146.5	10.2
DUN-11	1210	12/12	329.9	-46.2	62.8	5.5	157.3	-65.9	58.4	5.7
DUN-12	760	19/19	329.4	-46.3	190.0	2.4	139.5	-61.2	37.9	5.5
DUN-13	–	8/8	326.1	-53.0	502.3	2.5	167.2	-50.0	502.3	2.5
DUN-14	–	7/7	340.0	-59.6	75.2	7.0	154.8	-44.4	75.2	7.0
DUN-15	–	7/7	332.3	-57.4	154.1	4.9	160.7	-46.4	154.1	4.9
DUN-16	–	4/7	338.4	-58.2	54.5	12.6	156.0	-45.8	54.5	12.6
DUN-AF⋆	–	10	6.7	-59.4	20.6	10.9	153.4	-51.4	45.5	7.2
Mean	–	16	344.8	-60.9	26.3	7.3	149.3	-50.3	73.6	4.3
Kegaty section - KEL										
KEL-1	–	5/14	173.2	10.9	31.2	13.9	194.5	-51.4	27.7	14.8
KEL-2	–	4/6	178.2	26.8	72.0	10.9	180.5	-30.4	72.0	10.9
KEL-3	–	6/6	165.4	29.4	28.4	12.8	168.8	-35.3	28.4	12.8
KEL-4	–	5/10	152.3	22.4	27.6	14.8	155.7	-38.8	25.4	15.5
KEL-5	–	8/14	178.0	22.9	40.7	8.8	181.2	-35.0	37.4	9.2
KEL-6	–	3/7	169.3	-3.3	26.2	24.6	184.6	-34.2	26.2	24.6
Mean	–	6	169.5	18.5	28.3	12.8	176.2	-36.4	57.4	8.9

Site, sampling sites; h, height of sampled outcrop, where appropriate; N, number of samples (sites) used for calculating site (area) mean directions/number of measured samples. Declination (D) and Inclination (I) in degrees, Fisher precision parameter k (Fisher, 1953), Fisher radius (α_{95}) of 95per cent confidence in geographic (*in situ*) and bedding corrected (TC) coordinates, respectively. ⋆ Mean direction for 10 samples, which were treated with alternating field demagnetization, samples including sites DUN-3,-5,-9,-11,-12,-14,-15, because of the different sites, mean directions were not included into area mean direction.

A weak low temperature component (LTC) is present in samples from both sections. At DUN the LTC is, if at all, present only up to ~ 250°C (Fig. 3.3a–h). Combining results of 18 samples, where the LTC is separable, yields an *in situ* mean direction for the LTC of $D = 359.3°$, $I = 52.5°$, $k = 12.5$ and $\alpha_{95} = 10.2°$. At section KEL the LTC can be recognized in most samples up to ~ 350°C. The mean direction of this component is $D = 351.9°$, $I = 42.0°$, $k = 9.1$ and $\alpha_{95} = 10.1°$ using data from 25 samples.

After removal of the LTC a high temperature component (HTC) is present in all samples from section KEL, which is totally removed at tem-

peratures of 660 − 680°C. Combining site mean direction for all six sites results in an overall mean direction for this area of $D = 169.5°$, $I = 18.5°$, $k = 28.3$ and $\alpha_{95} = 12.8°$ before, and $D = 176.2°$, $I = -36.4°$, $k = 57.4$ and $\alpha_{95} = 8.9°$ after bedding correction (Fig. 3.4, Table 5.5).

Demagnetization data of section DUN show two HTCs (Fig. 3.3a–d),

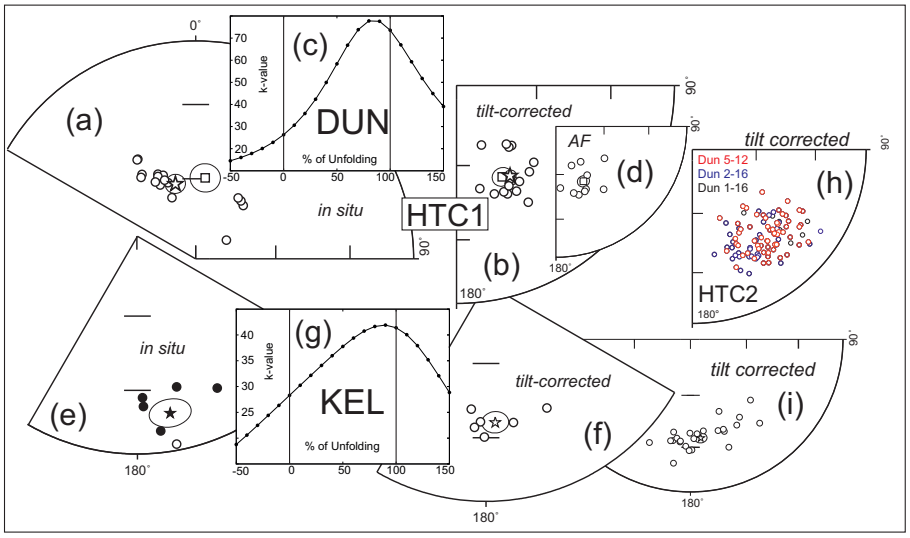

Figure 3.4: Site mean directions in geographic [*in situ*-(a and e)] and stratigraphic [tilt-corrected-(b and f)] coordinates for site DUN (uncorrected HTC1) and KEL (HTC). Stars mark mean values with associated 95per cent confidence intervals. Square indicates site mean direction of only component of 10 samples from DUN treated with alternating field demagnetization (Fig.3.3). (c and g) k-values versus percentage of unfolding. (d) Sample mean directions of samples from DUN treated with alternating field demagnetization and mean value with according α_{95} error interval. (h and i) All sample mean directions for section DUN [HTC2 and KEL (HTC)]. For DUN samples from within the continuous section (DUN5-12) are plotted in red, samples from the Jamanechke formation are plotted in blue and all samples in black.

a first HTC (high temperature component one, HTC1), identified between 300 and ∼ 600°C, and a HTC2, present between 600 and ∼ 690°C. Samples from DUN3 and DUN4 contain only a HTC1 and lose all their NRM intensity at ∼ 600°C (Fig. 3.3b). Combining site mean directions from 16 (HTC1) and 14 (HTC2) sites, respectively, yield mean directions of $D = 344.8°$,

$I = -60.9°$, $k = 26.3$ and $\alpha_{95} = 7.3°$ before, and $D = 149.3°$, $I = -50.3°$, $k = 73.6$ and $\alpha_{95} = 4.3°$ after tilt correction (Fig. 3.4, Tables 5.5 and 3.3) for HTC1 and $D = 10.6°$, $I = -69.3°$, $k = 29.6$ and $\alpha_{95} = 7.4°$ before, and $D = 139.6°$, $I = -35.1°$, $k = 71.6$ and $\alpha_{95} = 4.7°$ after tilt correction for the HTC2. It is noteworthy that all inclinations of the HTC2 are consistently lower than inclinations of the HTC1 in stratigraphic coordinates, whereas the declinations are rather similar. In order to get a first impression on the possibility of inclination shallowing of the HTC2, all sample mean directions of section DUN were plotted together. The fact that the distribution of directions is E-W elongated (Fig. 3.4h), suggests already that they might have been affected by a shallowing process (Tauxe and Kent, 2004). To verify this hypothesis a detailed rock magnetic analysis and tests for inclination shallowing will be presented in the next chapters.

Only samples from sites DUN3 and 4 lost all their magnetization at

Table 3.3: Palaeomagnetic site mean directions and overall mean directions of the haematite component (HTC2) of DUN.

Site	N	*In situ*				Bedding-corrected			
		$D(°)$	$I(°)$	k	α_{95} (°)	$D(°)$	$I(°)$	k	α_{95} (°)
Dungurme section - DUN, HTC2 (uncorrected)									
DUN-1	6/8	100.5	-62.0	87.4	7.2	129.1	-29.2	87.4	7.2
DUN-2	3/6	59.1	-50.1	720.1	4.6	131.2	-41.4	718.9	4.6
DUN-5	16/16	353.8	-62.3	64.6	4.3	139.5	-38.3	63.6	4.4
DUN-6	6/9	7.1	-69.8	57.0	8.9	138.8	-29.1	57.1	8.9
DUN-7	6/6	14.3	-68.1	58.6	8.8	135.4	-28.5	58.6	8.8
DUN-8	9/9	7.1	-64.7	53.6	7.1	135.0	-33.0	53.6	7.1
DUN-9	13/13	6.1	-72.0	69.2	5.0	141.2	-29.8	66.8	5.1
DUN-10	3/5	359.2	-67.8	46.7	18.2	127.7	-39.3	46.7	18.2
DUN-11	12/12	345.9	-58.0	44.1	6.6	141.0	-52.9	40.8	6.9
DUN-12	19/19	321.8	-64.7	44.4	6.6	149.2	-43.2	36.9	10.1
DUN-13	8/8	344.5	-69.8	88.9	5.9	153.9	-34.0	88.9	5.9
DUN-14	7/7	4.4	-70.0	31.9	14.3	146.4	-31.5	31.9	8.7
DUN-15	7/7	2.8	-68.9	108.0	5.4	146.3	-32.7	108.0	5.4
DUN-16	4/7	25.8	-70.4	14.1	25.4	140.7	-26.2	14.1	25.4
MEAN	14	10.6	-69.3	29.6	7.4	139.6	-35.1	71.6	4.7

Site, sampling sites; h, height of sampled outcrop, where appropriate; N, number of samples (sites) used for calculating site (area) mean directions/number of measured samples. Declination (D) and Inclination (I) in degrees, Fisher precision parameter k (Fisher, 1953), Fisher radius (α_{95}) of 95per cent confidence in geographic (*in situ*) and bedding corrected (TC) coordinates, respectively.

$\sim 600°$C (Fig. 3.3b). Consequently these sites only show up in calculation of site mean directions of HTC1 (Tables 5.5 and 3.3).

To get further demagnetization information about the two HTCs 14 samples from section DUN and four samples from section KEL were stepwise AF demagnetized (Fig. 3.3e–i). For samples from KEL and from the lower part

of DUN AF demagnetization was not successful in isolating stable components of magnetization (Fig. 3.3e and i). The greyish conglomerates (DUN3), on the other hand, lost more or less all of their initial intensity of NRM during AF demagnetization (Fig. 3.3f). Representative samples from the upper part of this area show, after removal of the viscous overprint, one component, which does not point directly towards the origin of the projection plane. Averaging mean directions of 10 samples from section DUN yields an AF mean direction of $D = 6.7°$, $I = -59.4°$, $k = 20.6$ and $\alpha_{95} = 10.9°$ before and $D = 153.4°$, $I = -51.4°$, $k = 45.5$ and $\alpha_{95} = 7.2°$ after tilt correction (Fig. 3.4d, Table 5.5) . Since the mean direction after tilt correction is identical within error limits with the HTC1 overall mean direction, AF demagnetization up to 200mT clearly isolates the first HTC1.

3.5.2 Rockmagnetic Results

Thermomagnetic Curves

The thermomagnetic curves are generally difficult to interpret due to the small amount of material and the resulting weak magnetic signal. Most of the studied samples show noisy decay of intensity until all magnetization is lost at $\sim$ 660°C, which corresponds to the unblocking temperature of haematite. Only some samples show distinct curvatures within the decay paths. Samples from KEL show a first decay of intensity at $\sim$ 150°C, before a component with an unblocking temperature of $\sim$ 650°C is identified (Fig. 3.5a). Sample DUN1-4 (Fig. 3.5a) shows a distinct curved decay, which would intersect with the $y = 0$ axis at $\sim$ 580°C. However, also this sample completely unblocks only at $\sim$ 660°C. In sample DUN5-2 (Fig. 3.5a) the proportion of these two phases (580 and 660°C) is rather equal but they are both still recognizable. The more the high-temperature phase dominates the unblocking temperature spectrum, the weaker the signal from the intermediate phase (at $\sim$ 580°C) becomes.

Demagnetization of Three Axis IRM

AF and thermal demagnetization of composite orthogonal three-axes IRMs yield the following results. Samples from KEL show a slightly increased decay of intensity at $\sim$ 500°C and then a drop to zero of all components at $\sim$ 680°C during thermal treatment. AF demagnetization removes the small amount of the 0.12T IRM and some 20 per cent of the 0.4T IRM. The 2.5T IRM has about double the intensity of the sum of the two other

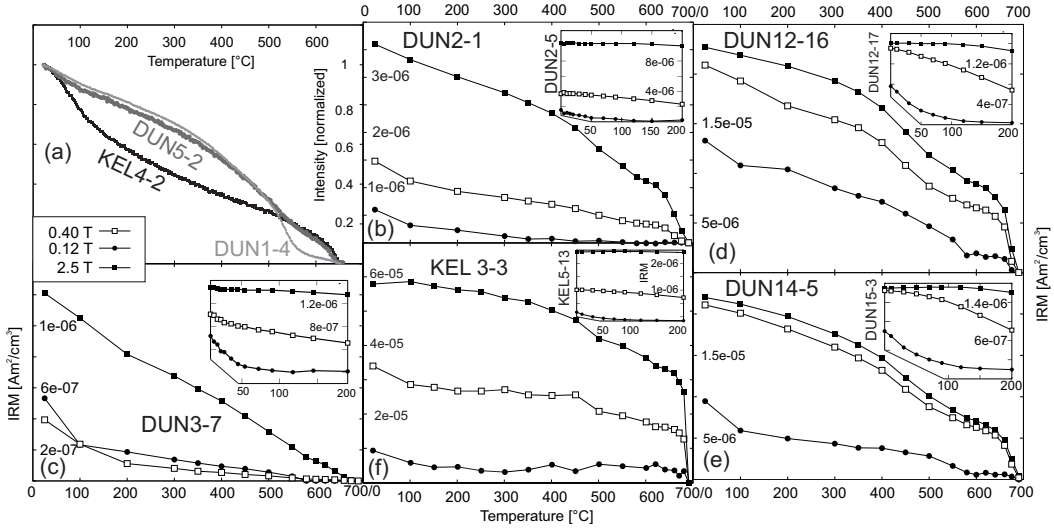

Figure 3.5: Rock-magnetic results from representative samples from both sections. (a) Thermomagnetic heating runs up to $\sim$ 680°C with a dc field of $\sim$ 370mT with normalized intensity of two samples from section DUN and one sample from KEL. (b-e) show results of thermal (large) and alternating field (small) demagnetization of three orthogonal imparted IRMs, using fields of 0.12 (circles), 0.40 (open squares) and 2.5 T (filled squares), respectively. Temperature is given in °C and alternating field (small insets) is given in mT.

fractions.

The matrix dominated, reddish conglomerates of DUN2 show comparable behaviour during thermal and AF treatment as samples from KEL (Fig. 3.5b and f). The more greyish conglomerates (DUN3) are characterized by a more linear decay of the 2.5T IRM up to 680°C, and a drop to zero of the 0.12T IRM before 600°C (Fig. 3.5c). AF demagnetization of a sister sample reveals a drop of the 0.4T IRM of about 50 per cent (Fig. 3.5c). Samples from the upper part (DUN5-16) show similar demagnetization results of the composite IRMs. Thermal demagnetization reveals a first curvature of all three IRMs, which would intersect with the x axis at $\sim$ 580°C. The 0.12T IRM component loses most of its intensity before 600°C (Fig. 3.5d and e). The remaining magnetizations drop to zero in a narrow interval at $\sim$ 680°C. AF demagnetization of these samples show a drop of the medium field component (0.4T) of more than 50 per cent (Fig. 3.5 d and e).

Somewhat unexpectedly, all IRM fractions of samples DUN12-16 and KEL3-3 (Fig. 3.5d and f) are persistent up to $\sim 680°C$. We speculate that these are carried by haematite in varying grain-sizes.

IRM Acquisition Curves

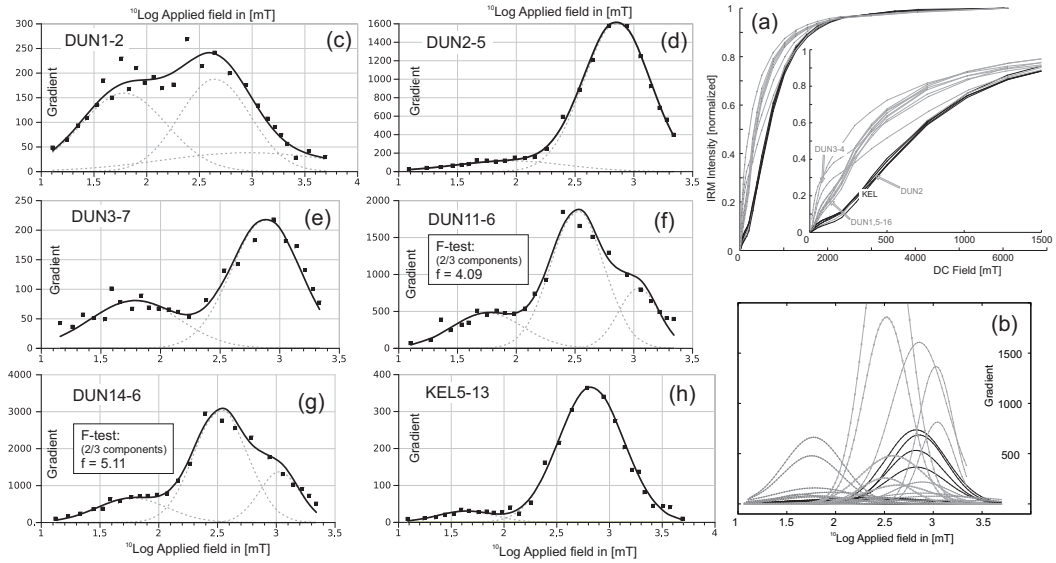

Figure 3.6: IRM acquisition modelling (Kruiver *et al.*, 2001) of representative samples of the DUN and KEL sections. (a) The raw IRM acquisition data and a zoomed interval from 0 to 1500 mT. Grey (black) curves represent samples from DUN (KEL). (b) All results from the fitted components of the first derivative plot (or gradient plot). (c-h) Individual gradient plots of samples from DUN and KEL. (f and g) F-test was performed to compare the quality of the fit using three components with respect to two. Both samples passed the test on a 99 per cent confidence level (Kruiver *et al.*, 2001), which indicates, that three components significantly improved the fit.

The first derivative of the IRM acquisition curve was modelled using the approach of Kruiver *et al.* (2001). Most of the representative samples, from section KEL and from the whole lower part of DUN (DUN1-4) can be modelled adequately using two components (Fig. 4.3c-e and h). The proportion of the two components, which are a low field component with peaks at $50-100$mT and a high field component with peaks at $600-800$mT,

however, changes from 40/60 (DUN1), to 30/70 (DUN3) and 10/90 (DUN2 and KEL). Modelling of IRM acquisition curves of samples from the upper part of DUN can be significantly improved using three components instead of two (Fig. 4.3g and h), including two high field components with peaks at about $300 - 400$mT and above 1000mT. Taken together the modelling results of all measured samples in one gradient plot (Fig. 4.3b) highlights the occurrence and varying proportion of the low and high field components.

Rockmagnetic Implications

Summarizing, we identify two or three magnetic components in the sampled material. Based on the thermal demagnetization of composite IRMs and the thermomagnetic curves (Fig. 3.5) we correlate two of these components with HTC1 and HTC2, which unblock at ~ 580 and ~ 680°C, respectively. Since HTC1 was also identified during AF demagnetization, we interpret this component to be carried by magnetite. The fact that both NRM and composite IRM finally can be reduced in intensity within a very narrow interval during thermal demagnetization, suggests that the HTC2 can be explained by the presence of haematite, likely specularite (Stamatakos and Kodama, 1991), as will be discussed in more detail further. Though it might not be contributing much to the remanence, pigmentary haematite is certainly also present, being responsible for the red colour of the rocks. The additional third very high field component, which is only occasionally visible, might be carried by goethite, corroborated by the slight drop in intensity at ~ 100°C (Fig. 3.5a). Another possibility might be, however, that this component can be correlated with the signal of the pigmentary haematite, which can have a similar unblocking temperature as the specularite but higher coercivities (Dunlop, 1972).

It is also important to note, that even in samples where the NRM loses all the intensity after heating to ~ 600°C there is still a significant amount of haematite present (Figs. 3.3b and 4.3f). On the contrary, samples which are dominated by the haematite fraction still contain a small amount of magnetite (Fig. 4.3e and i).

Magnetic Fabrics

AMS studies for both sections reveal bedding parallel fabrics in tectonic-corrected coordinates, with mostly subvertical minimum principal axes and subhorizontal maximum and intermediate axes (Fig. 3.7a–d), supporting a primary sedimentary fabric. On a Flinn diagram [L versus F, Flinn (1962)],

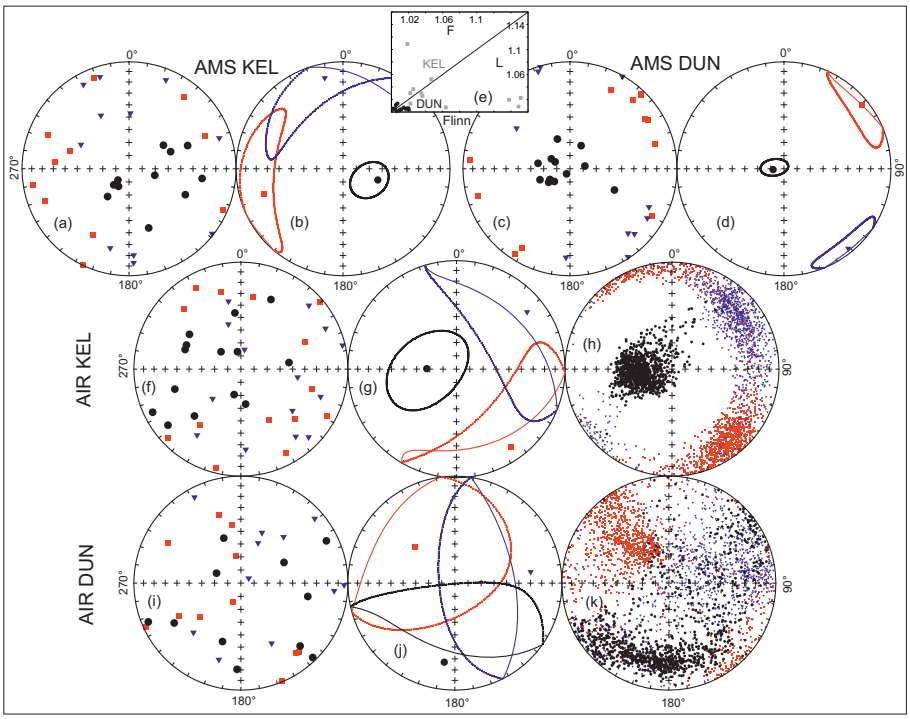

Figure 3.7: Low and high field anisotropy of susceptibility (a–d) and IRMs (f–k), respectively (black circles: minimum axes, blue triangles: intermediate axes, red squares: maximum axes). (a and b), (c and d): Results of anisotropy of susceptibility (AMS) measurements and respective hext error ellipses for sections KEL and DUN. (e) Flinn diagram for all AMS data from both areas (black circles – DUN, grey squares – KEL. (f, g and h) and (i, j and k): Results of anisotropy of isothermal magnetizations (AIR), with respective hext error ellipses (g and j) and bootstrap eigenvectors (h and k). Plots are made using software *PmagPy2.16* from Lisa Tauxe.

samples from the DUN section plot close to the origin and in both the prolate and oblate fields of the diagram, indicating a triaxial fabric with small anisotropy. Samples from KEL, on the contrary, have larger anisotropies but also plot in both the prolate and oblate fields of the diagram, though are predominantly oblate (Fig. 3.7e).

Unlike for AMS, the magnetic fabrics measured using the SIRM technique yield different results for the two studied sections (Fig.3.7f–k).

The fabric for DUN does not show a distinct clustering of principal axes,

suggesting an un-oriented isotropic fabric (Fig.3.7i–k). On the contrary, the fabric of KEL, although with some scatter, shows a preferential clustering of principal axes, which is enhanced by the parametric bootstrap (Fig.3.7h): the minimum axes plunge steeply to the W, whereas the maximum and intermediate axes are distributed in a subhorizontal plane (Fig.3.7f–g), suggesting a sedimentary origin. Because the ChRM for this section is carried by haematite, a sedimentary fabric supports the notion that the remanence for these sediments is carried by detrital haematite.

Conversely, the lack of a distinct fabric of the AIR for DUN would rule out detrital haematite. Reminding the reader that the anisotropy technique utilized isolates the contribution of the haematite grains, by eliminating the contribution of both magnetite (via AF demagnetization) and goethite (via 125°C thermal demagnetization), we infer that the fabric measured for DUN is that of pigmentary haematite, for which a randomly oriented isotropic fabric is expected (Tauxe *et al.*, 1990). On the other hand, the AMS fabric of DUN is dominated by the magnetite signal, which shows a primary, sedimentary fabric.

These observations are consistent with the high-temperature ChRMs isolated for both KEL (in the haematite unblocking temperature range) and for DUN (in both the magnetite and haematite unblocking temperature range).

In the next section on inclination shallowing we show how the remanence carried by the haematite pigment in DUN must have been acquired soon after deposition and have been affected by some post-depositional compaction. As Heslop *et al.* (2014) demonstrate, very small degrees of alignment are sufficient to produce reliable palaeomagnetic directions: therefore it is not surprising that the haematite pigment in DUN possess a reliable CRM direction, though shallow, despite yielding an un-oriented magnetic fabric.

3.5.3 Inclination Shallowing

Palaeomagnetic results from Central Asian red beds have been suspected for a long time to be affected by inclination shallowing and not be reliable recorders of the earth magnetic field (e.g., Gilder *et al.*, 2001; Tauxe and Kent, 2004). More and more authors relate this inclination bias to compaction or depositionally caused shallowing of detrital haematite (Gilder *et al.*, 2001; Dupont-Nivet *et al.*, 2002; Gilder *et al.*, 2003; Tan *et al.*, 2003). This process was identified also in laboratory redeposition experiments (e.g., Tauxe and Kent, 1984). Tauxe and Kent (2004) proposed a method to iden-

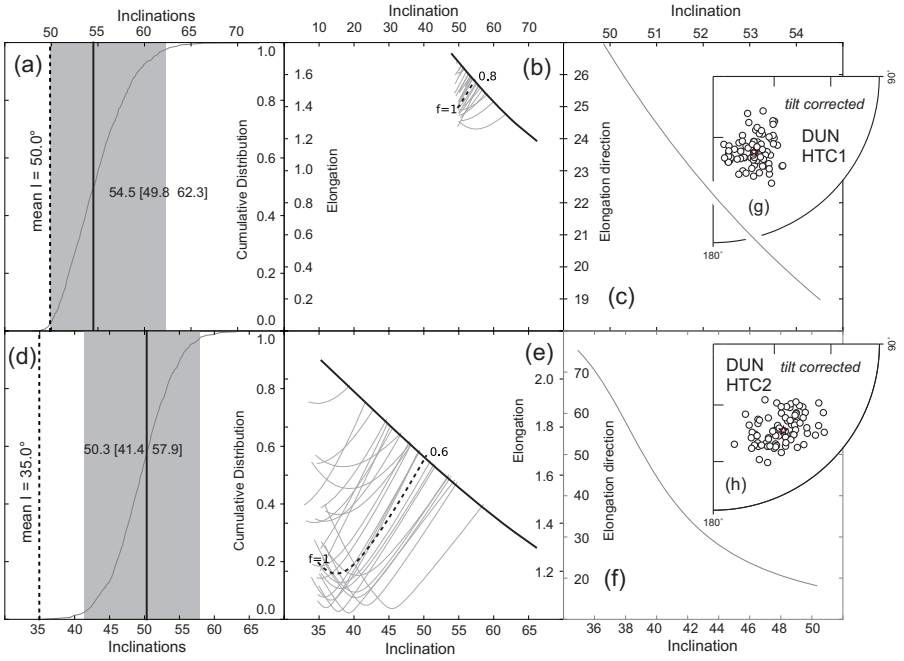

Figure 3.8: Elongation/inclination method of Tauxe and Kent (2004), for correcting inclination shallowing for the HTC1 (a–c) and the HTC2 (d–f) of section DUN. (b and e) Plots of elongation versus inclination for the data (red line) and for the TK03.GAD model (green line). Additionally, results from 20 bootstrapped datasets (beige lines). The intersection represents the inclination/elongation pair, which is most consistent with the TK03.GAD model. (c and f) Cumulative distribution of crossing points from 5000 bootstrapped datasets. (g and h) Mean directions prior to correction. (Method was performed using *PmagPy2.16* from Lisa Tauxe)

tify the flattening factor *f*, to reconstruct the original inclination based on the variation of elongation of the distribution of palaeomagnetic directions E/I-method).

The method utilizes the expected distribution of recorded magnetic directions during secular variation. Therefore, each direction should represent a spot reading of the actual geomagnetic field. This justifies the usage of directions obtained from individual sedimentary rock samples. On the other hand, the data set used should be large enough to have a sufficient number of recordings of secular variation (Tauxe and Kent, 2004). In order to

fulfil these requirements we combined all individual sample data from the large continuous section (DUN5-12) with the remaining sites (DUN1-4 and 13-16).

Applying the method on 115 samples from both components (HTC1 and HTC2) of section DUN yields the following: The HTC1 results in a mean absolute inclination of 50.0° (for simplification only positive or absolute inclination values are given in this chapter) prior to correction and 54.5° after correction (Fig.3.8). The error interval is $49.7 - 62.5°$, which includes the mean inclination prior to correction. This result suggests that, if at all, only minor shallowing affected this component. The HTC2 has a mean absolute inclination of 35.0° prior and 50.3° after correction (Fig.3.8). The error interval is $41.4° - 57.9°$. Flattening factors are 0.8 and 0.6 for the HTC1 and HTC2, respectively.

The corrected absolute inclination of HTC2 of 50.3° is identical within error limits to the mean absolute inclination of the HTC1 of all samples (50.3°). This might be explained by a process of compaction-induced inclination shallowing, which mainly affected the pigmentary haematite grains leaving the magnetite grains mostly untouched. The fact that the corrected directions carried by the haematite pigment closely resemble that carried by the magnetite grains strongly suggests that the pigment carries a chemical remanence, which was acquired shortly after deposition. The platy nature of the haematite grains, makes these more susceptible to post-depositional compaction than the more spherical magnetite grains. The low degree of anisotropy of susceptibility at DUN (Fig.3.7e), where the AMS is probably dominated by magnetite, strengthens this conclusion. Section KEL also shows an elongation of directions of the HTC within the horizontal plane (Fig.3.4h), however, there are not enough demagnetization directions available to perform the E/I-correction method. To investigate the supposed inclination bias in samples from section KEL, haematite remanence inclinations were corrected using the anisotropy-based correction of Tan *et al.* (2003, Fig.3.7), using anisotropies of high-field IRMs (hf-AIR method, Tauxe *et al.*, 2008; Bilardello and Kodama, 2009). The AIR measurement technique, which was also successfully used by Bilardello and Jackson (2014) in a comparative study of different anisotropy techniques, was applied to samples from both sections. Only results from section KEL yield a distinct clustering of principal anisotropy axes, as expected for sedimentary fabrics (Fig.3.7f–k).

The average experimental difference between the theoretically identical off-diagonal terms is 5.6per cent of the average IRM (Mirm/3), however it

is < 5per cent for 7/14 calculated ellipsoids and < 10per cent for 12/14. These results give confidence in the validity of the technique for measuring haematite anisotropy when using high-field IRMs. Only the anisotropies with off-diagonal difference < 10per cent of the average IRM were used for the inclination corrections.

The average anisotropy measured for section KEL was used, together with an average haematite particle anisotropy value of 1.38 (e.g., Bilardello and Kodama, 2010; Bilardello *et al.*, 2011).

Inclination corrections were performed on the site level, after correction, the ChRM absolute inclination of section KEL steepens from $\sim 36.4^{\circ}$ to 75.2°, corresponding to a flattening factor of 0.2.

This is a large inclination correction that exceeds by $\sim 25^{\circ}$ the corrected absolute inclination obtained for section DUN using the E/I technique of Tauxe and Kent (2004) and is not within the uncertainty of the E/I correction of DUN (low and high inclinations of 41.4 and 62.3, respectively).

3.6 Discussion

3.6.1 Reliability of the correction methods

Bilardello *et al.* (2011) have shown how the E/I technique underestimates the corrected inclination when using too few directional data ($\leq$ 100 samples). For section DUN, more than 100 samples were used, lending some confidence in the E/I correction. Another argument in favour of the robustness of the E/I technique is the agreement of the HTC1 direction including results obtained with AF demagnetization with the corrected HTC2 direction of section DUN. On the other hand, the anisotropy measurement technique employed here, indistinctly measures the contributions from both detrital and pigmentary haematite. If the detrital grains only are responsible for the ChRM, as proposed for section KEL, then the measured anisotropy may be inaccurately correcting the inclination bias. The lack of a sedimentary haematite fabric for DUN (Fig.3.7i–k) rules out the possibility of making a true comparison between the two techniques. We treat these results as a positive detection of inclination shallowing at both sites. We note, however, that both correction techniques might carry uncertainties, deriving from a small sample number on one hand and/or inaccuracies in measuring the fabric of the characteristic remanence carrying haematite grains on the other.

To get further confidence in the correct application of the E/I method, we

obtained values for palaeosecular variation (PSV) of the HTC2 component. We used VGPs based on the individual DUN sites (Table 3.3) to obtain a within-site corrected VGP scatter (Biggin *et al.*, 2008). This procedure results in a S_B value of 12.2° for the 14 sites of the HTC2. Investigating new PSV compilations of the Cretaceous Normal Superchron (CNS) and the Jurassic (Biggin *et al.*, 2008) shows that our value is comparable with the CNS and low but still within the observed range of the Jurassic for similar palaeoaltitudes ($\sim$ 30°N). PSV data from within the Permo-Carboniferous reversed superchron (PCRS) from low palaeolatitudes yield somewhat lower S_B values (Haldan *et al.*, 2009), which might be related to either the lower palaeolatitudes of their study or the occurrence of this study during the superchron. After all, this result contradicts a very low sedimentation rate, which would doubt the application of the E/I method, because in this case a very low PSV value would be expected. Also severe tectonic activity recorded in the palaeoamgnetic data is unlikely, because this would result in a increased PSV value. Any further implications using our PSV value is, however, difficult due to the sparse PSV data available for the Palaeozoic.

3.6.2 Palaeo- and rock-magnetic Results

Based on the rock-magnetic results we conclude that most probably the HTCs are carried by magnetite and haematite. Haematite is more abundant in samples from section KEL and appears to be detrital. In contrast, we relate the haematite phase HTC2 of DUN to secondary pigmentary haematite, which was acquired shortly after deposition. The haematite component holds a shallower inclination, which can be explained by compaction-induced shallowing of the platy haematite grains, whereas the more spherical magnetite grains are less prone to shallowing. This conclusion is supported by the consistency of the HTC2 inclination corrected using the elongation-inclination (E/I) method (Tauxe and Kent, 2004), and the inclination of the HTC1, in stratigraphic coordinates. Due to this conclusion we regard the uncorrected HTC1 as the primary magnetization direction of this section (DUN) and use it for the further palaeogeographic analysis.

Inspection of the maximal clustering of site mean directions versus unfolding percentage from both sections lead to a positive fold test (Enkin, 2003), which indicates an acquisition age of the primary magnetization prior to the folding process (Fig.3.4c and g).

3.6.3 Palaeoposition

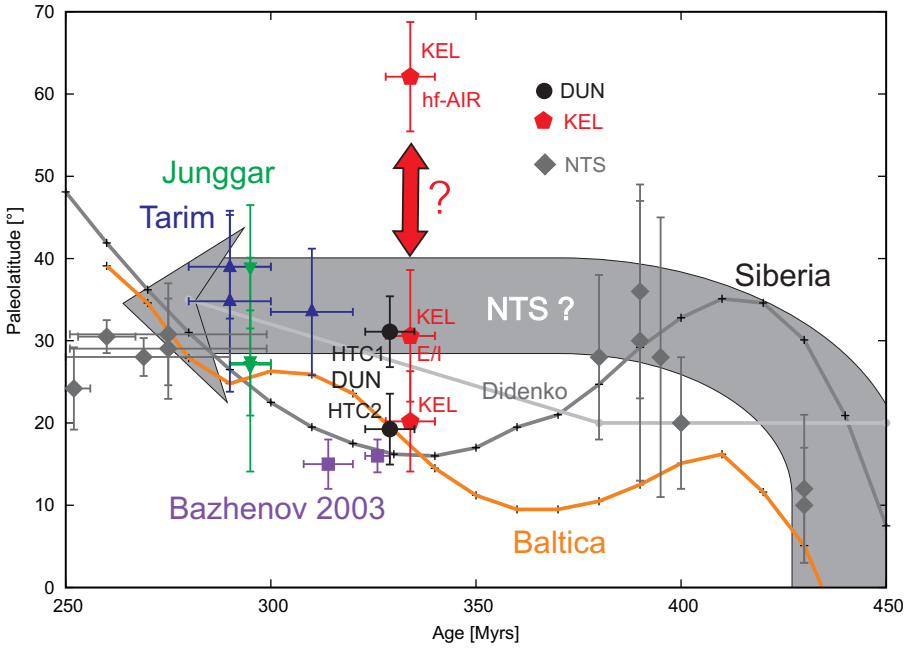

Figure 3.9: Palaeolatitude diagram, showing data from the literature together with the palaeolatitude curves from Siberia and Baltica (Cocks and Torsvik, 2007; Torsvik *et al.*, 2012) for a reference site within the NTS mountains. Black circles indicate palaeolatitude value for both high-temperature components of DUN (HTC1 and 2). Red pentagons indicate values for KEL (uncorrected), inclination corrected by elongation-inclination (E/I) with a flattening value of 0.6 and by the hf-AIR method. Grey diamonds represent published data for the North Tianshan zone (Bazhenov *et al.*, 1999; Abrajevitch *et al.*, 2007) for Silurian and Devonian plus Permian rocks. Purple squares show most recent study from the NTS (Bazhenov *et al.*, 2003). Blue and green triangles show palaeolatitudes based on palaeopoles from Tarim (upright) and Junggar (turned, Wang *et al.*, 2007). Light grey line indicates suggested palaeolatitude of palinspastic reconstruction by Didenko *et al.* (1994). Red arrow highlights the ambiguity of the correction results of KEL.

Application of two different techniques to correct inclination shallowing in red sediments yields inclination values for two early Carboniferous sites in

Kyrgyzstan of $-50.3°$ and $-75.2°$ with error limits of approximately $\pm 10°$ and $\pm 4°$, respectively. These inclinations translate to palaeolatitudes of 31.1°N (error range of $23.7° - 40.1°$) and 62.1°N (error range of $55.8° - 69.1°$ (Fig.3.9). These results imply a north–south directed convergence of the two basins between the early Carboniferous and the final amalgamation of the whole area in the late Carboniferous to Permian of about 30° (more than 3000km). It seems very unlikely, that these two areas, even though they represent two separate geologic basins (Fig.3.1) with slightly different but overlapping age ranges (Fig.3.2), were deposited with such a large latitudinal difference. Especially taken the most recent palaeogeographic reconstructions of this area into account (Didenko *et al.*, 1994; Şengör and Natal'in, 1996; Filippova *et al.*, 2001; Windley *et al.*, 2007; Xiao *et al.*, 2010) the amount of 30° seem unlikely. Partly the difference in palaeolatitudes might represent north-south convergence accompanying the subduction of the Turkestan ocean. The exact amount of subducted oceanic crust is still a matter of debate but might be as large as 2500 km (Samygin and Burtman, 2009) for the whole Turkestan ocean. If the Kazakh basin, however, is part of the Junggar-Balkhash ocean a latitudinal difference of up to $\sim 10°$ might be reasonable. We might speculate that the remnants of the inferred dry land of Devonian age (Mikolaichuk and Djenchuraeva, 2000; Bakirov and Mikolaichuk, 2009, Fig.3.1) represent a much larger continental piece than previously proposed.

Assuming a similar flattening history (f value of ~ 0.6) at KEL compared to DUN, however, would imply a palaeolatitude of KEL at $\sim 30.6°$N (error range $39.4° - 23.4°$). This would reduce the subducted area between the two basins below the distance detectable by palaeomagnetism.

It seems evident now that the NTS zone moved from the southern hemisphere towards a position at $\sim 30°$N between the Ordovician and the Devonian (Bazhenov *et al.*, 2003; Alexyutin *et al.*, 2005; Bazhenov *et al.*, 2012). After that Bazhenov *et al.* (2003) suggested an evolution attached to the East European craton (Baltica). Our results contradict these conclusions and favour a stable position of the NTS zone at $\sim 30°$N between Devonian and Carboniferous times (Fig.3.9). During this interval we propose some north-south directed compression accretion accompanying the closure of the Turkestan palaeoocean basins (Fig.3.1).

3.6.4 Age of Magnetization

For the NTS province, we show that reported data, which indicate low palaeolatitudes (Bazhenov *et al.*, 2003), are probably biased by inclination shallowing.

Compaction induced inclination flattening, which has been identified in both of our data sets, is the most important argument for a formation age of the magnetic signal during or close after deposition. Because most of the visible folding took place probably after the Jurassic, the positive fold tests only indicate a magnetization age between deposition and Jurassic times. The post-Jurassic folding is indicated by a very minor angular unconformity between the Carboniferous and Jurassic sequences in the whole NTS zone (e.g. Bachmanov *et al.*, 2008). Since most reported remagnetization events in this area took place in the Late Palaeozoic (e.g. Kirscher *et al.*, 2013) a positive fold test does not prove non-remagnetized results.

3.7 Conclusions

Early Carboniferous sedimentary rocks from the Sonkul (DUN) and the Kazakh (KEL) basins, NTS mountains, were investigated palaeomagnetically. Representative samples were subjected to rock-magnetic analyses to determine the carriers of the magnetic remanence. Thermomagnetic runs, thermal and AF demagnetization of composite three axes IRMs and modelling of IRM acquisition curves indicate the presence of magnetite and haematite in varying proportions in all samples. Thermal demagnetization experiments were applied to samples from both areas.

At section DUN thermal demagnetization allowed to separate a LTC, which is broadly aligned with the present day field in *in situ* coordinates, as well as two HTCs, up to ~ 600°C (HTC1) and up to ~ 680°C (HTC2), respectively. The sufficiently large number of samples at DUN allows to test for inclination shallowing using the Tauxe and Kent (2004, E/I) method. The results show that the HTC2, carried by haematite, has suffered approximately 15° of shallowing, yielding a flattening factor of 0.6. In contrast, flattening of the HTC1 was less than 5°. The fact that the corrected direction of the HTC2 and the noncorrected direction of the HTC1 are identical suggests that the HTC1 ($T_B = 580$°C), which was also successfully identified by AF demagnetization, is carried by magnetite and can be interpreted to be of primary origin. Combining site mean directions of 16 sites of the uncorrected HTC1 results in a mean direction of $D = 344.8°$, $I = -60.9°$,

$k = 26.3$ and $\alpha_{95} = 7.3°$ before and $D = 149.3°$, $I = -50.3°$, $k = 73.6$ and $\alpha_{95} = 4.3°$ after tilt correction. The increase of k of 47.3 indicates a prefolding age of this component.

At section KEL, six sites yield a LTC, which is also broadly aligned with the present day field before bedding correction, and a HTC, which points up and south. Combining site mean directions results in a mean direction of $D = 169.5°$, $I = 18.5°$, $k = 28.3$ and $\alpha_{95} = 12.8°$ before, and $D = 176.2°$, $I = -36.4°$, $k = 57.4$ and $\alpha_{95} = 8.9°$ after tilt correction. The increase of the precision parameter k by 29.1 suggest a prefolding, albeit Jurassic, age of this magnetic component.

For KEL not enough samples were available for the E/I correction and inclinations were corrected with an anisotropy-based technique (Tan *et al.*, 2003) yielding a corrected inclination of $75.2° \pm 4°$. Since the degree of AIR in samples from DUN is extremely low and lacks a sedimentary fabric the AIR correction technique could not be applied. Therefore, a comparison between the two methods is not possible. At section KEL, application of the AIR method indicates that massive shallowing affected these rocks with a flattening factor f of 0.2. Compared to most available studies on haematite bearing rocks (Kodama, 2012) our f value seems rather low and we suspect some unresolved uncertainties still present in our results.

Another argument why the corrected inclination of KEL seems too high

Table 3.4: Resulting regional mean directions together with results corrected for inclination bias.

Site	Corr.meth.	D (°)	I(°)	k	α_{95} (°)	Lat (°N)	Lon (°E)	dp	dm	λ(°)
KEL	None	176.2	–36.4	57.4	8.9	–67.5	84.5	10.4	6.0	20.2
KEL	E/I	176.2	–49.8	57.4	8.9	–77.7	90.7	7.9	11.9	30.6
KEL	hf_AIR	176.2	–75.2	–	4.0	–70.2	249.8	7.3	6.7	62.1
DUN	None (HTC1)	149.3	–50.3	73.6	4.3	–63.3	150.8	5.8	3.9	31.1

Site, area; Corr.meth., correction method for inclination bias; E/I, Elongation-Inclination method (Tauxe and Kent, 2004); AIRM, anisotropy based method of Tan *et al.* (2003); mean tilt corrected direction with declination (D), inclination (I), precision parameters k and α_{95}. Resulting palaeopole with latitude (Lat) and longitude (Lon) and error ellipse dp and dm, λ: palaeolatitude for study area.

is based on palaeogeographic arguments. Transferring the HTC1 inclination of DUN (unaffected by inclination shallowing), the HTC2 inclination of DUN (corrected with a f value of 0.6, E/I method) and the inclination of KEL (corrected with a f value of 0.2, AIR method) would imply a latitudinal difference between the two basins of $\sim 30°$, which is equivalent to roughly 3000km. Even though the two basins might have been separated in the early Carboniferous by several hundreds of kilometres (Mikolaichuk and

Djenchuraeva, 2000), there is no geologic evidence for subduction of any large scale (e.g., Filippova *et al.*, 2001; Bakirov and Mikolaichuk, 2009; Samygin and Burtman, 2009). The larger amount of samples and the identification of two components, which coincide after inclination shallowing correction, gives strong confidence in the position of DUN at $\sim 30°$N. There is some space for north-south convergence (within the error margins) but a palaeoposition of KEL further north than $\sim 40°$N seems to be highly unlikely.

The detection of inclination shallowing in rocks from both sections further constrain the age of acquisition of the magnetic remanence to during or shortly after the deposition time.

The resulting palaeopoles (Table 4.3) show rotational deviation compared to the APWP of Baltica and Siberia (Cocks and Torsvik, 2007; Torsvik *et al.*, 2012) of up to $\sim 100°$ (DUN) and $\sim 70°$ (KEL, corrected by $f = 0.6$), respectively. These values are within range of earlier published results from the same area and are consistent with complex deformation pattern accompanying the collision of Baltica, Siberia and Tarim (Natal'in and Şengör, 2005; Van der Voo *et al.*, 2006; Kirscher *et al.*, 2013).

Acknowledgements

We thank the editor Sylvia Hales, Roberto Molina Garza and especially Andrew Biggin for their critical and very constructive comments on the manuscript. Their remarks lead to a significant improvement of the paper. This study was funded by projects to Valerian Bachtadse from the German Funding Agency DFG, Ba1210/12-1 and Ba1210/12-3 and a visiting grant from the DAAD to Alexander Mikolaichuk. Assistance in the field by Matthias Hackl and Yvonne Koch is greatly appreciated.

4

Early to middle Paleozoic evolution and terrane accretion in Central Asia – Paleomagnetic confirmation for a collision event in the Ordovician

by ***U. Kirscher, V. Bachtadse, A. Mikolaichuk, and A. Kröner***
Submitted to Gondwana Research

Abstract

Triggered by the benchmark paper on the evolution of the Central Asian Orogenic Belt (CAOB) by Şengör *et al.* (1993), the geological evolution of Central Asia has again moved into the focus of the geoscientific community. Yet, the validity of recently published models for the paleogeographic evolution of the CAOB still remains to be tested. The main reason being that the paleogeographic information on microplates and terranes now assembled into the CAOB is still sparse and occasionally ambiguous for some time in-

tervals prior to amalgamation of Eurasia in the late Paleozoic.

Here we present new paleomagnetic data for well-dated volcanic and sedimentary rocks from seven sampling areas within the Kyrgyz North Tianshan zone (NTS), ranging from Cambrian to Ordovician in age. The areas are located on the Kyrgyz, Terskey Ala-too, Suusamyr-too and Kapka-Tash Ranges.

Rock magnetic analysis indicates that a high unblocking temperature component (HTC) of the NRM is associated with magnetite and/or haematite, whereas magnetizations with low (LT) and intermediate (IT) blocking temperatures are carried by goethite and/or maghemite. The LT and IT components of magnetization are characterised by directions of the NRM that, in *in-situ* coordinates, are very close or identical to the direction of the present-day magnetic field in the area. These are consequently interpreted to reflect a secondary magnetic overprint. In cases where the blocking temperatures of LT and HT components overlap, the combined analysis of remagnetization circles with stable endpoint data was successful in identifying the magnetic direction of the HT component.

The HTC component, after bedding correction, is widely dispersed depending on the age of the rocks, and plots in a declination interval between 90° and 300° with various inclinations between −20° and +70°. The interpretation of being primary is based on a positive local fold and a positive reversal test at one area, respectively, in the Ala-too and Suusamyr-too areas as well as a regional fold test including data from three areas of the Suusamyr-too and Terskey Ala-too Ranges sampled. Additionally, *in-situ* data from all areas interpreted to hold a primary magnetic signal, do not coincide with the expected direction of magnetization of younger ages, especially during the late Paleozoic period. Data from two entire areas (Kyrgyz and Terskey Ala-too Ranges) clearly fail the fold test and are therefore interpreted to represent remagnetized signals during a deformation event.

Combining these results by assigning a reversed polarity with published paleolatitude data from Kyrgyzstan and Kazakhstan, a reasonably well-defined reconstruction for the evolution of the NTS zone can be established, significantly improving the paleogeographic position of the entire area. Based on the data presented here it seems most likely that an accretion event in the Ordovician at $\sim$ 460 Ma can be documented in the Tianshan. Subsequently, the amalgamated Kyrgyz- Kazakh terrane (also known as the Kazakhstan continent or Kazakhstania) moved northwards to $\sim$ 30°N between Ordovician and Devonian times. It then occupied a stationary latitudinal position and presumably experienced further accretion

until the early Carboniferous in agreement with geological evidence.

Apparently, Kazakhstania was not connected to Baltica or Siberia prior to amalgamation beginning in the late Carboniferous, because the two cratons show separate movements during the middle Paleozoic. Most likely Kazakhstania collided with Baltica and Siberia to form Eurasia not before the middle to late Carboniferous.

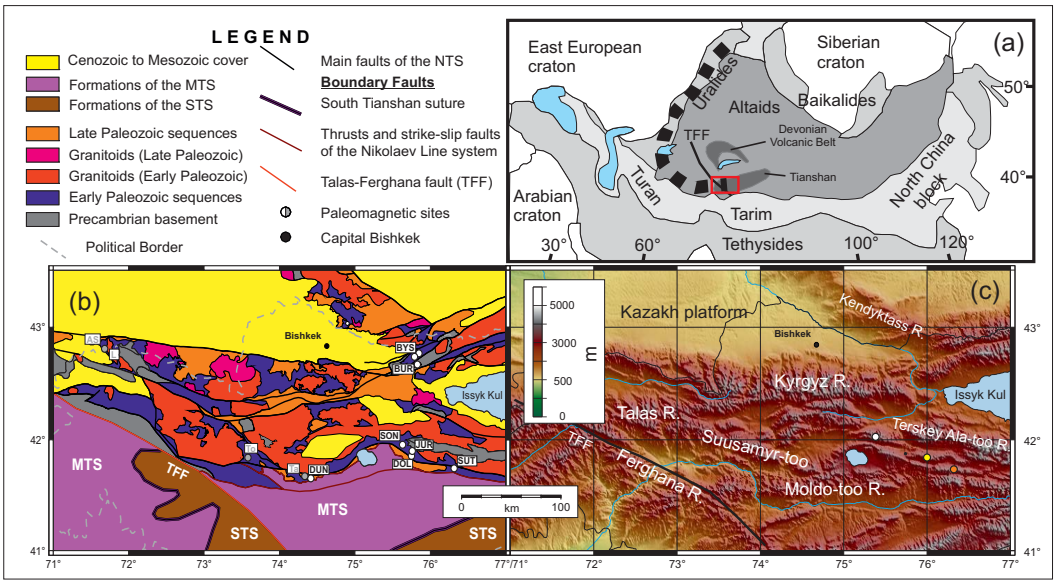

Figure 4.1: (a) Global map of Eurasia showing the CAOB in dark grey in the middle. Also indicated are the major cratons and blocks, the Uralide-Tianshan mountain belt, the Talas-Ferghana Fault (TFF), the Devonian volcanic belt of Kazakshtan, and the study region with a red rectangle. (b) Geological map of the study region. White dots indicate studied sections, grey dots mark sections studied by Bazhenov *et al.* (2003). North, Middle and South Tianshan (NTS, MTS, STS) are indicated. (c) Topographic map of the study region with major mountain ranges of the area [created using GMT of Wessel and Smith (1998) and topographic dataset ETOPO1 (Amante and Eakins, 2009)]. Dots mark the position of the Karakatty (white), Karadzhorgo (yellow) and Kapka-Tash (orange) Ranges.

4.1 Introduction

The Central Asian Orogenic Belt (CAOB, Yanshin, 1965) is one of the world's largest accretionary orogens. It was active during the Neoproterozoic and the entire Paleozoic until its growth ceased, and the newly formed continental crust finally became trapped between Siberia, Baltica and the Tarim and Turan microplates (Fig. 4.1). The region has attracted the interest of many geological studies, not only concerning paleogeographic reconstructions (e.g., Windley *et al.*, 2007, and references therein), but also attempting to decipher the mechanisms controlling the growth of continental crust in general (e.g. Kröner *et al.*, 2014). The interpretations and models published can generally be categorized into two groups and derivates. Şengör *et al.* (1993) proposed a giant arc model, where the individual arc components were subsequently welded together whereas several authors (e.g., Windley *et al.*, 2007, and references therein) suggested an archipelago type nucleus for the paleo-Asian domain, which is comparable to the plate tectonic situation in the present-day South West Pacific (e.g. Hall, 2009).

The southwestern segment of the CAOB, situated mostly in Russia, Kazakhstan and Kyrgyzstan, is characterized by markedly curved geologic structures (Şengör *et al.*, 1993). Lithostratigraphic terranes are arcs striking North-South along the Ural mountains and east-west along the Tianshan Mountains at the outer western and southern rims of the CAOB (see figure 6 in Windley *et al.*, 2007). This suggests a major orocline with the hinge situated under the Caspian basin. Geological evidence, such as collisional or oriented subduction features (e.g., Samygin and Burtman, 2009), seem to support the hypothesis that the Ural Mountains, the Karatau Range, and the Tianshan Mountains are structurally linked (Samygin and Burtman, 2009). Kirscher *et al.* (2013) presented paleomagnetic evidence from the Karatau Range suggesting that the area indeed became bent during late Paleozoic amalgamation. Going towards the center of the orogen, within the Tianshan Mountains, the geologic arrangement becomes more complex and the simple overall pattern cannot be reconstructed solely using paleomagnetic data (e.g., Van der Voo *et al.*, 2006).

It is now generally accepted that the Kyrgyz Range of the North Tianshan (NTS) and the Chingiz Range in Kazakhstan represent two branches of a horse-shoe shaped formerly straight volcanic arc that was bent during the amalgamation of Eurasia (e.g., Abrajevitch *et al.*, 2007; Levashova *et al.*, 2007; Abrajevitch *et al.*, 2008).

Prior to this rather well constrained late Paleozoic history, the paleo-

geographic evolution is less well defined. Paleomagnetic data only constrain the position of Baltica (Cocks and Torsvik, 2005) and Siberia (Cocks and Torsvik, 2007) after the break-up of Rodinia in the Neoproterozoic (Meert and Torsvik, 2003) and before the amalgamation of Eurasia, and to a lesser extent that of Tarim (Zhao *et al.*, 2014). It has been shown that all three plates traveled northwards and crossed the paleoequator between the Ordovician and the Silurian (Bazhenov *et al.*, 2003; Abrajevitch *et al.*, 2007; Levashova *et al.*, 2007). After that, Tarim was proposed to have occupied a stationary position at $\sim 15°$N until the late Carboniferous (Zhao *et al.*, 2014), when it moved farther northwards and collided with Kazakhstania, Siberia and Baltica. Concerning the NTS, Bazhenov *et al.* (2003) proposed a somewhat similar northward drift between Ordovician and Devonian times up to about 30°N (Abrajevitch *et al.*, 2007, and references therein) where it remained stationary until final amalgamation during the late Paleozoic (Kirscher *et al.*, 2014).

The origin of the Precambrian and early Paleozoic continental or oceanic fragments remains highly speculative. Paleontological evidence suggests an affinity of the NTS zone with the margin of Gondwana and especially Tarim (Popov *et al.*, 2007). The common presence of $\sim$ 1.1Ga Grenville-age basement rocks, that are also known from other Gondwana domains, also indicates rifting of these blocks off the northern margin of Gondwana (Kröner *et al.*, 2014). Geochemical results and zircon chronology indicate two subduction accretion events. Additional to the late Paleozoic amalgamation, there seems to have been an accretion event during the Ordovician (Konopelko *et al.*, 2012), representing the formation of Kazakhstania (Filippova *et al.*, 2001; Windley *et al.*, 2007).

The degrees of freedom in paleogeographic reconstructions reflect patchy information on a) the early Paleozoic drift history of individual terranes prior to amalgamation of the Kazakhstan microcontinent, b) motion of the Kazakhstan microcontinent during the middle and late Paleozoic and the mechanisms of its incorporation into Eurasia, and c) the overall kinematics of late Palaeozoic Kazakhstania and the relative role of rotations, bending, and wrenching prior to- and during the process of multiple collisions during the late Carboniferous and Permian.

To address this debate and further constrain the paleogeographical evolution of this area, we present new paleomagnetic data for Cambrian to Ordovician rocks from the Kyrgz NTS zone.

Table 4.1: Position, age and number of samples of studied sections.

Site	Lat. [°N]	Long. [°E]	Age	Formation	#
Ordovician					
BUR	42.6823	75.8291	M.Ord.	Oktorkoy	26/4
BYS-1-4	42.7190	75.6881	L.Ord	Borybay	34/4
BYS-5-8	42.7295	75.7077	L.Ord.	Cholok	29/4
DOL-A	41.8806	75.7360	Darriwilian	Kumoinok	28/4
DOL-B	41.8887	75.7404	Darriwilian- Sandbian	Unkurtash	22/3
DOL-C	41.8625	75.7280	Darriwilian- Sandbian	Unkurtash	46/5
DUN	41.6585	74.3414	Sandbian	Tertmasu	30/5
Ordovican-Cambrian					
JUR	41.8866	75.7589	L.Cambr.-E.Ord.	Karadjorgo	42/6
SON	41.9440	75.6790	Cambrian	Karakatty	36/5
SUT-1-10	41.7769	76.3015	E.Cambr.	Bel'tepshy	85/10
SUT-11-13	41.7769	76.3015	E.Cambr.	Sultansary	30/3

Site: sampling site. Lat. and Long.: coordinates in ° north (N) and east (E). Age: proposed age of sedimentation. E./M./L.Ord.: Early/Middle/Late Ordovician, E./L.Cambr.: early/late Cambrian. Formation: formation name, # Total number of obtained samples/sites.

4.2 Regional Geology and sampling

The Kyrgyz part of the Tianshan mountain belt can be subdivided into the Southern Tianshan (STS), the Middle Tianshan (MTS) and the Northern Tianshan (NTS, Fig. 4.1). In the NTS the basement consists of Precambrian microcontinental fragments and early Paleozoic oceanic and island arc complexes (Kröner *et al.*, 2012, 2013, and references therein). The entire assemblage is pierced by S-type stitching granites marking the consolidation of Kazakhstan in Late Ordovician to Silurian times (Bakirov and Mikolaichuk, 2009; Biske and Seltmann, 2010). Whereas Silurian sediments are practically unknown in this region, probably caused by uplift during this time, Late Devonian and early Carboniferous imposed basin fillings overlay the early Paleozoic formations with a regional angular unconformity. In the late Carboniferous Kazakhstania collided with Baltica (Puchkov, 1997, 2000). Subsequently, the area underwent several phases of oblique intracontinental deformation, including folding and faulting until the early Mesozoic (Bazhenov *et al.*, 1999; Alexeiev *et al.*, 2009).

Within the territory of Kyrgyzstan eleven locations in four regions, namely the Kapka-Tash, Terskey Ala-too, Kyrgyz and Moldo-too Ranges

(Fig. 4.1, Table 4.1), were studied paleomagnetically. The age of these locations ranges from early Cambrian to Late Ordovician (Table 4.1). In general, only arc-related volcanic rocks and back arc basin-related sediments such as graywacke were studied. All lithologies sampled were deposited in an early Paleozoic arc-back-arc setting. A total of 408 oriented drill cores were taken from these rocks at 53 sites (Table 4.1).

Kapka-Tash Range

Thirteen sites (SUT) and a total of 115 samples were studied covering the Bel'tepshy and the Sultansary Formations in the Sultansary area (Table 4.1), which is situated within the Kapka-Tash Range (Fig. 4.1). Samples were mostly taken from pillow basalt of the Bel'tepshy Formation (ten sites) and, to a lesser extent, from well-stratified basalt and tuff layers (three sites). Macroscopically, the leucocratic basalts are of light green color and show a non-differentiated, tholeiitic island arc chemical signature (Mikolaichuk *et al.*, 1997). Vasilev (1991) described sponge macroscleras, which are known since the early Cambrian in this area. A rich collection of lower Cambrian trilobites, brachiopods, hyolithes, hyolithelminths, and gastropods was found within the overlying tuff formation (Techar, Fig. 4.2), which is interbedded with limestones (Mikolaichuk and Mambetov, 1998).

Terskey Ala-too Range

Three areas were studied in the Karadzhorgo and Karakatty Ranges and along Dolon Pass (Fig. 4.2), which are continuations of the large Terskey Ala-too Range (Fig. 4.1). A late Cambrian to Early Ordovician sedimentary section was sampled near the Dolon Pass at 6 sites (JUR) with 42 samples in the Karadjorgo Formation (Table 4.1). Samples were only taken from layers of reddish tuff siltstones (Fig. 4.2). Late Cambrian to Tremadocian conodonts were described from the middle part of the section (Mikolaichuk *et al.*, 1997).

Five sites (SON) with 36 samples were taken from pillow basalts of the Karakatty Formation, along the Tulek River (Table 4.1). Conodonts of late Cambrian age were identified within cherts of the overlying Tuyuksay Formation (Fig. 4.2, Mikolaichuk *et al.*, 1997).

Three locations were sampled at the Dolon Pass along the asphalt road. DOL-A and DOL-B represent four and three sites from arkose and graywacke of the Kumoinok and Unkurtash Formations, respectively. 28 and 22 samples were taken from these locations. Additionally, five sites with 46 samples

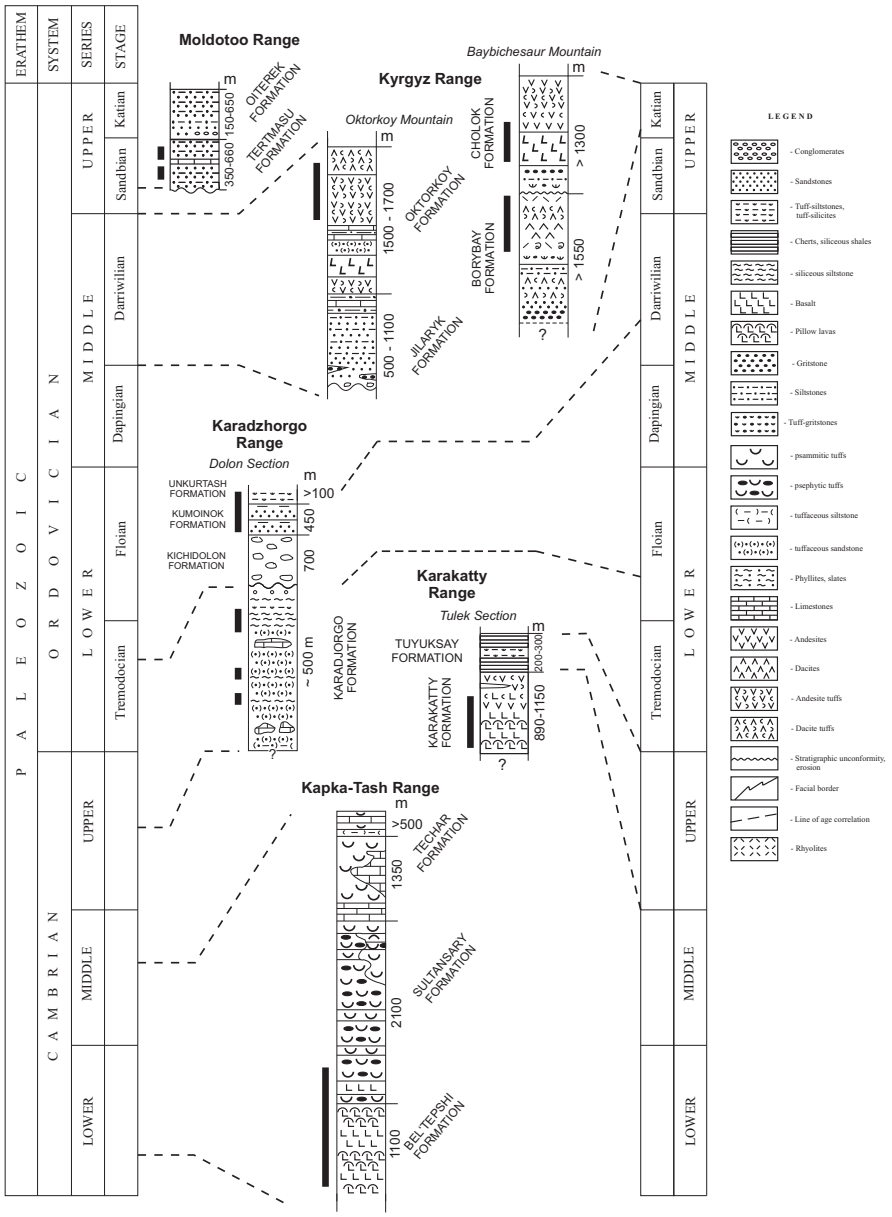

Figure 4.2: Lithological columns of Lower Paleozoic formations, which were sampled for paleomagnetic investigation in the North Tianshan. Rocktypes are indicated. Sampling position is marked by thick black lines.

were taken from a tuff section of the Unkurtash Formation (DOL-C). The upper Floian to Darriwilian age of these formations is firmly based on the findings of graptolites (Mikolaichuk *et al.*, 1997). Furthermore, the age of this sequence is bracketed by the occurrence of Tremadocian granitic pebbles in the underlying Kichidolon Formation (Fig.4.2, Mikolaichuk and Mambetov, 1998) and Darriwilian tephroids in the overlying Unkurtash Formation (Mikolaichuk and Mambetov, 1998).

Kyrgyz Range

Two sequences of Ordovician island arc volcanic rocks and sediments were studied in the Baybichesaur and Oktorkoy mountain ranges within the Kyrgyz Range (Figs. 4.1, 4.2). Four sites (BUR) and 26 samples were obtained from pillow basalts of the Oktorkoy Formation near the village of Burulday (Table 4.1). These are dated by Darriwillian brachiopods identified in interlayers of limestone within the Oktorkoy Formation (Fig. 4.2; Morozov, 1993; Djenchuraeva, 1997).

Four sites (BYS) with 63 samples were drilled in rhyolites, tuffs and basalts of the Borybay and Cholok Formations, respectively, near the village of Bystrovska (old Russian name, today known as Kemin). Here, the age of the sampled rocks is constrained by SHRIMP U-Pb zircon data (Kröner *et al.*, 2012), fixing the emplacement ages to 452 ± 5 and 449 ± 6 Ma, respectively.

Moldo-too Range

Five sites and 30 samples were studied in graywacke rocks of the Tertmasu Formation (Fig. 4.2, Klishevich and Kolobova, 1990) at the Moldo-too Range, below a large section of Carboniferous rocks of the Dungurme Formation, which were studied paleomagnetically (Bazhenov *et al.*, 2003; Kirscher *et al.*, 2014). Within the according stratotype section, which is located about 60 km away (Burg and Mikolaichuk, 2009), numerous brachiopods, nautiloids, trilobites, gastropods and bryozoans were found (Klishevich and Kolobova, 1990). Recently, this formation has been related to Sandbian age (Caradocian in the old stratigraphic scheme, Popov *et al.*, 2007).

4.3 Applied methods

Samples were drilled in the field and oriented with a standard Brunton compass. A local declination of +5° was used to correct the azimuth of both orientation measurements (compare IGRF 2011). Samples were subjected to both thermal (TH) and alternating field (AF) demagnetization during an extensive pilot study. Depending on the outcome of these experiments (whether stable endpoint or interpretable remagnetization circle data were identified) one or both methods were used for routine demagnetization experiments at each area. Stepwise thermal demagnetization experiments were performed using a Shoenstedt thermal demagnetizer with peak temperatures of 700°C. AF demagnetization was carried out using the homemade automated system at the University of Munich (Wack and Gilder, 2012) with peak fields of 90 mT. Magnetization directions were measured with a 2-G squid magnetometer in a shielded room at the University of Munich. Magnetic components were identified using at least five consecutive demagnetization steps and applying principal component analysis (Kirschvink, 1980). The Lowrie (1990) algorithm was applied to characterize the magnetic minerals carrying the magnetic signals. A composite orthogonal three axis Isothermal Remanent Magnetization (IRM) was imparted using field strengths of 0.12 T, 0.4 T and 2.5 T, respectively. The samples were then thermally demagnetized with peak temperatures at $\sim$ 700°C. The statistical robustness of the directional data was determined by application of Fisher (1953) statistics.

4.4 Results

4.4.1 Rock magnetic results

Thermal demagnetization of three IRMs imparted orthogonally (Lowrie, 1990) revealed two groups of results. The magnetic properties of samples from BUR, BYS, DOL-C, DUN and SUT are dominated by a low coercivity component (activated by DC fields of 0.12 T) with maximum unblocking temperatures below 600°C (Fig. 4.3). Samples from sites DOL-A, JUR, SON and to a lesser extent DOL-B are characterized by a substantial contribution of high coercivity components (activated in DC fields between 2.5 and 0.4 T), with unblocking temperatures around $\sim$ 680°C (Fig. 4.3).

In addition, decay plots of samples from BUR, BYS, DOL-B, DUN,

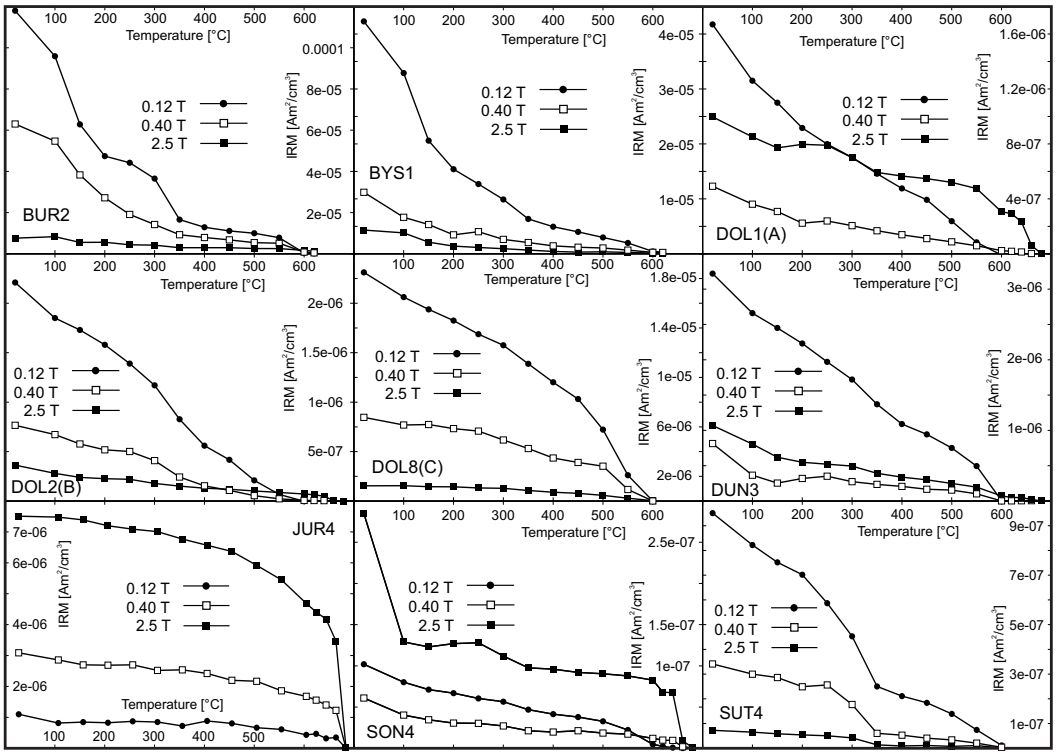

Figure 4.3: Results of thermal demagnetization experiments of orthogonal 3-axis IRMs (Lowrie, 1990). DC fields of 0.12, 0.4 and 2.5 T, respectively, have been used.

SON and SUT show a deflection of the low field IRM and mostly the intermediate IRM (activated with fields between 0.12 and 0.4 T) which intersects the x-axis at $\sim 350-400$°C (Fig. 4.3). A strong low temperature component is obvious only in results from samples from BUR, BYS and SON. This component vanishes completely at ~ 200°C and is interpreted to be diagnostic for goethite.

The 'intermediate temperature component' (drop at ~ 350°C), may be explained by the presence of fine-grained maghemite (de Boer and Dekkers, 1996). Similar results of thermomagnetic experiments from Asia with an *in-situ* direction close to the present-day field were related to post formational low temperature oxidation of magnetite (e.g. Choulet *et al.*, 2013). Except for site JUR, there is also strong evidence in samples from all sections for

low coercivity magnetite. In samples from DOL-A, SON, JUR, and to a very small amount, DOL-B there is evidence for the presence of hematite.

4.4.2 Demagnetization Results

After removal of a viscous overprint, a low temperature component (LTC) was identified in all samples analyzed. This LTC survives TH demagnetization up to $\sim$ 300°C, occasionally up to above 500°C (sections JUR and SON). LTC data from samples from BUR (six samples), BYS (26), DOL (40), DUN (22), JUR (14), SON (15) and SUT (49) were combined to obtain area LTC mean directions. Combining these seven individual mean directions yielded a total LTC mean direction of $D = 353.2°$, $I = 60.3°$, $k = 86.4$ and $\alpha_{95} = 6.5°$ in geographic coordinates. This value is in good agreement with the expected present-day value of the geomagnetic field in this region and is therefore interpreted to represent an overprint of the present geomagnetic field.

After removal of the LTC a first high temperature component (HTC_M) with an unblocking temperature range from $\sim 300 - 400$°C to $\sim$ 600°C was identified and is carried by magnetite. Occasionally, a second HTC_H is present with unblocking temperatures up to $\sim$ 700°C, diagnostic of hematite. HTC results from three areas (SON, JUR and BUR) do not show a well-defined demagnetization behavior with a clear linear trend towards the origin of the projection plane. Here, only a few stable endpoint results could be obtained. Therefore, instead of calculating site mean directions, a few individual directional data were combined with remagnetizaiton great circles to obtain a mean direction for the respective area following the procedure of McFadden and McElhinny (1988b).

BUR

Combination of five sample mean directions and four demagnetization great circles from section BUR yielded a mean direction of $D = 124.3°$, $I = -80.6°$, $k = 116.7$ and $\alpha_{95} = 4.9°$ before, and $D = 98.7°$, $I = -69.8°$, $k = 63.3$ and $\alpha_{95} = 6.7°$ after bedding correction.

BYS

The HTC_M of section BYS is present up to $\sim$ 600°C (Fig. 4.4c, d) and points towards the origin of the projection plane. Taken together the eight

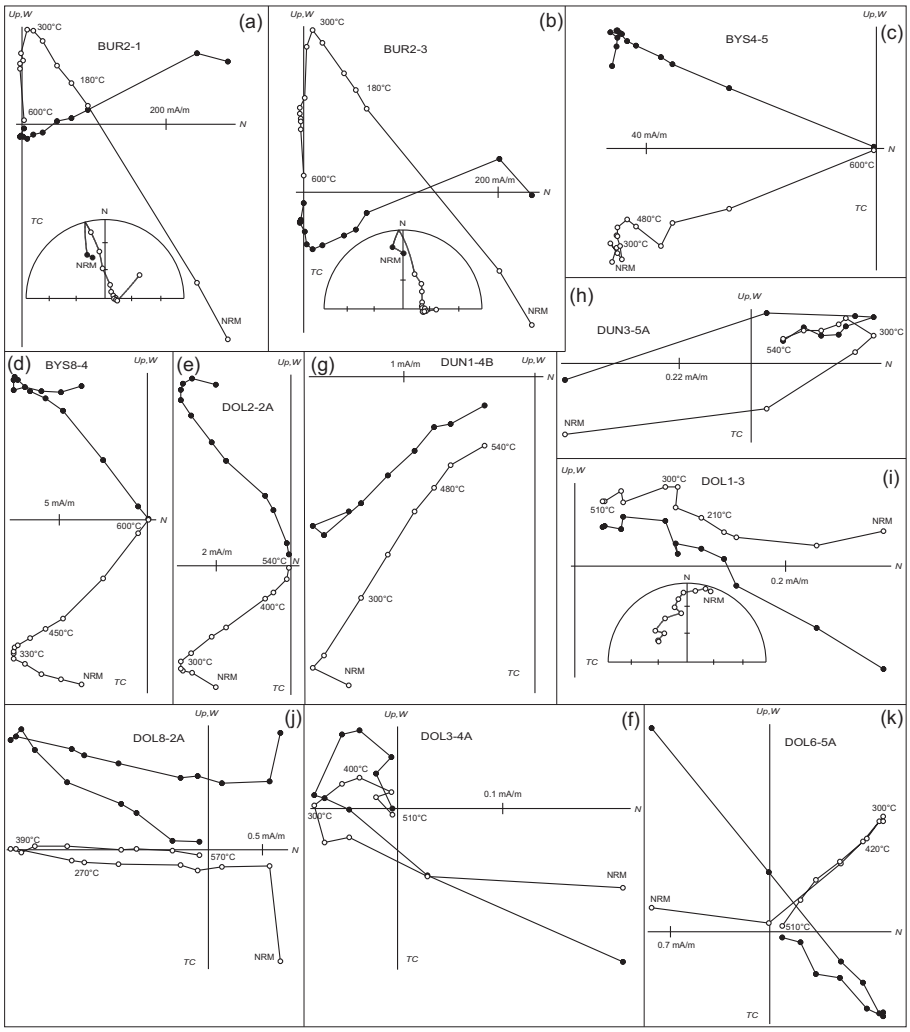

Figure 4.4: Results of thermal demagnetization experiments plotted as orthogonal vector diagrams (Zijderveld, 1967) in geographic (in situ) and stratigraphic (TC) coordinates. Solid and open dots represent vector endpoints projected onto the horizontal and vertical planes, respectively. Temperature steps in °C are indicated. For areas BUR (a,b) and DOL-A (i) stereographic projections of according Zijderveld diagram are also shown.

site mean directions (Table 4.2) yielded a regional mean direction of $D = 210.0°$, $I = -0.4°$, $k = 50.9$ and $\alpha_{95} = 7.8°$ before, and $D = 205.6°$, $I = 33.3°$, $k = 11.6$ and $\alpha_{95} = 17.0°$ after bedding correction. Plotting

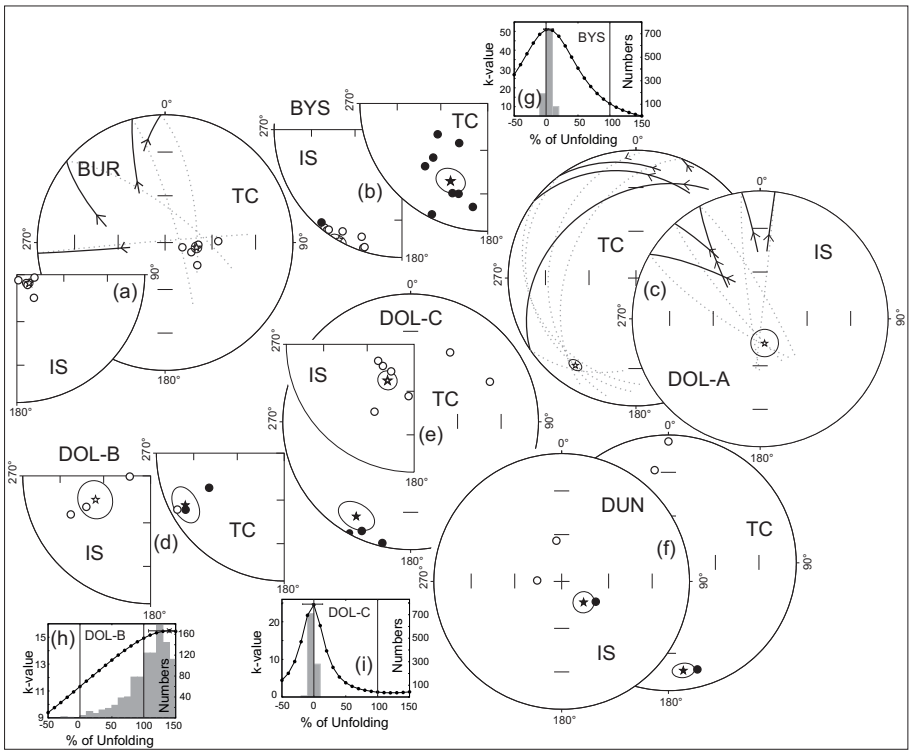

Figure 4.5: Stereographic projections of site mean directions from rocks of Middle to Late Ordovician age (a-f). Area mean directions are plotted as stars with according α_{95} error interval. Remagnetization great circles are shown for areas BUR (a) and DOL-A (c). Solid and open dots represent projection on the upper and lower hemispheres, respectively. Maximum k value is plotted versus stepwise percentage of unfolding for areas BYS, DOL-B and DOL-C (g-i), together with histograms of 1000 parametric simulations (Watson and Enkin, 1993).

the precision parameter k versus percentage of unfolding clearly shows that the magnetization was probably acquired after folding. Application of the parametric fold test of Watson and Enkin (1993) yielded a maximum k value at $4.0 \pm 8.7\%$ of unfolding with 1000 simulations (Fig. 4.5g).This confirms the post-folding age of remanence acquisition of the rocks.

Table 4.2: Site mean directions from areas BYS, DUN and DOL.

Site	N	In situ				Bedding-corrected				GC
		D[°]	I[°]	k	α_{95} [°]	D[°]	I[°]	k	α_{95} [°]	
BYS1	5	201.4	-13.6	35.8	13.3	209.3	1.2	22.3	17.0	1
BYS2	6	216.7	1.5	15.2	17.7	202.0	28.5	13.1	19.2	–
BYS3	6	198.2	-1.9	89.2	7.3	188.2	19.4	89.2	7.3	1
BYS4	3	210.3	-8.7	137.7	10.5	201.5	25.7	137.7	10.5	–
BYS5	5	216.4	-2.2	106.7	7.7	215.8	58.8	106.7	7.7	–
BYS6	9	220.9	4.4	75.5	6.2	238.3	52.2	75.5	6.2	–
BYS7	8	216.9	-0.9	1595.3	1.4	225.2	39.9	1595.5	1.4	–
BYS8	13	218.4	-1.8	75	4.8	224.9	31.4	87.7	4.5	2
DUN1	8	352.6	-63.8	8.3	20.5	360.0	-5.7	9.1	19.5	–
DUN2	8	272.4	-74.5	10.3	18.1	351.5	-27.7	10.3	18.1	–
DUN3	6	120.7	64.7	17.7	17.0	164.8	14.7	17.7	17.0	2
DOL-A										
DOL1	5	349.5	77.7	42.2	17.4	35.0	17.8	236.5	7.3	5
DOL-B										
DOL2	3	244.2	-31.4	56	16.6	245.2	35.7	56	16.6	–
DOL3	5	268.2	-76.8	30.8	14.4	242.2	-6.1	22.8	16.8	1
DOL4	6	244.3	-43.7	15.9	18.5	240.2	12.1	18.1	17.3	3
DOL-C										
DOL5	5	186.1	-56.6	35.8	13.9	63.2	-31.2	23.8	17.1	2
DOL6	6	245.3	-64.8	41.9	10.9	29.7	-37.7	41.9	10.9	2
DOL7	6	210.5	-38.9	19.5	16.6	204.1	7.2	86.8	7.8	3
DOL8	18	235.3	-65.8	24.5	7.2	208.9	0.6	28.3	6.7	9
DOL9	4	220.4	-67.4	29.4	18.2	193.1	3.0	29.4	18.2	1

Site: sampling sites. N: number of samples used for calculating site mean directions. Declination (D) and Inclination (I) in degrees, Fisher precision parameter k (Fisher, 1953), Fisher radius (α_{95}) of 95% confidence in geographic (*in situ*) and bedding corrected (TC) coordinates, respectively. GC: number of included remagnetization great circles for calculating mean directions, if used.

DOL

No useful directional data for the HTC_M could be obtained from the first four sites of DOL-A. Only five samples show well-defined remagnetization great circle results (Fig. 4.4i). Combining these great circles resulted in an intersection at $D = 169.5°$, $I = -77.7°$, $k = 42.2$ and $\alpha_{95} = 17.4°$ before, and $D = 215.0°$, $I = -17.8°$, $k = 236.5$ and $\alpha_{95} = 7.3°$ after bedding correction (Fig. 4.5c). Since none of the samples showed a well-defined linear demagnetization trend towards the origin, this result has to be treated with caution.

At **DOL-B** demagnetization results are much better defined (Fig. 4.4e, f). Three site mean directions resulted in a mean direction of $D = 67.0°$, $I = 50.0°$, $k = 9.6$ and $\alpha_{95} = 23.1°$ before, and $D = 242.3°$, $I = 13.7°$, $k = 12.3$ and $\alpha_{95} = 19.3°$ after bedding correction (Fig. 4.5d). Plotting the precision parameter k versus percentage of unfolding (Fig. 4.5h) suggests a pre-folding age of acquisition for the magnetic signal.

The tuffs at **DOL-C** show again well-defined demagnetization behavior. Five site mean directions resulted in an area mean direction of $D = 36.8°$, $I = 60.6°$, $k = 16.4$ and $\alpha_{95} = 12.1°$ before, and $D = 209.9°$, $I = 15.8°$, $k = 8.0$ and $\alpha_{95} = 19.8°$ after bedding correction (Fig. 4.5e). Inspection of the plot of the precision parameter k versus percentage of unfolding

(Fig. 4.5i) clearly indicates the time of acquisition of the magnetic signal after folding.

DUN

The HTC_M of the magnetically weak sediments of section DUN was only possible to distinguish in samples from three sites. The regional mean direction based on these three site mean directions is $D = 133.6°$, $I = 70.8°$, $k = 21.6$ and $\alpha_{95} = 13.4°$ before, and $D = 172.1°$, $I = 16.1°$, $k = 28.9$ and $\alpha_{95} = 11.4°$ after bedding correction. Two sites comprise samples with reversed polarity, whereas the other site yielded results with a normal polarity. These polarities are antipodal (Fig. 4.5f). However, to perform a proper reversal test, three data points are not sufficient. Nevertheless, we interpret the tilt-corrected direction to represent a primary magnetic signal that was acquired during sedimentation.

JUR

Five samples of section JUR show a well-defined demagnetization behavior between ~ 370 and ~ 700°C, yielding a mean direction of $D = 248.8°$, $I = -43.9°$, $k = 103.5$ and $\alpha_{95} = 7.6°$ in geographic coordinates. Since the mean inclination coincides, before tilt correction, with the expected value for the late Carboniferous to early Permian, it is interpreted as a remagnetization signal due to tectono-thermal orogenic processes. This is a common feature in this region (e.g., Bazhenov *et al.*, 2003; Kirscher *et al.*, 2013).

Only five samples showed demagnetization results with usable directional data that are different from the Permo-Carboniferous directions. Taken together these five mean directions with ten remagnetization great circles yielded a mean direction of $D = 270.1°$, $I = -0.9°$, $k = 12.7$ and $\alpha_{95} = 11.4°$ before, and $D = 283.0°$, $I = 30.1°$, $k = 12.2$ and $\alpha_{95} = 11.6°$ after bedding correction (Fig. 4.7a). The variation in bedding orientation is not sufficiently high to perform a robust fold test (Fig. 4.7d).

SON

Combining ten remagnetization great circles with the five reliable stable endpoint data from section SON yielded a mean direction of $D = 230.6°$, $I = 70.2°$, $k = 20.1$ and $\alpha_{95} = 9.0°$ before, and $D = 115.6°$, $I = 43.7°$, $k = 20.6$ and $\alpha_{95} = 8.8°$ after bedding correction (Fig. 4.7b). Uniform bed-

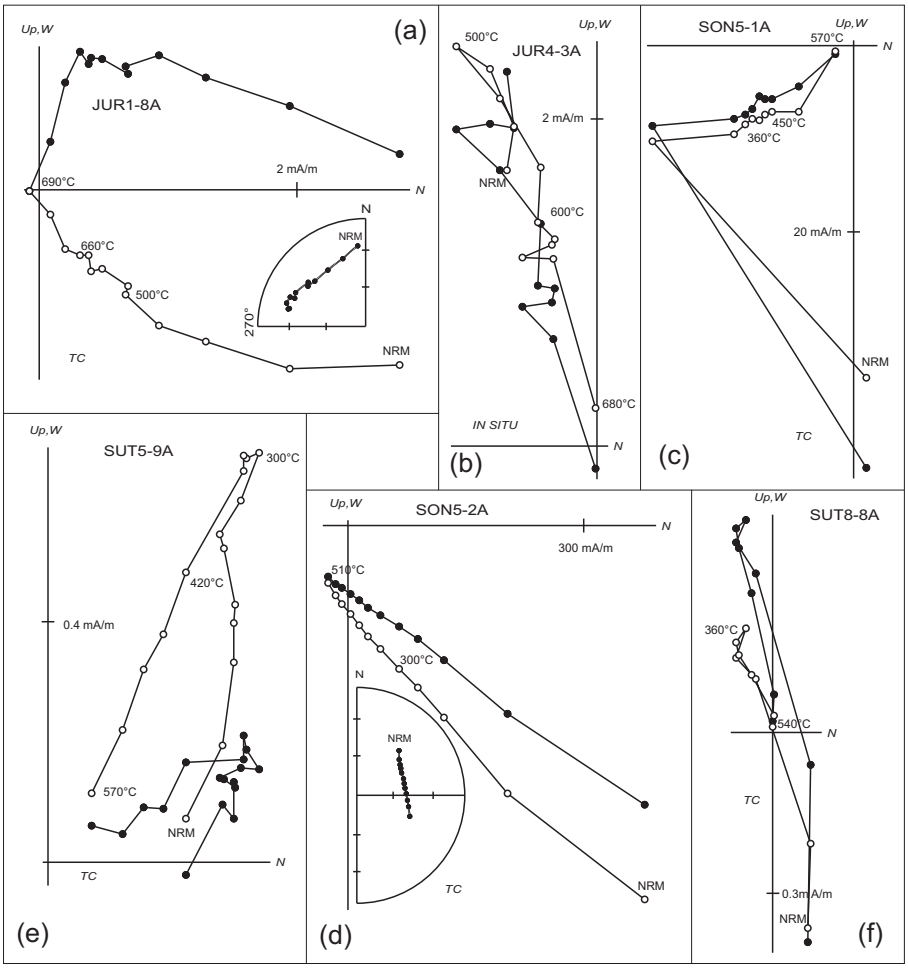

Figure 4.6: Results of thermal demagnetization experiments plotted as orthogonal vector diagrams (Zijderveld, 1967) in geographic (in situ) and stratigraphic (TC) coordinates from Cambrian sections. Solid and open dots represent vector endpoints projected onto the horizontal and vertical planes, respectively. Temperature steps in °C are indicated. For areas JUR (a) and SON (d) stereographic projections of according Zijderveld diagram are also shown.

ding orientations resulted in stable k values between 0 and 100% unfolding (Fig. 4.7e).

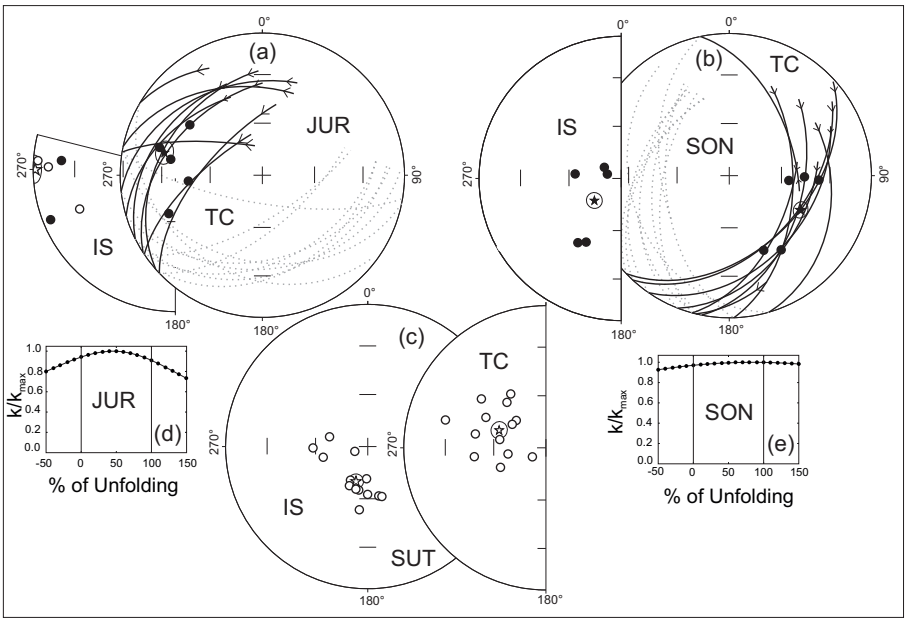

Figure 4.7: Stereographic projections of site mean directions from rocks of Ordovician and Early Cambrian age (a-c). Remagnetization great circles are shown for areas JUR (a) and SON (b). Maximum k value is plotted versus stepwise percentage of unfolding for areas JUR (d) and SON (e). Solid and open dots represent projection on the upper and lower hemispheres, respectively.

SUT

The HTC_M of section SUT is rather well-defined and present up to $\sim$ 600°C (Fig. 4.6e, f). Site mean directions were obtained and resulted in a mean direction of $D = 206.1°$, $I = -69.9°$, $k = 26.2$ and $\alpha_{95} = 8.3°$ before, and $D = 291.0°$, $I = -59.4°$, $k = 21.0$ and $\alpha_{95} = 9.3°$ after bedding correction (Fig. 4.7c). Again, the variation in bedding orientation together with uncertainties in identifying the precise bedding values at these old pillow basalts, prevented the application of a fold test. However, the more circular distribution of directions after bedding correction provides some confidence that the magnetic signal was acquired before folding.

Table 4.3: Site mean directions from Soltan Sary Section.

Site	N	In situ				Bedding-corrected			
		D[°]	I[°]	k	α_{95} [°]	D[°]	I[°]	k	α_{95} [°]
Soltan Sary section									
SUT1	5	263.1	-65.8	39.2	12.4	288.9	-38.2	23.4	16.1
SUT2	5	256.5	-63.8	21.2	17.0	296.9	-51.0	26.4	15.2
SUT3	8	284.3	-67.5	33.3	9.7	307.2	-42.6	36.7	9.3
SUT4	4	207.2	-68.5	352.1	5.2	246.7	-61.6	352.1	5.2
SUT5	10	249.5	-82.2	22.2	10.5	319.4	-55.5	23.5	10.2
SUT6	3	195.0	-63.5	408.5	6.1	261.6	-68.3	911.2	4.1
SUT7	4	200.6	-68.1	9.2	32.1	286.4	-61.8	11.5	28.4
SUT8	4	187.6	-53.2	32.7	17.3	263.0	-48.1	22.5	20.9
SUT9	4	205.1	-65.3	190.1	7.1	281.1	-48.2	73.1	11.5
SUT10	5	167.5	-61.0	79.0	8.7	312.8	-66.9	79.0	8.7
SUT11	6	164.2	-60.2	88.9	7.1	236.3	-80.8	98.6	6.8
SUT12	5	195.5	-64.7	24.0	15.9	304.9	-66.5	31.2	13.9
SUT13	7	182.2	-71.6	34.1	10.5	326.9	-52.8	30.1	11.2

Site: sampling sites, Age. N: number of samples used for calculating site mean directions. Declination (D) and Inclination (I) in degrees, Fisher precision parameter k (Fisher, 1953), Fisher radius (α_{95}) of 95% confidence in geographic (*in situ*) and bedding corrected (TC) coordinates, respectively.

4.4.3 Summary of Results

There is a more or less strong LTC present in most samples. Combining data of this component from all seven areas with a total of 146 directional results yielded an overall mean value of $D = 353.2°$, $I = 60.3°$, $k = 86.4$ and $\alpha_{95} = 6.5°$ for this component. Therefore, we associate this component with an overprint caused by the present geomagnetic field.
Most abundantly a HTC_M is present in the studied rocks and is carried by a low coercivity phase that is activated at 0.12T (Fig. 4.3) and is completely removed after heating to 600°C (sections BUR, BYS, DOL-A, DOL-C, SON and SUT). We interpret this phase as being syn formational (hmm???) magnetite. In rocks from two areas (JUR and SON) and, to a lesser extend, at DOL-B, hematite is also present (Fig. 4.3).
The directions of samples from BYS and DOL-C are dominated by the HTC_M and fail the fold test (Table 4.4). These two areas show an increase of the confidence angle α_{95} of 9° and 7.7°, respectively, during unfolding.

Due to more or less uniform bedding attitudes (Fig. 4.8) no fold tests were possible for DOL-B, SUT, SON, and BUR. Normal and reversed polarites of the HTC_M identified in DUN suggest a primary origin for the ChRM. At section JUR two sets of HTC mean directions are present after the removal of the LTC. Five samples show only a HTC_H, which is broadly in agreement with the point of intersection of the remagnetization great circles of ten samples. Another five samples show a combined HTC_M and HTC_H with similar directions that plot very close to the direction of the expected late Paleozoic overprint direction. This adds some confidence that the solely occurring HTC_H together with the remagnetization great circles were acquired before the late Paleozoic remagnetization event. No stable endpoint

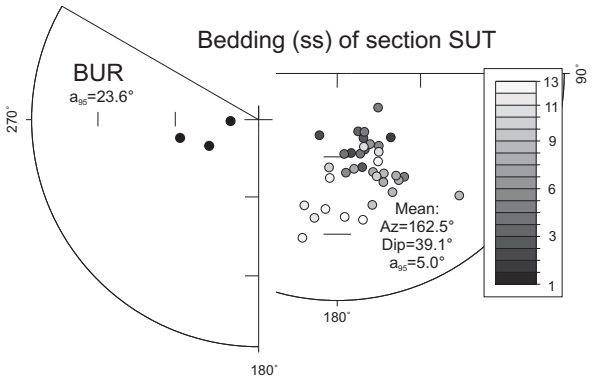

Figure 4.8: Stereographic projections of normal vectors on bedding planes from sections SUT and BUR. Badding vectors of SUT are grey-coded with respect to the measured position, 1-18 indicates sampled sections.

Table 4.4: Regional mean directions from all areas with a reversed polarity.

Site	N	In situ				Bedding-corrected				Pol	GC
		D[°]	I[°]	k	α_{95} [°]	D[°]	I[°]	k	α_{95} [°]		
Remagnetized Signals											
DOL-C	5	216.8	-60.6	16.4	12.1	29.9	-15.8	8.0	19.8	-	–
JUR	5	248.8	-43.9	103.5	7.6	239.3	2.3	103.5	7.6	-	–
BYS	8	212.5	-2.9	64.6	6.9	211.3	33.0	13.1	15.9	-	–
Primary Signals											
DUN	3	133.6	70.8	21.6	13.4	172.1	16.1	28.9	11.4	+/-	–
DOL-B	3	67.0	50.0	9.6	23.1	242.3	13.7	12.3	19.3	-	–
BUR	9	304.3	80.6	116.7	4.9	278.7	69.8	63.3	6.7	+	4
DOL-A	5	169.5	-77.7	42.2	17.4	215.0	-17.8	236.5	7.3	-	–
JUR	15	270.1	-0.9	12.7	11.4	283.0	30.1	12.2	11.6	-	10
SON	15	230.6	70.2	20.1	9.0	115.6	43.7	20.6	8.8	-	10
SUT	13	26.1	69.9	26.2	8.3	111.0	59.4	21.0	9.3	+	–

Site: sampling sites. N: number of samples used for calculating area mean directions. Declination (D) and Inclination (I) in degrees, Fisher precision parameter k (Fisher, 1953), Fisher radius (α_{95}) of 95% confidence in geographic (*in situ*) and bedding corrected (TC) coordinates, respectively. Pol: Present polarity, +/-: normal/reversed polarity. GC: included remagnetization great circles for calculating area mean direction (McFadden and McElhinny, 1988a).

directions could be isolated at DOL-A where a mean direction is exclusively based on intersecting remagnetization great circles. We therefore treat this result with caution.

Reported Paleozoic paleomagnetic data from the entire region contain mostly counterclockwise deviated directions of various amounts related to the amalgamation of Eurasia (Van der Voo *et al.*, 2006). In this respect we assign the most suitable polarity to our results. This translates into paleo-southpoles with longitudes between $\sim 330°$ and $\sim 85°$ and latitudes between $+40°$ and $-60°$ (Table 4.5). These poles satisfy our criteria of counterclockwise rotations of the study area when compared to the APWPs of Baltica, Siberia and Gondwana. The resulting paleolatitudes range from ca.$+30°$

Table 4.5: Regional mean directions after refolding procedure at maximal k values with resulting paleo-southpoles.

Site	λ_S[°]	Φ_S[°]	Age [Ma]	λ_P[°]	Φ_P[°]	dp[°]	dm[°]	Plat	α_{95} [°]
Remagnetized Signals									
DOL-C	41.87	75.73	∼250	-62.8	333.8	18.4	14	41.6	12.1
JUR	41.89	75.76	∼280	-32.1	338.7	9.5	5.9	25.7	7.6
BYS	42.72	75.70	∼440	-39.6	31.5	6.9	3.5	-1.5	6.9
Primary Signals									
DUN	41.66	74.34	455.7±3.0	-39.6	84.5	11.7	6.0	-8.2	11.4
DOL-B	41.89	75.74	462.5±1.6	-15.2	10.1	19.7	10.1	-6.9	19.3
BUR	42.68	75.83	464.2±5.8	37.7	28.0	11.5	9.9	-53.7	6.7
DOL-A	41.88	75.74	467.9±3.9	-45.1	22.4	7.6	3.9	9.1	7.3
JUR	41.89	75.76	483.5±13.5	20.3	349.6	12.9	7.1	-16.2	11.6
SON	41.94	75.68	491.2±5.8	-0.1	130.2	11	6.9	-25.5	8.8
SUT	41.77	76.30	525.0±16.0	13.1	123.3	14.0	10.5	-40.2	9.3

Site: sampled area. λ_S[°] and Φ_S[°]: latitude and longitude of studied area. Age: age of studied rocks. λ_P[°] and Φ_P[°]: resulting paleopole based on area mean directions with according error dm and dp in °. Plat: paleolatitude based on inclination of area mean direction. α_{95} [°]: Fisher radius of confidence (Fisher, 1953).

for the remagnetized areas DOL-C and the overprint direction of JUR, via slightly negative values for DUN and DOL-B, towards values which indicate increasingly high southerly positions for the older areas BUR, SON, JUR and SUT (Table 4.5).

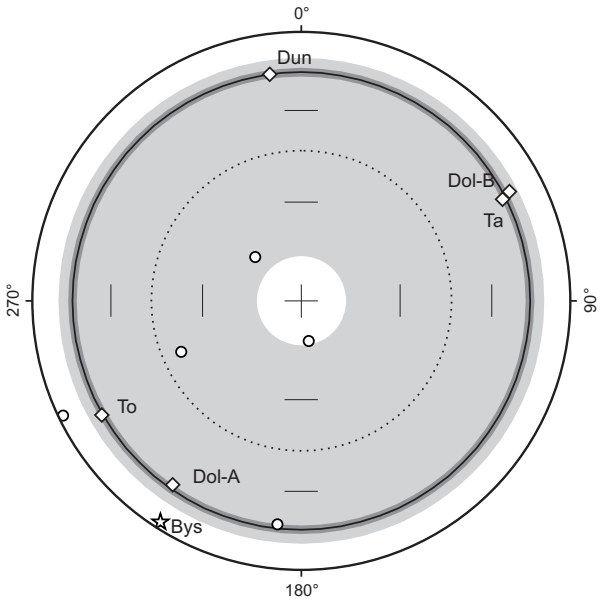

Figure 4.9: Comparison of inclination data of Late Ordovician data from areas DOL, DUN (this study) and To, Ta (Bazhenov *et al.*, 2003), from the North Tianshan. Circles and diamonds indicate mean directions prior and after tilt correction, respectively. Dotted circle with light grey error interval represents fitted small circle centered at the origin with according standard deviation for *in situ* data points. Black line with dark grey interval shows results for data after tilt correction.

4.5 Conclusions

We analysed middle Cambrian to Late Ordovician rocks from nine areas in the Kyrgyz Tianshan (Fig. 4.2, Table 4.1). Rock magnetic analysis revealed the presence of magnetite and/or haematite as the carrier of the characteristic remanent magnetization in all samples (Fig. 4.3).

Site mean directions for two areas (BYS and DOL-C) yielded negative fold tests (Enkin, 2003), demonstrating a post-folding age of the magnetic signal. Samples from the other areas are interpreted to reflect a primary magnetic signal due to several reasons. Two areas (DOL-B and DUN) are characterized by positive fold and reversal tests, respectively. Mean directions of three areas (DUN, DOL-A and DOL-B), together with results of

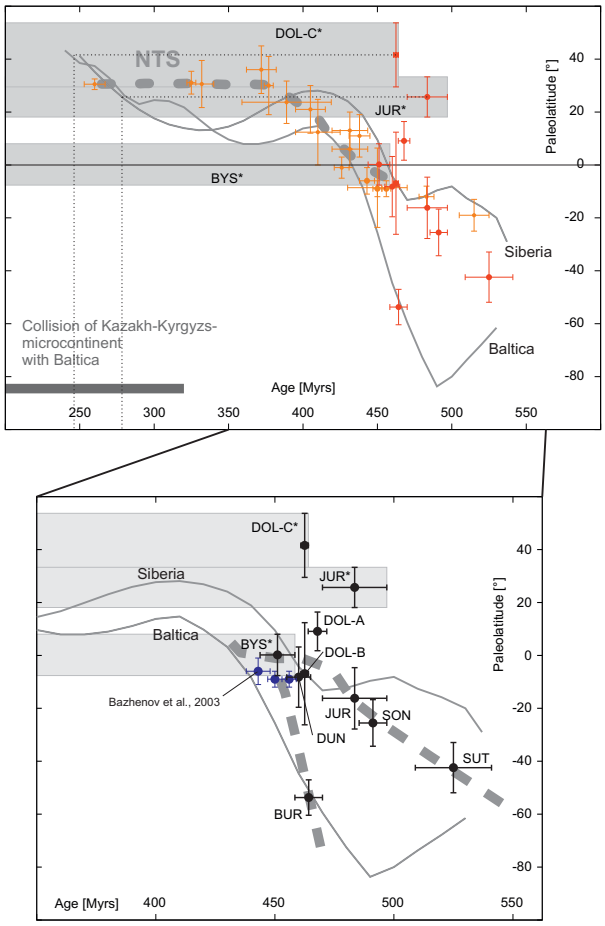

Figure 4.10: Plot of paleolatitude versus age for all obtained area mean directions. Also shown are paleolatitudes based on the APWP of Siberia and Baltica (Torsvik *et al.*, 2012) for a reference site in the North Tianshan. Also plotted are paleolatitude values of other studies from the North Tianshan Zone, the Chingiz Range and south Kazakhstan (Bazhenov *et al.*, 2003; Alexyutin *et al.*, 2005; Abrajevitch *et al.*, 2007; Levashova *et al.*, 2007; Kirscher *et al.*, 2014) in orange.

a study of nearby situated rocks of the same age (Bazhenov *et al.*, 2003), show a well-defined regional fold test (Fig. 4.9). Finally, the pre-folding area mean directions resulting from samples in seven areas (BUR, SON, JUR, SUT, BYS, DUN, DOL-A) do not coincide with the most common

remagnetization direction reflecting the late Paleozoic deformation event. The common overprint in these areas has been reported in several studies (e.g. Bazhenov *et al.*, 2003; Kirscher *et al.*, 2013), and is also present in the remagnetized areas DOL-C and in a LTC of area JUR (Table 4.4).

Transforming the above results into paleolatitudes (Fig. 4.10) has the following implications:
(1) Paleolatitudes for DOL-C and the secondary component of area JUR overlap each other within error limits and most likely represent a remagnetized signal from the collision of the Kazakh-Kyrgyz microcontinent with Baltica. Their paleolatitude intersects with the corresponding curve for Baltica at $\sim$ 250 Ma (Torsvik *et al.*, 2012).
(2) Area BYS, however, is more likely to have become remagnetized during the early Paleozoic collision event when the area was situated close to the paleo-equator.
(3) At least two fragments of the NTS terrane were separated during the Early Ordovician.
(4) A Middle Ordovician collision event led to amalgamation of a microcontinent at low southern latitudes (Fig. 4.10).

These results, in combination with published data for this area, infer a paleogeographic evolution for this region ranging from early to late Paleozoic. We suggest that the Kyrgyz North Tianshan is made up of at least two, and probably more, crustal fragments that are likely to have been derived from the northern margin of Gondwana. These continental terranes were located at mid-low latitudes, probably below Australia and in proximity to India. Tarim was probably also one of these fragments (Fig. 4.11). After separation of these fragments from Gondwana, some were amalgamated in the Middle Ordovician at low latitudes (Fig. 4.10) and south of the paleo-equator to form Kazakhstania (Filippova *et al.*, 2001) or the Kazakh continent (Windley *et al.*, 2007). As proposed by Alexeiev *et al.* (2011), this microplate was the locus of further accretion of small blocks to the east (present coordinates). The microplate slowly migrated to the north until it reached a position at roughly 30°N in the Devonian. Thereafter, the collage of Precambrian fragments and early Paleozoic arc-related rocks occupied a stable position and acted as a subduction epicenter. Baltica and Siberia most likely collided with this area only during the amalgamation of Eurasia in the late Paleozoic.

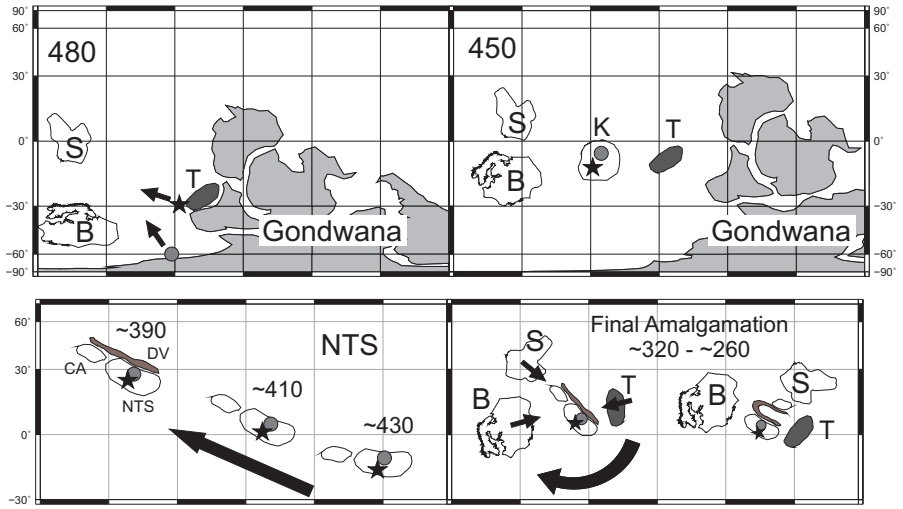

Figure 4.11: Schematic reconstruction of the paleogeographic evolutionary history of the North Tianshan zone and adjacent areas during the Paleozoic. Numbers from 480 to 260 indicate age in millions of years BP. Gondwana reconstruction and positions of Baltica and Siberia are based on Torsvik *et al.* (2012). Position of Tarim is based on Li (1990). Following abbreviations are used: B - Baltica, S - Siberia, T - Tarim, CA - Chingiz Arc, DV - Devonian volcanic belt, NTS - North Tianshan. Black arrows show direction of movement. Circle and star show proposed origin of northern and southern part of the North Tianshan zone at the margin of Gondwana, respectively. Position of Chingiz arc and Devonian volcanic belt is based on Bazhenov *et al.* (2012), and references therein.

Acknowledgments

We thank Matthias Hackl for support in the field. This study was financed by grant Ba1210/14-1 and 14-3 of the Deutsche Forschungsgemeinschaft (DFG) to V.B. and a visiting grant from the DAAD to A.V.

5

Palaeozoic Palaeomagnetism of the South-Western Segment of the Central Asian Orogenic Belt – A Critical Review

by ***U. Kirscher, and V. Bachtadse***
Accepted for the Book on composition and evolution of Central Asian Orogenic Belt, Kroener, A.(ed), E. Schweizerbart'sche Verlagsbuchhandlung (Publisher)

Abstract

Despite significant progress made in understanding the tectonic evolution of the Central Asian Orogenic Belt (CAOB) during the Palaeozoic there are still a number of competing models for the tectonic and geodynamic evolution of Central Asia in these times. Here we present a critical review of the existing palaeomagnetic data set for the southwestern part of the CAOB.

Data has been taken from the Global PalaeoMagnetic DataBase (GPMDB) containing all published data until the year 2004 and extended by data published thereafter. A general query of all available data points without known secondary magnetic signals was evaluated and compared to high quality data points. The high quality data includes studies with positive palaeomagnetic tests of stability, such as reversal and fold tests. All data are then compared to apparent polar wander paths (APWPs) for stable Europe (Baltica) and Siberia (Angara) in order to identify the drift history of individual tectono- stratigraphic terranes making up the CAOB and to quantify and date the rotations they have been subjected to during and/or after amalgamation. Palaeolatitudes for individual blocks derived from palaeomagnetic data show agreement with palaeolatututudes derived from the apparent polar wander paths of both Baltica and Angara, at least since $\sim$ 400 Myrs. Before this time, palaeolatitudes suggest affinities rather to Siberia (Angara) than to Baltica, not exceeding palaeolatitudes of 15° South until $\sim$ 470 Myrs ago. Declination deviations of the investigated date with respect to expected values derived from th APW path for Siberia do not show any systematic distribution. A steady decrease with decreasing formation ages, which would indicate a successive deformation history through time, cannot be observed. Despite the fact that changes in structural strike and changes in magnetic declination seem to be related, this relationship appears only to be qualitatively and oroclinal bening of the CAOB is definitely not the only mechanism at work.

In contrary, palaeopoles define small circles centered on the study areas indicating various counterclockwise rotations with respect to the APWP for Baltica and Siberia as being the dominant tectonic feature. We interpret these observations as reflecting a long-lived zone of deformation, in an oblique compressional setting. The marked horseshoe shaped deformational pattern observed in Devonian volcanic arcs in central Asia (oroclinal bending) is well documented and quantified by both structural and paleomagnetic studies in central Kazakhstan although paleomagnetic data show some considerable scatter. Nevertheless it seems that the deformation pattern observed here cannot be applied to the whole CAOB. Tectonic processes like arc slicing or shaving, occurrence of small faults, and diffuse deformation accompanying the large fault systems might have affected the palaeomagnetic data, and might have smeared out the palaeopole positions.

The existence of areas with different rotation histories is best suited to explain the palaeomagnetic results. More precise definition of the small areas seems not promising, because the spatial cover of available Palaeozoic

outcrops suitable for palaeomagnetic testing is sparser than the size of the tectonic units. Defining Early Palaeozoic terranes is therefore only promising using palaeolatitudes.

5.1 Introduction

Despite the fact that the Central Asian Orogenic Belt (Yanshin, 1965) (or Altaids, Figs. 5.1+5.2) is probably one of the largest accretionary structures on planet Earth, it was only in rather recent times that it moved back in the focus of the Earth sciences community (see thorough review by Windley *et al.* (2007)), since the first description of the complex area by Eduard Suess in 1901 (see reviews by Şengör *et al.* (2014); Kröner and Rojas-Agramonte (2014). Consequently, it does not come as a surprise that a series of competing models have been brought forward since then (Windley *et al.*, 2007) which can be grouped as modifications of (a) the multiple island arc or (b) the single arc model. The multiple island arc model (a) is based on postulated similarities in the structural evolution of the Central Asian Accretionary Belt (CAOB) or Altaids (sensu Şengör *et al.* (1993)) between 1.0 Ga to 250 Ma and the western Pacific as a modern analogue where crustal growth is basically controlled by complicated interactions of islands arcs, oceanic islands, sea-mounts, accretionary wedges and microcontinents (Xiao *et al.*, 2010). In this model, originally designed by Zonenshain *et al.* (1990) and later been taken up by mostly Russian authors (Windley *et al.* (2007) and references therein), the Precambrian micro continents, now integrated into the Altaids show affinities either to Gondwana or to Siberia. In their original model (b) Şengör *et al.* (1993) argue in favor of a primarily continuous island arc (Kipchak-Tuva-Mongol arc), about 7000km in length. Early Palaeozoic roll-back of the arc is related to the formation of the Khanty-Mansi backarc ocean (Windley *et al.*, 2007). Subsequent differential rotation of Siberia and Baltica caused segmentation and duplication of the arc by strike-slip shuffling and oroclinal bending associated with the final closure of the Khanty-Mansi Ocean by late Carboniferous times. By this time the general amalgamation and large scale tectonic organization of all microblocks and arc related structures was completed. Subsequently, oblique northward directed subduction of the Palaeotethys lead to transpressional conditions (Samygin and Burtman, 2009) including the formation of large strike-slip fault systems (Buslov, 2011). Despite the increasing number of palaeomagnetic studies in the region (e.g. Alexyutin *et al.*, 2005; Bazhenov

et al., 1999; Bazhenov and Mikolaichuk, 2004; Levashova *et al.*, 2007), one of the main questions, the origin and precise evolutionary history of these microplates has not been fully answered yet. However, all palaeomagnetic results from the area indicate large scale counterclockwise rotations with respect to Baltica, which do not seem to follow an underlying pattern. Yet, no general accepted tectonic model has been brought forward to explain all observation.

In the following we attempt to unify and generalize present palaeomagnetic data of Palaeozoic rocks from the south-western segment of the CAOB. Additionally, we try to formalize them, and give the furthest possible constraints to the Palaeozoic evolution of the whole region, which can be extracted from palaeomagnetic data. The quality of the existing palaeomagnetic data set will be evaluated by comparing it with data satisfying modern reliability criteria. Then the data is used to reconstruct the palaeolatitudinal history of tectonic blocks and to quantify rotations based on the difference in declination between observed and reference values. The latter is being calculated from the reference apparent polar wander path of Baltica (Torsvik *et al.*, 2012). It is therefore an attempt to generalize the large amount of palaeomagnetic data, which mostly are incompletely used only for palaeolatitude estimation of small terranes.

5.2 Geological setting and tectonic field characteristics

The south-western part of the CAOB is bordered by the Ural and Baikalide mountain ranges to the north and by the Alay-Tarim cratonic units to the south (Figs. 5.1+5.2). Internally, their main orographic features are either large sedimentary basins, like for example the Caspian depression, or Palaeozoic mountain chains, such as the Tianshan or the Karatau.

Precambrian lithospheric fragments mark the pre- Altaid core of the accretionary orogen. These relicts are thought to represent parts of isolated allochtonous blocks or microplates within a Palaeo-Asian ocean (Windley *et al.*, 2007). It has been proposed, that they are derived either from East-Gondwana (Mossakovsky *et al.*, 1993) or from the Siberian margin (Berzin and Dobretsov, 1994). Subsequently, rifting processes and eustatic sea level changes lead to the formation of large carbonate seamounts in this region. Changes in subduction activity, along with changes in arc environments (see Samygin and Burtman (2009) for detailed description) generated a com-

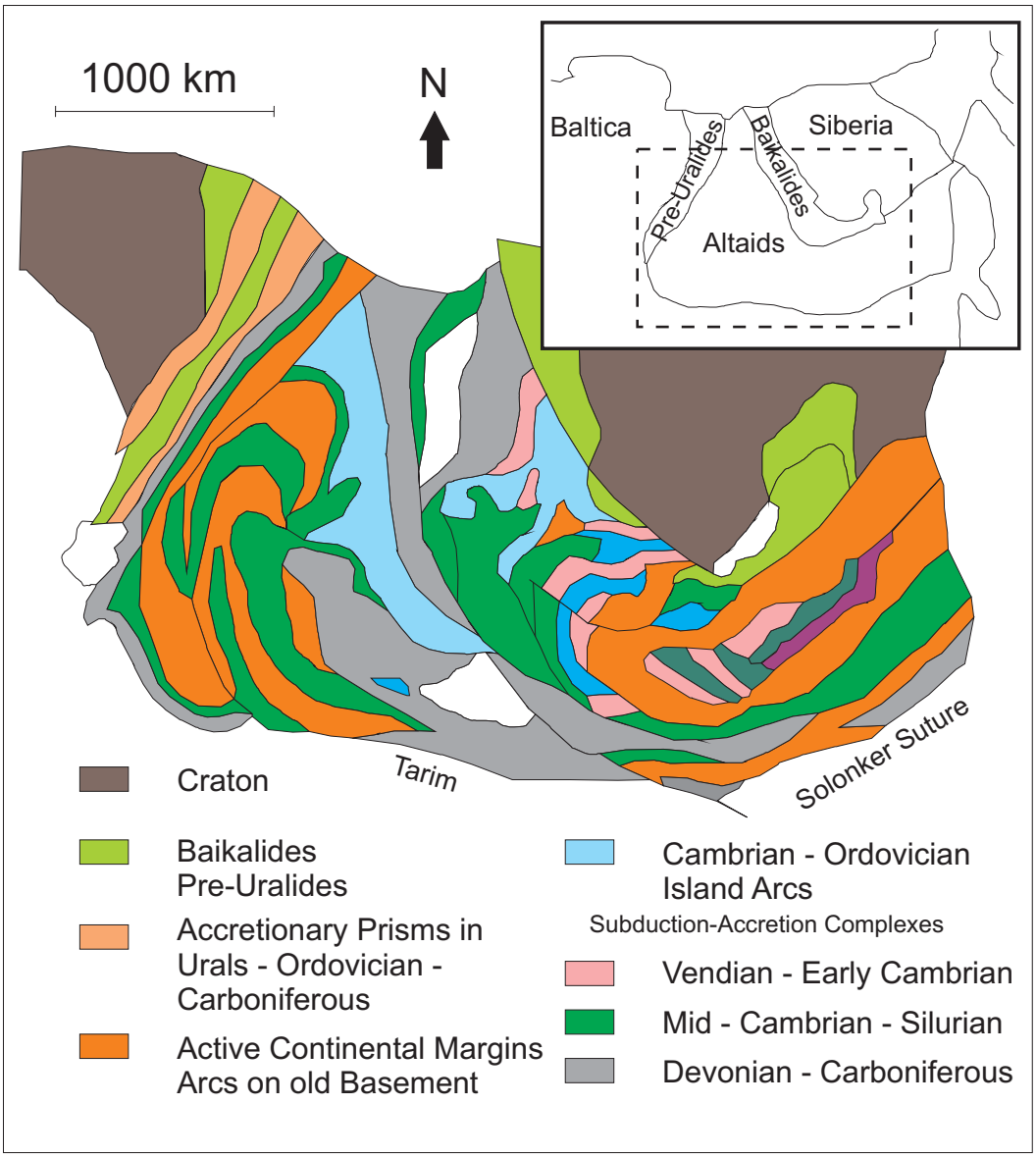

Figure 5.1: Simplified tectonic map of the Central Asian Orogenic Belt, modified from Windley *et al.* (2007), showing the most important microblocks and sutures of the area.

plex palaeogeographic setup, which has been described in numerous publications (Zonenshain *et al.*, 1990; Şengör *et al.*, 1993; Filippova *et al.*, 2001;

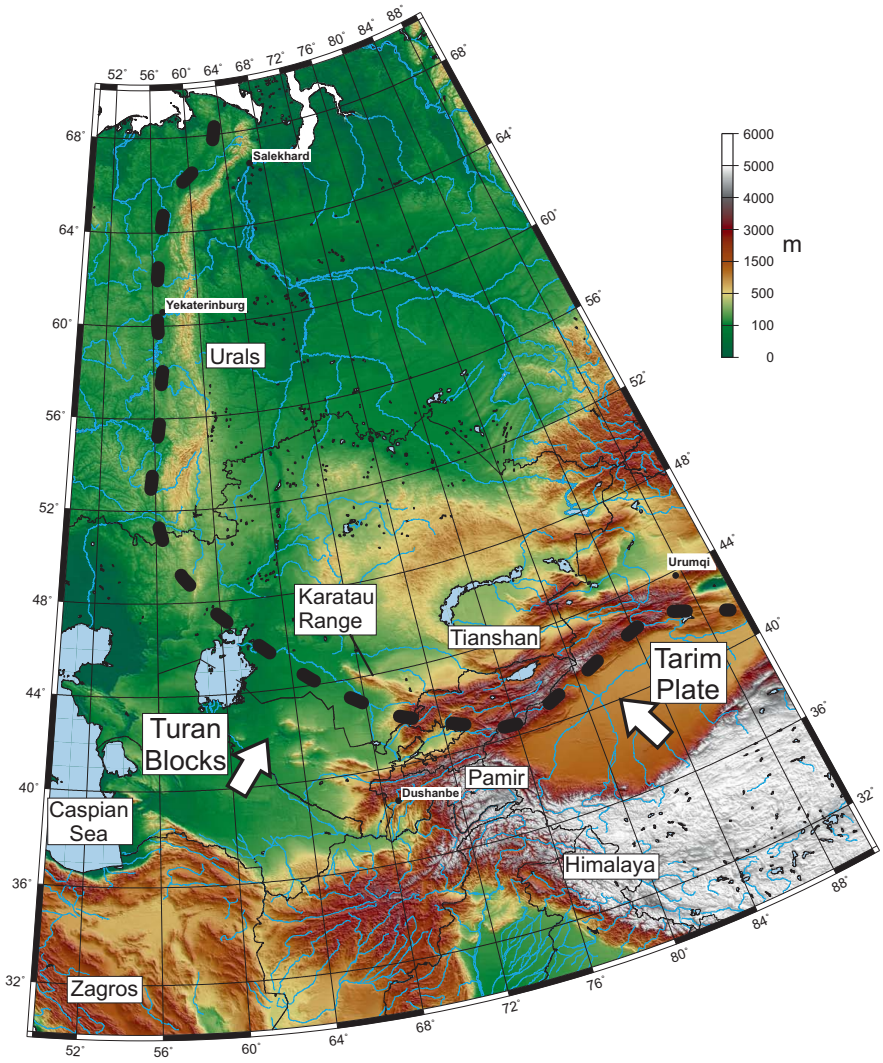

Figure 5.2: Topographic map of the Western part of the Central Asian Orogenic Belt. Important orogenic features are indicated. White arrows show the suspected direction of collisional movement of the Tarim and Turan microblocks during the final amalgamation of Central Asia. Dotted line represents the Ural-Tianshan orogenic belt. Map was created using GMT of Wessel and Smith (1998) and topographic dataset ETOPO1 (Amante and Eakins, 2009).

Windley *et al.*, 2007; Xiao *et al.*, 2010). There is some agreement about an assemblage of microblocks and island arcs, which formed a proposed Kazakhstan-Tianshan microcontinent in Ordovician times (Filippova *et al.*, 2001; Kheraskova *et al.*, 2003), marked by voluminous collisional granite plutonism. This process, however, is not an element of the Şengör *et al.* (1993) model, who instead associate the Kazakhstan fragments with the Cambrian Kipchak island arc, which formed the Kazakhstan orocline. During the remaining Palaeozoic period, between Middle Ordovician and Permian times, the complete Turkestan oceanic domain was subducted along various active continental margins, leading to subsequent collision of the Kazakh-Tianshan continent with Baltica, Siberia, Alay-Tarim and the Turan blocks (Fig. 5.2). Subduction processes, and the amalgamation of Laurasia came to an end in the Moscovian (Samygin and Burtman, 2009). Due to northward to north-westward subduction of the Palaeoethys in the late Palaeozoic period, the whole area was subjected to large scale compressional tectonics, involving major strike slip fault systems and rotational reorganization (Bazhenov *et al.*, 1999; Buslov, 2011).

After complete closure of the Palaeotethys the northern passive margin of the Neotethys was activated (Stampfli *et al.*, 2002). It has been suggested by several palaeomagnetic studies (Bazhenov *et al.*, 1999; Bazhenov and Mikolaichuk, 2004), that after Permian times large scale rotational reorganization in Central Asia was localized in the Pamirs and east of Tibet. Even though Cenozoic Alpine deformation rejuvenated some older faults (Bazhenov *et al.*, 1999), amounts of overall displacements and rotations during the Cenozoic are suggested to be only moderate to negligible (Dewey *et al.*, 1989; Bazhenov and Mikolaichuk, 2004).

The majority of Palaeozoic rocks studied palaeomagnetically is located in this, south-western part of the CAOB and are geographically concentrated in the Tianshan Mountains and the central Kazakhstan uplands (Fig. 5.3).

5.3 Major Plate Tectonic concepts for the evolution of the CAOB

The complexity of active continental deformation has been intensively studied in the past (Gordon (e.g. 1998); Thatcher (e.g. 2009) and references therein) and it became evident that the concept of well defined, narrow plate boundaries is not always strictly applicable. Plate boundaries are also expressed in wide deformation zones, diffuse plate boundaries, reaching widths

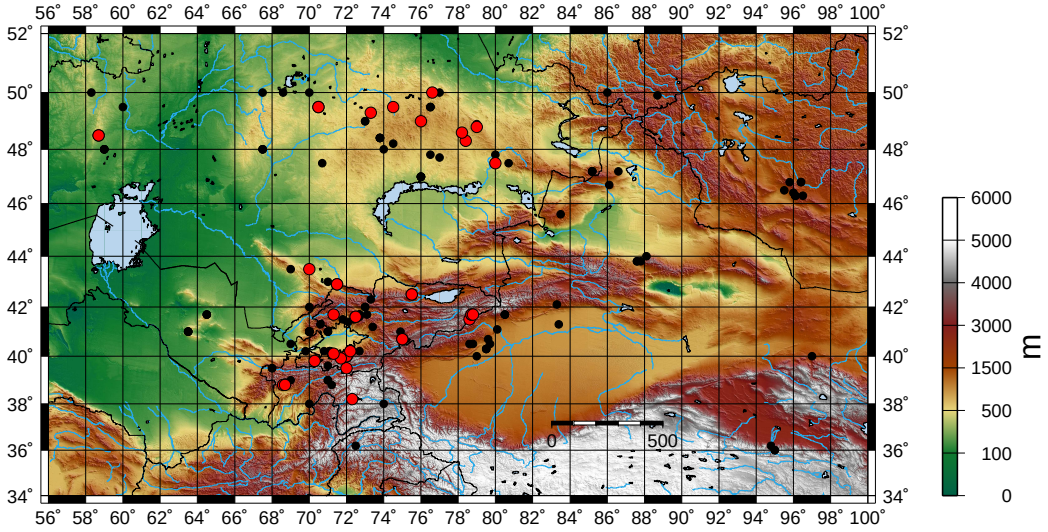

Figure 5.3: Topographic map of the south-western segment of the Central Asian Orogenic Belt, dots indicate study locations of (a): black dots represent general database query, (b) red dots represent selected high quality studies. Map was created using GMT of Wessel and Smith (1998) and topographic dataset ETOPO1 (Amante and Eakins, 2009).

exceeding 1000 km and covering about 15% of the Earths surface (Gordon, 1998). This consequently leads to disintegration of wide areas of the continental lithosphere and to the formation of a great number of tectonic (sub-) plates which are incorporated within the diffuse plate boundary. In terms of vertical axis rotation, which can be especially investigated by palaeomagnetic data, the disintegration of the uppermost brittle lithosphere can lead to a complex pattern of rotational movements.

During the whole evolution of the CAOB oblique subduction and oblique continent-continent collision took place several times.

5.3.1 Subduction zones

During amalgamation of Laurasia, subduction of the Palaeoasian Ocean caused the major stress fraction of the area. This large subduction system, like most of modern analogues, is thought to show oblique geometry (Natal'in and Şengör, 2005). Oblique subduction results in the formation of large

strike slip fault systems rearward to the major subduction front (M.E. Beck, 1991) and consequently Natal'in and Şengör (2005) explain the formation of the Altaids by arc-slicing and arc-shaving, induced by oblique subduction under a giant arc structure.

5.3.2 Collision zones

Collision related strike slip fault systems are often linked to oblique convergence and accommodate the non-orthogonal stress direction. Block rotations associated with these strike slip fault systems can follow a structured mechanisms (Mandl, 1987), or complex movements of brittle, crustal pieces, reacting to trans-tensional deformation (Taylor *et al.*, 2008). Additionally, Peacock *et al.* (1998) emphasize the importance of small faults during rotational movements, accompanying oblique compression.

A more simple approach of collisional movements is the concept of

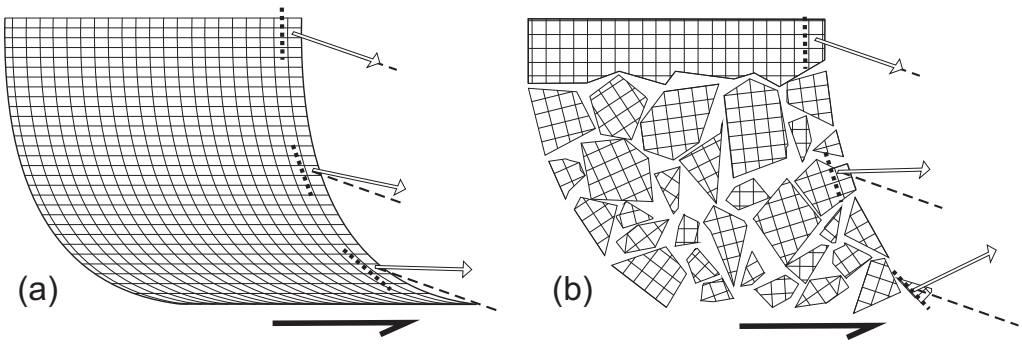

Figure 5.4: Block models for deformation zone due to shearing, modified after Nelson and Jones (1987), with global strike (thick dotted line), local declination (thin dotted line) and deviated declination (white arrow).

oroclinal bending. It describes rather homogeneous bending of originally straight structures (e.g. Van der Voo, 2004). Nelson and Jones (1987) describe principal models for deformation pattern in a shear zone, based on palaeomagnetic data. Two important end members of these models are the smooth oroclinal bending model and a small block model, where the brittle crust is broken up into small units (Fig. 5.4). They found varying amounts in declination deviation on a very small scale of a few kilometers in southern Nevada and explain this observation by a highly fragmented crust, which

shows the expected clockwise rotations in response to continuous left lateral oblique deformation at greater depths. This occurs, however, in an incoherent manner ((b) in figure 5.4).

Based on the geodynamic evolution, involving the collision of Alay-Tarim blocks with Kazakhstan and squeezing of the Kazakh terranes between them, Baltica, and Siberia, it is not remarkable, that oroclinal bending has been assumed. Connecting the North-South striking Urals with the East-West striking Tianshan via the Northwest-Southeast striking Karatau suggests that this orogenic system is an orocline (Kirscher *et al.*, 2013), which agrees with a geodynamic setting where Kazakhstania is situated and deformed between Baltica to the West, Siberia to the East and Alay-Tarim to the South.

5.4 Recent palaeomagnetic Studies of the Area and their Interpretations

Most Russian palaeomagnetic studies (Filippova et al. [2001] and references therein) were primarily designed to yield information on palaeogeographic settings attempting to incorporate the Kazakh terranes and the remnants of palaeo-oceans in a global plate tectonic framework.

Alexyutin *et al.* (2005) investigated Ordovician and Silurian limestones from the Kendyktas ridge and Chu- Yili Mountains in south Kazakhstan. They identified primary pre-folding components of magnetization and conclude a latitudinal agreement of their data with Baltica since the Ordovician. In addition, they report deviations in declination with respect to the Baltica reference data, which indicate counterclockwise rotation of the area of up to 140°. The good agreement of these data with data from the North Tianshan was used as an argument not in favor of oroclinal bending as dominant deformation feature at least in this part of Kazakhstania. Their apparent polar wander path (APWP) for south Kazakhstan, defines a loop swinging across the southern tip of Africa (in present coordinates) towards the east ($\sim 100°$E) from the Ordovician to the Permian, down towards the south pole ($> 60°$S) and back to the southern Atlantic.

This is in contrast to the results of **Abrajevitch *et al.* (2008)** who interpret their results from Devonian and Permo- Carboniferous rocks of central Kazakhstan to be in accord with the oroclinal bending concept and in agreement with structural data from the region. They explain the observed deviation in declination which follows the change in regional strike to

reflect the bending of an originally straight volcanic arc, during the collision of Siberia, Baltica and Tarim. This process came to an end in Late Permian times.

Bazhenov *et al.* (2003) studied Ordovician and Carboniferous rocks from Kyrgyzstan and Kazakhstan. They identified a northward drift of the North Tianshan zone during most of the Palaeozoic. Additionally, they found a spread in declination values, which they explained by small scale relative rotations of a not entirely rigid body.

Van der Voo *et al.* (2006) investigated Upper Palaeozoic volcanics and sediments from southeast Kazakhstan and report inclinations in good agreement to the Baltica reference values. In contrast, the declinations reported in this study reveal a high degree of scatter prompting the original authors to adopt Natal'in and Şengör (2005)'s line of argumentation, which explains these observations by wrench faulting during collision accompanied by strike slip faults and caused by subduction.

Most recently, **Kirscher *et al.* (2013)** presented a study from the Karatau Range, where they show, that the remagnetization of Devion and older rocks in the region are linked to major deformational events in this area. There, amounts of vertical axis rotations are only present up to $\sim 60°$. They concluded that this is an indication for the structural coherence of the Ural-Karatau-Tianshan junction, and that deformation, expressed by vertical axis rotation, is increasing from the Urals towards the Tian Shan.

5.5 Evaluation of All Available Data

To address this debate we evaluate palaeomagnetic data, extracted from the IAGA GPMDB[1] covering a geographic spread between $35° - 52°$ latitude and $56° - 100°$ longitude (black dots in figure 5.3). These data without any further threshold criteria besides the exclusion of known secondary magnetic signals ('Eliminate known secondaries' option of the database query), were compared with selected high quality studies containing positive tests of reliability, such as reversal-, conglomerate- and fold- tests (red dots in figure 5.3, figure 5.5). The main selection criteria of the high quality data is the presence of these tests of reliability. We choose 44 paleomagnetic studies. The selected studies were also examinated using the 'Van der Voo criteria of reliability' (Van der Voo, 1990). Rock age was treated as reliable, if the age is reported within a range of less than 20 Ma, demagnetization when the

[1] http://www.ngu.no/geodynamics/gpmdb (January, 2012)

No.	Rock unit	Sed.	Vol.	Age low	Age high	VGP Lat.	VGP Long.	dp	dm	Test	Q	Reference
1	East Kazakhstan Volcanics		x	245	251	42.0	140.0	5.3	6.5	F	3	Rusinov, 1986
2	Tuzkul Formation			251	260	52.9	186.5	5.3	8.4	M	3	Bazhenov et al., 1995
3	Tuzkul Formation			251	260	44.2	196.3	4.5	8.2	M	3	Bazhenov et al., 1995
4	Hanaka Formation			251	271	78.2	212.0	3.5	5.5	F	3	Bazhenov et al., 1993
5	Gundara Formation			268	271	72.9	252.9	5.3	9.1	F,G	4	Bazhenov, 1996
6	Alaisky Range	x	x	251	299	59.1	342.2	2.9	4.2	F	3	Didenko and Pechersky, 1986
7	Alaisky Range	x	x	251	299	69.8	338.5	15.1	21.3	F	3	Didenko, 1989
8	Northern Tien Shan Volcanics and Sediments	x	x	251	299	63.4	181.8	5.5	8.3	F	3	Audibert and Bazhenov, 1992
9	Northern Tien Shan Volcanics and Sediments	x	x	251	299	70.8	306.5	5.2	8.0	F	3	Audibert and Bazhenov, 1992
10	Arpa and Masail suites			271	299	75.5	284.7	21.3	33.2	F	2	Biske et al., 1993
11	Luchob Formation			271	299	55.8	319.7	3.5	5.8	F,G	3	Bazhenov et al., 1993
12	Arpa and Masail suites			271	299	72.8	299.5	16.0	25.0	F	2	Biske et al., 1993
13	Kipchak seria			307	312	27.4	312.4	6.5	12.8	F	3	Biske et al., 1993
14	Kyzylkanat Group			299	330	63.0	194.0	5.7	8.9	F	3	Sholpo and Rusinov, 1971
15	North Tien Shan sediments	x		312	318	53.8	202.1	4.2	4.2	F	4	Bazhenov et al., 2003
16	Alaisky Range	x		307	335	60.2	335.0	13.4	20.0	F	2	Didenko and Pechersky, 1989
17	Tabylgaty Red Beds	x		318	345	61.6	287.2	5.4	5.4	F	3	Bazhenov et al., 2003
18	Saribel suite			345	359	28.3	302.3	6.8	13.2	F	3	Biske et al., 1993
19	Saribel and Kaychin suite			345	375	29.3	301.7	7.9	15.2	F	2	Biske et al., 1993
20	Kokshaay Range	x		359	385	15.0	337.0	6.0	12.0	F,R	3	Biske, 1993
21	Alaisky Range		x	359	416	48.7	327.1	3.4	5.9	F	3	Didenko and Pechersky, 1989
22	Tyuritayskaya suite			359	416	58.0	208.0	2.9	4.8	F	2	Grishin et al., 1991
23	Chingiz Range		x	385	392	-11.3	85.1	13.2	13.2	N	3	Levashova et al., 2003
24	Kurkudukskaya suite			392	398	8.5	135.8	5.4	9.9	F,R	3	Pechersky and Didenko, 1995
25	Shuldaksky Complex	x		392	398	4.9	129.9	4.1	7.4	U,R	3	Pechersky and Didenko, 1995
26	Southern Tien Shan	x		398	416	42.3	323.7	3.9	7.1	F,R	3	Klishevich and Khramov, 1995
27	Southern Tien Shan	x		398	416	42.8	297.5	3.8	7.6	F,R	4	Klishevich and Khramov, 1995
28	Southern Tien Shan	x		398	416	45.2	296.7	3.6	7.1	F,R	5	Klishevich and Khramov, 1995
29	Southern Tien Shan	x		398	416	45.1	301.7	3.9	7.7	F,R	5	Klishevich and Khramov, 1995
30	Zhalair Range			398	416	-6.8	316.0	9.5	15.5	G,R	4	Pechersky and Didenko, 1995
31	Ferghana Dolerites and Gabbros		x	398	416	-10.3	31.3	3.2	5.1	G,F,R	3	Pechersky and Didenko, 1995
32	Ferghana Dolerites and Gabbros		x	398	428	33.1	340.6	1.7	3.0	G,F	2	Pechersky and Didenko, 1995
33	Chingiz Range	x	x	428	444	-33.6	32.7	9.4	9.4	F,G,R	5	Levashova et al., 2003
34	Mayljen sediments	x		444	461	38.0	264.0	5.0	10.0	F	3	Grishin et al., 1991
35	Northern Tien Shan Sediments	x	x	444	461	31.1	214.7	2.9	2.9	F	4	Bazhenov et al., 2003
36	Bazarbaysky	x	x	461	472	-30.0	60.0			F	3	Turmanidze et al., 1991
37	Chingiz Range	x		472	488	-43.9	127.8	11.5	11.5	F	4	Collins et al., 2003
38	Chu-Yili and Kendyktas	x		400	430	56.7	279.3	7.1	13.4	F,R	4	Alexyutin et al., 2005
39	Chu-Yili and Kendyktas	x		458	470	59.8	174.6	5.4	8.0	F(-)	3	Alexyutin et al., 2005
40	Chu-Yili and Kendyktas	x		470	490	37.7	243.3	8.0	15.5	F	4	Alexyutin et al., 2005
41	Kyrgyz Kokchetav-North Tien Shan		x	364	370	34.4	3.5	9.3	12.9	G	4	Levashova et al., 2007
42	Devonian volcanic belt		x	275	305	42.2	178.8	5.2	3.1	F,R	5	Abrajevitch et al., 2008
43	Devonian volcanic belt		x	251	275	56.3	180.6	5.5	3.7	F	4	Abrajevitch et al., 2008
44	Devonian volcanic belt		x	275	305	13.5	138.0	8.5	5.7	F,G	5	Abrajevitch et al., 2008

Figure 5.5: High quality studies from the South- Western segment of the CAOB. Sedimentary (Sed.) and/or volcanic (Vol.) are used for the analysis, age range (with lower and upper limit), latitude and longitude with errors (dm and dp), conducted palaeomagnetic tests of reliability (F - fold test, M - rock magnetic test, G - conglomerate test, R - reversal test, N - no tests, U - unconformity test, (-) indicates negative test) and Q - quality factor (Van der Voo, 1990) are noted.

DMC code exceeded 4 (for details see the description of the Global Paleo-

magnetic database, http://www.ngu.no/geodynamics/gpmdb/). Over 86% of the studies have a Q value larger or equal to 3, whearas 34% have a Q value larger than 3 (Fig. 5.5).

This high quality data includes most recent results on palaeogeography of this area. For comparison, two palaeomagnetic poles from the south-easternmost part of the Ural Mountains are also included in the data compilation (Slautsitais, 1971; Svyazhina, 1971; Pechersky and Didenko, 1995; Burakov and Didenko, 1984). Most of the available palaeomagnetic studies have been carried out either in the Tianshan Mountains, or in the central Kazakhstan upland, north of Lake Balkhash. These two areas are differently color-coded in all plots to identify possible systematic differences. All plots are based on data resulting from the general query of the GPMDB, indicated by small symbols. Results fulfilling high quality requireements are indicated by larger and/or different symbols. The oroclinal bending test, comparing deviation in declination from the expected values vs. deviations in regional strike with respect to the Ural Mountains was carried out using only high quality data (e.g. primaty character of magnetization established by positive stability tests). The two major areas, Tianshan and Kazakhstan upland, are illustrated also differently. The two data compilations are compared with the respective values of the APWP of Siberia and Baltica. They are extracted from the studies of Cocks and Torsvik (2007) and Torsvik *et al.* (2012), which represent most recent high quality APWPs of the two cratons.

These two craton represent the bordering plates, which on one hand are thought to exist since the Early Palaeozoic, and from which on the other hand palaeomagnetic data is available from a huge variety of rocks with different formation ages. Palaeomagnetic data from Tarim, Junggar and the Turan blocks, which are adjacent to the CAOB to the South, is sparse and prior to the late Carboniferous only very few studies are available. Therefore, for our global approach only the comparison with Baltica and Siberia was made.

5.6 Palaeolatitudes

In a first step, palaeopole positions (Fig. 5.5) were converted into palaeolatitudes for the individual studied areas in order to detect major latitudinal differences between individual tectonic units and differences with Baltica and/or Siberia, respectively. As pointed out by several authors (e.g. Bazhenov *et al.*, 2003; Alexyutin *et al.*, 2005; Abrajevitch *et al.*, 2008), there

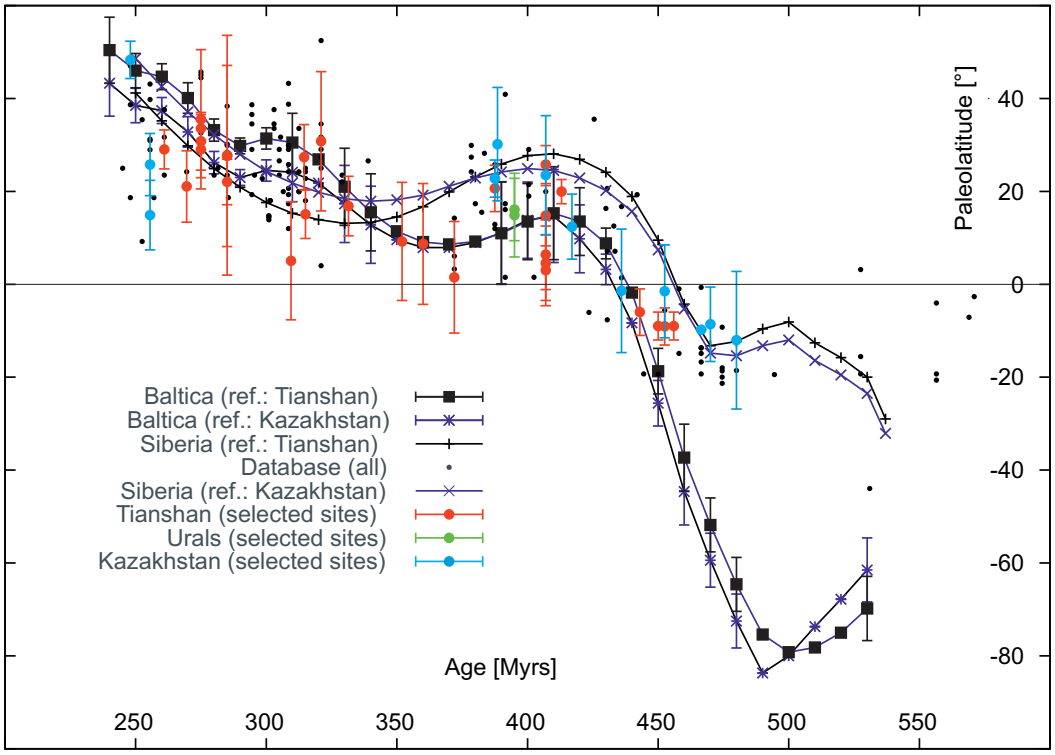

Figure 5.6: Palaeolatitudes plotted versus age, for all data points (small black dots) and for the high quality studies (large circles). Different colors indicate different study area. Lines represent respective palaeolatitude values for the Baltica/Siberia APWP (Cocks and Torsvik, 2007; Torsvik *et al.*, 2012), calculated for reference sites in the Tianshan and Kazakhstan upland, respectively.

seems to be latitudinal agreement between the major cratons and tectonic units from the south-western part of the CAOB. Within the Fisherian error limits (Fisher, 1953) (Fig. 5.6) there is no major latitudinal difference between the Kazakhstan blocks or microcontinents and the major cratons to the east or west. This also implies that there is no significant difference in palaeolatitude between individual blocks. However, a northward movement of these small tectonic units can be identified between $\sim$ 470 Myrs and $\sim$ 380 Myrs, similar to both cratonic units, but before $\sim$ 450 Myrs, a vicinity to Siberia rather than to Baltica is visible.

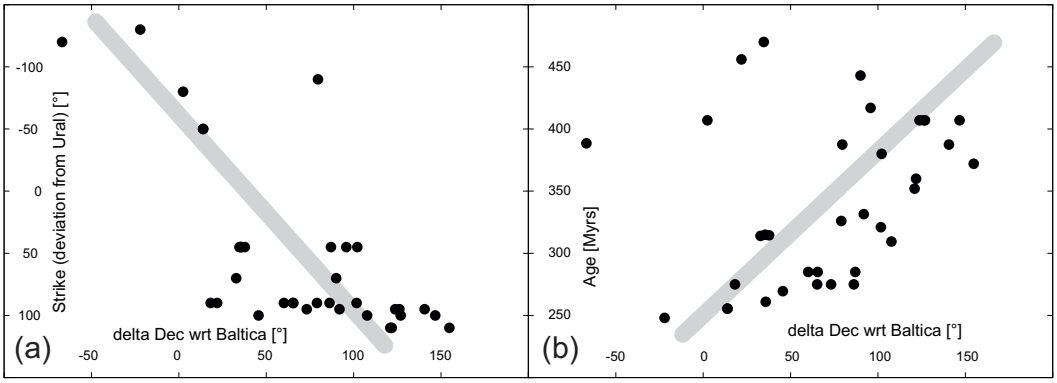

Figure 5.7: Plot of declination deviation between measured declination and declination obtained from associated values of the APWP of Baltica versus (a) strike deviation with respect to the Ural Mountain Chain, where 0 strike is equal to a roughly N-S orientation. Positive values represent rotational deviation with counterclockwise sense. (b) plot of declination deviation versus age of acquisition of magnetization. Grey line indicates broad trend in both plots.

5.7 Oroclinal Features

A second approach to structure the data is made by calculating declination differences between the declination of the studied rocks and appropriate declinations obtained from the apparent polar wander path of Baltica for a reference site located in the Tianshan and the Kazakhstan upland, and compare them with age and strike deviations, which follow the curved shape (Figs. 5.1+5.2). This procedure is undertaken to associate the curved geologic features with bending during the orogenic event, which would have affected all primary declinations from this area. Since the main collisional phase in this area took place in the Late Palaeozoic (Windley *et al.*, 2007), all declinations investigated in this work should show declination deviations. One u-shaped flexure within the North Tianshan and Chingiz Range has already been shown by palaeomagnetic data (Abrajevitch *et al.*, 2007) to represent a formerly straight structure now bent into an orocline.

To test whether this concept can also be applied to other parts of the orogeny, firstly the declination deviations were plotted against general strike deviation with respect to the Ural Mountains (0, 0 represents the Urals in

declination of Baltica and strike with north/south, + corresponds to counterclockwise sense of deviation, and vice versa), following the 'Schwartz-plot' to detect oroclinal bending (Schwartz and Van der Voo, 1983) (a in figure 5.7). Secondly, the declination deviation is plotted against age, to identify possible time dependant increase of rotation values (b in figure 5.7). Declination deviations versus strike deviation show only minor correlation, which would suggest an increase of declination deviation with increasing structural deformation. Additionally, the Kazakhstan upland show positive strike deviation, which means clockwise strike deviation compared to the Ural Mountains, and negative or counterclockwise declination deviations. These results would be in agreement with the suggested oroclinal bending of the central core of the Kokchetav-North Tianshan domain (Levashova *et al.*, 2007; Abrajevitch *et al.*, 2007). However, the correlation is highly spread, showing a huge variety of declination deviations, especially in the Tianshan Mountains (strike deviations of $-50°$ up to $-120°$).

Inspection of figure 5.7 (b) suggests that the amount of rotation decrease with decreasing formation age of the magnetization. However, the spread is again very large.

5.8 Interpreting Palaeopole positions

Finally the palaeopole positions were investigated, which were deduced from the overall mean directions of the studies. The palaeopoles were transformed into palaeo south-poles and compared with the APWP of Siberia and Baltica. Poles obtained from the general query are circles and smaller than poles obtained from the selected studies. All of the poles and the running mean poles of the APWP are color-coded with age.

Inspection of figure 5.8 reveals a huge spread of palaeopoles in the southern hemisphere between 0° and 180° in longitude. To allow interpretation of the 2D projection, small circle bands centered on the sampling regions are indicated in grey. Vertical axis rotations should lead to rotation of the poles on this paths. Clustering of poles in certain areas of these bands would indicate the existence of larger areas, which suffered the same rotational history. It seems, however, that the distribution of poles is rather uniform, and all amounts of rotations are present in the data. A focus on the high quality studies does not simplify the picture very much. Especially Permo-Carboniferous rocks show this pattern. Older rocks, which are less abundant, display a somewhat more difficult behavior. This might also re-

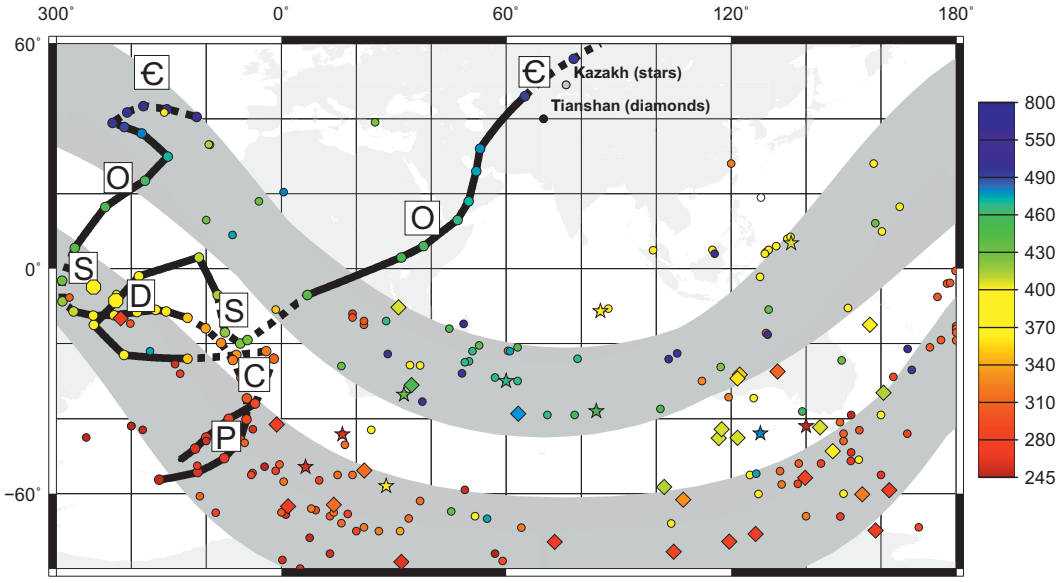

Figure 5.8: Palaeo- south poles of all data points (small circles) color-coded with age plotted together with the APWPs of Siberia and Baltica (Cocks and Torsvik, 2007; Torsvik *et al.*, 2012). Larger diamonds (Tianshan) and stars (Kazkahstan upland) represent the high quality studies. Dashed and solid lines of the APWPs indicate different periods of the Palaeozoic, namely P: Permian, C: Carboniferous, D: Devonian, S: Silurian, O: Ordovician and ∈: Cambrian.

flect the loops of the APWP. The uniform distribution of poles of the same ages (intervals of less than 40 Myrs), argues against a separate polar wander path of a Kazakh terrane, which behaved as a single block since Ordovician times. The fast and large scale latitudinal movement of this terrane, which is indicated by palaeopoles, which have been recorded between $\sim$ 280 and $\sim$ 430 Myrs ago (Fig. 5.8) is also rather unlikely.

5.9 Conclusion

An attempt has been made to summarize all available palaeomagnetic data of Palaeozoic rocks from the southern segment of the CAOB. They were compared with high quality studies from the area. It turned out, that all

the data shows several features, which can not be simplified by considering only high quality data. Concerning palaeolatitudes, the data is consistent with a palaeoposition adjacent to Baltica and/or Siberia since Ordovician times. Before the Ordovician, a closer affinity only with Siberia would be possible. In general, both the Tianshan mountains and the central Kazakhstan uplands seem to represent rocks from one single palaeogeographic area since ~ 470 Ma in terms of palaeolatitudes, and different early Palaeozoic micro terranes might have been amalgamated or close together since that time. The palaeopoles of all Palaeozoic rocks are deviated away from the APWPs of Baltica and Siberia in a counterclockwise sense with amounts of $0° - > 100°$. These rotation values are only very broadly a function of age or position but are uniformly distributed. A more detailed description for the whole area, like the construction of an APWP of the area, has become impossible due to the various amounts of vertical axis rotations, which lead to a smeared distribution of palaeopoles.

We interpret these observations by the deformation, including shortening and faulting, of the amalgamated accretionary orogen in the Late Palaeozoic, caused by oblique stress directions. Within this zone the degree of rotation can vary largely in narrow intervals (Fig. 5.9).

A true and detailed verification of the paleogeographic history of this area is difficult based only on palaeomagnetic data. Only at a smaller scale, like the Devonian volcanic belt (Abrajevitch *et al.*, 2007), the detection of homogeneous oroclinal bending by palaeomagnetic data is promising. On the global scale, the bending of the whole area, which accompanied the closure of the Palaeoasian Ocean, is affected by complex tectonic deformation during and after the amalgamation in the Late Palaeozoic. Features like arc slicing and arc shaving (Natal'in and Şengör, 2005), bookshelf pattern (Mandl, 1987), occurrence of small faults with various orientation (Peacock *et al.*, 1998) or the response of a brittle crust to lithosphere movements (Nelson and Jones, 1987), evidently obscured the simple bending enormously (Fig. 5.9).

The identification of small early Palaeozoic terranes seems therefore only feasible using exclusively palaeolatitudes and accept any amount of declination deviation of 0° to above 100°.

It also has to be noted, that our rough approximation using all available palaeomagnetic data underlines the limitations of palaeogeographic reconstructions using this technique only, even though this is the only direct procedure of obtaining them. Based on all published palaeolatitudes from the discussed area, for example, it is already difficult to decide to which cra-

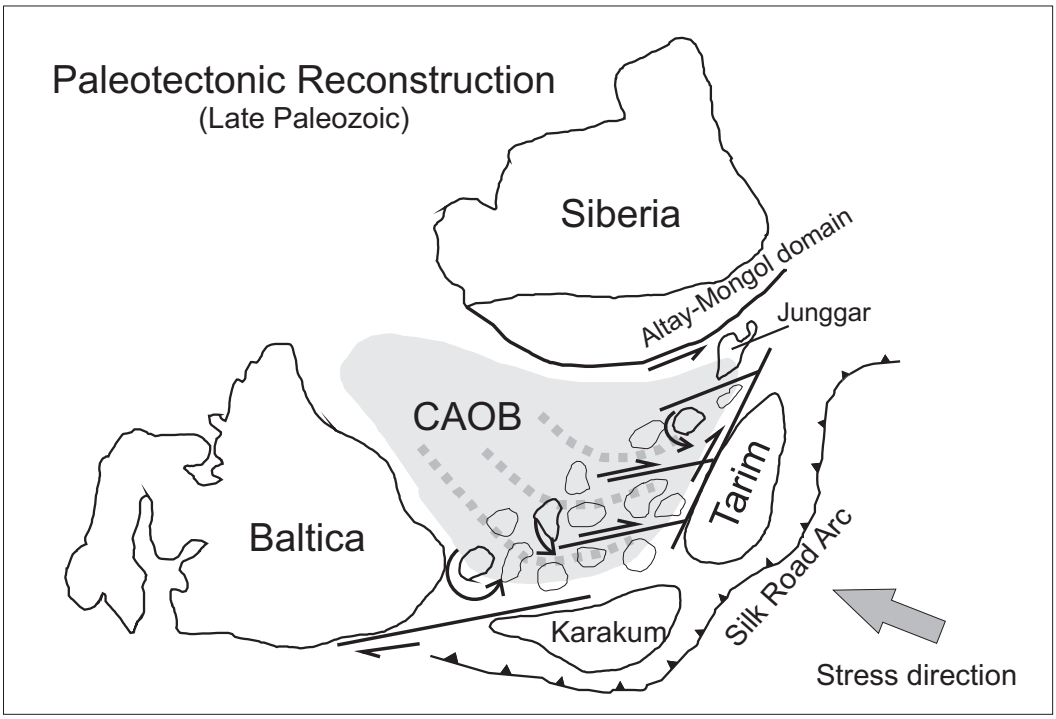

Figure 5.9: Proposed simplified palaeotectonic scenario of the Late Paleozoic deformation pattern (modified after Natal'in and Şengör (2005)). Arc slicing, collision of Tarim, Karakum Siberia and Baltica and the brittle crustal response of the CAOB deformation zone is responsible for the observed variations in the palaeomagnetic data set. Small brittle units within the deformation zone can have suffered different amounts of vertical axis rotations. Large strike slip faults are indicated as well as subduction system under the Silk-Road Arc. Dotted lines mark the general bending behavior.

ton potential pieces of the CAOB might have been associated to. It seems evident, however, that all microterranes of the south-western segment of the CAOB have been located at low latitudes close or to the south of the palaeoequator in the Ordovician. Whether this supports amalgamation of a large Kazakh microcontinent in the Late Ordovician, as suggested by Filippova *et al.* (2001), the coherence of all microterranes with Siberia (Fig. 5.6), or points towards Gondwanan affinities of these terranes Popov *et al.* (2007) cannot be solved palaeomagnetically based on the currently available data set. Therefore, we are still in urgent need for more high quality studies in

order to solve the palaeogeographic puzzle of the CAOB and its detailed evolution prior to the final amalgamation in the Late Paleozoic.

6

Preliminary investigation of recent and active rotational movements within the study area

by ***U. Kirscher in cooperation with M. Hackl and A. Bande***

6.1 Introduction

In the previous chapters, especially chapters 2, 3, and 4 it has been shown that paleomagnetic analysis can be applied very successfully even in tectonically complex areas such as the CAOB. Based on the compilation of all paleomagnetic data available for the region (chapter 5) it has been show that the rotational history, however, of tectonic elements within the CAOB is not easily reconstructed. One explanation for the homogeneous distributed paleopoles would be a brittle fragmentation of the upper crust during the final amalgamation of Eurasia at the end of the Paleozoic. On the other hand the area of interest was subjected to further deformation

more or less throughout its entire history caused by the subduction of the Tethys ocean and the India/Asia collision. Therefore, another explanation for the diffuse distribution of paleopoles might be that the old paleomagnetic signals got obscured by younger phases of deformation. It is known that especially large faults can cause large amounts of vertical axis rotations in their surroundings.

Additionally, according to the micro block model, active deformation should be localized along the boundaries of rigid areas. If those blocks and their recent deformation rates can be defined, it might also be possible in the future to subtract Cenozoic and/or Mesozoic rotation amounts and by this decompose the complex Paleozoic rotational pattern indicated by paleomagnetic data. If the active deformation indicates separable blocks with differing rotational movements, it might be possible to relate these areas with old Paleozoic terranes. Complications of this approach include (a) a missing agreement between active and recent tectonic movement and (b) that the young brittle response represents only the Cenozoic fragmentation and can therefore not be related to Paleozoic terranes at all.

The Talas-Ferghana Fault (TFF) is a reactivated late Paleozoic strike

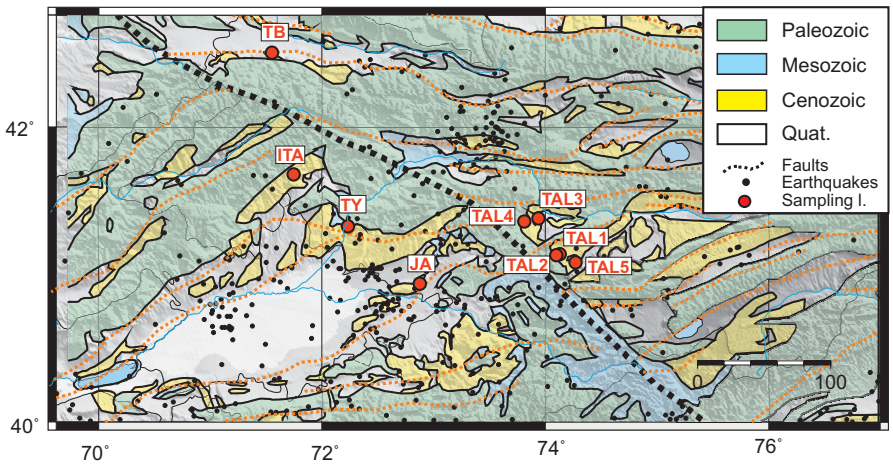

Figure 6.1: Simplified geologic map of the Kyrgyz Tianshan with Cenozoic paleomagnetic sampling sites. Also indicated are the TFF (black) and other major faults in this area (red). Small black dots represent recent earthquakes in the area.

slip fault with an estimated offset of several hundred kilometers. It is known

to have caused considerable amounts of rotation in its vicinity, and might therefore serve as a representative example to investigate the recent rotational history and its correlation to the present day deformation field.

Several sites of Paleogene to Neogene age on the territory of Kyrgyzstan (Fig. 6.1) have been studied paleomagnetically and were compared to the present day deformation field base on GPS observations (Zhang *et al.*, 2004; Zubovich *et al.*, 2010).

In contrast to the interpretation of Bazhenov and Mikolaichuk (2004), that rotational reorganization did not significantly affect the south-western part of the CAOB after late Paleozoic amalgamation, there are indications suggesting considerable rotational movements in the Tianshan during the Cenozoic. These rotations total up to $\sim 20^\circ - 30^\circ$ between the Ferghana and Issyk-Kul basins (e.g., Thomas *et al.*, 1993; Wack *et al.*, 2014).

The Cenozoic tectonic evolution of the Tianshan and the southern part of the CAOB is controlled by the India-Asia collision. After a phase of tectonic quiescence between Cretaceous and most of the Paleocene (Molnar and Tapponnier, 1975), the collision of India with Eurasia triggered tectonically controlled sedimentation within the Tianshan in the Oligocene with the predominance of Molasse type red and grey sediments (Bakirov *et al.*, 2001; Bakirov and Mikolaichuk, 2009).

It has been pointed out that up to one half of the total north south convergence of India-Eurasia is taken up within the Tianshan causing formation of strike slip fault systems and rotational movements of individual blocks and/or basins confined within large deformational zones (Zubovich *et al.*, 2010; Buslov, 2011).

Several theories exist, how strike slip faults can cause different reactions in terms of vertical axis rotations, especially if the fault is not confined by a narrow zone of several kilometers but widespread (Nelson and Jones, 1987; Aubele *et al.*, 2012).

6.2 Paleomagnetic results of Paleogene to Neogene deposits

In order to gain information about the general feasibility of this approach, preliminary samples for paleomagnetic analysis were taken at nine sites with different distances to the TFF (Fig.6.1). Some of the data were provided by Alejandro Bande and sampled within a project granted to Prof. Ed Sobel, Potsdam (SO 436/4-1).

The sampled material comprises terrigenous coarse grained grey (sam-

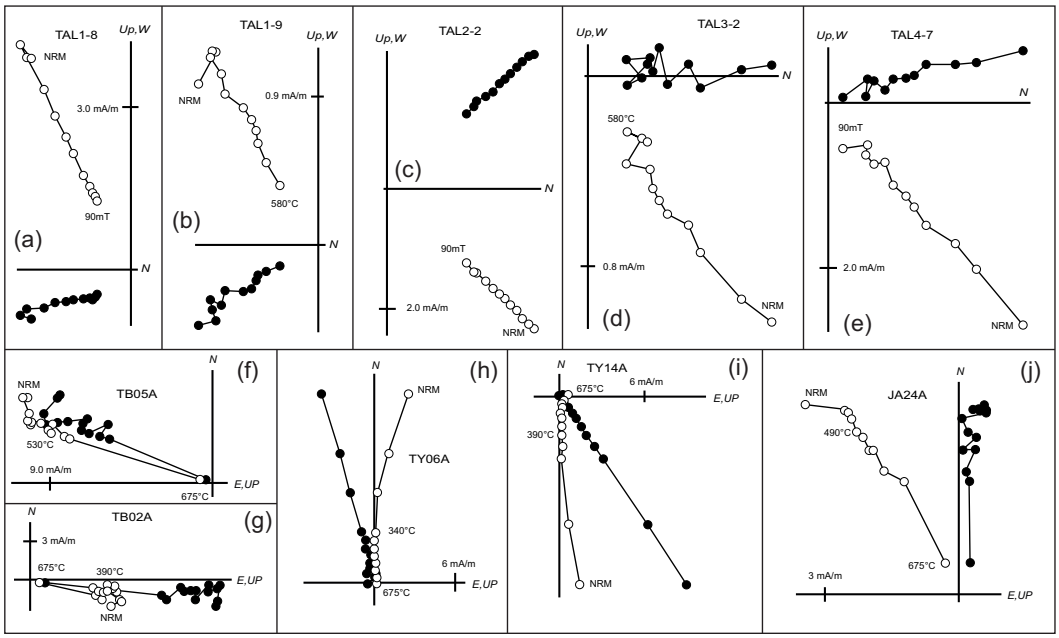

Figure 6.2: Representative results of thermal and alternating field demagnetization experiments plotted as orthogonal vector diagrams (Zijderveld, 1967) in stratigraphic coordinates of Neogene sediments. Solid and open dots represent vector endpoints projected onto the horizontal and vertical planes, respectively. Temperature and alternating field steps in °C and mT are indicated.

pling region TAL) to red (remaining sites) sedimentary rocks of Paleogene to Neogene age. As for almost all terrigenous rocks, it is intrinsically difficult to obtain precise age control due to the lack of magnetostratigraphic information or fossil remains. However, since the region studied formed an integral part of Eurasia at least since the Permian, it is probably sufficient to now the age of the rocks studied on a rather large scale in order to interpret the paleomagnetic data.

All samples were analyzed with thermal demagnetization techniques, with peak temperatures of 600° (TAL) and 700°, respectively. The demagnetization diagrams are characterized by a stable high temperature component (HTC), which points towards the origin of the projection plane (Fig.6.2).

The five sites of TAL show exclusivly positive (TAL-2,3,4) or reversed

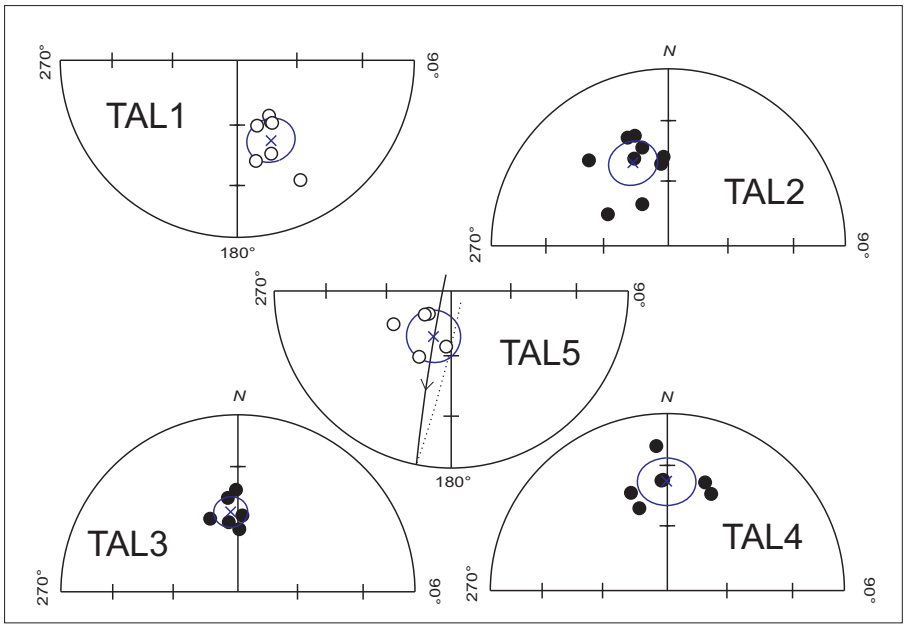

Figure 6.3: Stereographic projection of sample mean directions of results from TAL sites, plotted together with site mean direction and according α_{95} error interval. Solid and open dots represent projection on the upper and lower hemispheres, respectively. One remagnetization great circle is also indicated at site TAL5.

(TAL-1,5) polarities (Fig.6.3), respectively. They agree well with each other and the combined sample direction are antipodal. At one site (TAL-5) one remagnetization great circle was used for calculating the site mean direction. The resulting mean declinations of these sites do not always, however, agree with each other within the α_{95} error interval (Tab.6.3).

The red sediments of sites TB, ITA, TY' (including sub sites TA, TR and TY) and JA show a somewhat more complex demagnetization behavior. Except site TB all sites show very shallow inclinations (less than 10°, in contrast to an expected inclination of $\sim 60°$, Fig.6.4). It is possible that this is related to an inclination shallowing process, which is especially affecting the sedimentary and more needle like hematite grains (Kirscher *et al.*, 2014). To proof this a more detailed study would be necessary. Sites ITA, TB and TY show few but antipodal dual polarity directions (Fig.6.4). Directional data from site ITA was combined with remagnetization great circles to obtain a statistical robust mean direction (Fig.6.4).

Summarizing, our results yield counterclockwise deviations to the ex-

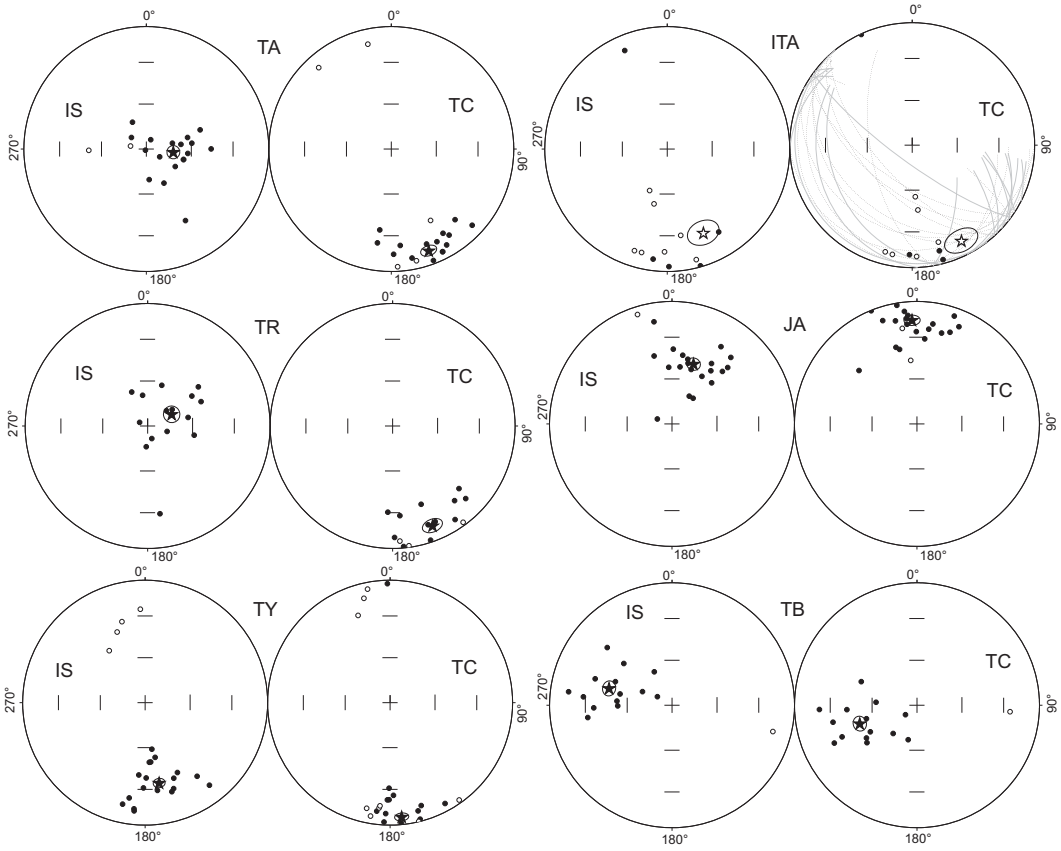

Figure 6.4: Stereographic projection of sample mean directions of results from sites TA, ITA, TR, JA, TY and TB (TA, TY and TR are summarized as TY in the map, because they are situated close together). Solid and open dots represent projection on the upper and lower hemispheres, respectively. Also plotted is the site mean direction (star) and the according α_{95} error interval. One remagnetization great circle is also indicated at site TAL5.

pected declination values for the region calculated for Paleogene to Neogene times (Besse and Courtillot, 2002) of 2° to 30°. Sites TB and TAL5 show a very different pattern of $\sim 110°$ counterclockwise and $\sim 20°$ clockwise deviations. However, our results are in principal agreement with the results of Thomas *et al.* (1993) and do not reduce the ambiguity of the paleomagnetic data from this area. Therefore, even if some of the declination deviations

are still within each others error limits, the rotational changes on a small scale might reflect a primary pattern.

6.3 Active deformation within Kyrgyzstan

Zubovich *et al.* (2010) presented an extensive compilation of active deformation within the Tianshan and adjacent regions. They concentrated on overall north south movements and showed several transsections of GPS velocity data that about two-thirds of the India-Eurasia convergence is taken up by the Tianshan, which was therefore probably built up in only about 10 Ma. We used their data set, in combination with surrounding data of Zhang *et al.* (2004) from China and Eurasia, to calculate a rotational deformation field using the method of Hackl *et al.* (2009).

This technique allows to define rigid blocks and calculate their present day rotation rates (Hackl *et al.*, 2009). However, the results in Figure 6.5 show that the deformation across the Tianshan is rather continuous and rigid blocks cannot be defined easily. In agreement with Zubovich *et al.* (2010), most areas show a slight counterclockwise rotation of $\sim 1^\circ - 2^\circ$ per Myr. Small areas of clockwise rotational movements do not contain GPS stations (Fig. 6.5), which could be a result of interpolation artifacts. Since this area has been under constant stress for at least $\sim$ 10 Myr (Zubovich *et al.*, 2010, and references therein), rocks older than 10 Ma are expected to show a declination deviation of $10^\circ - 20^\circ$ counterclockwise. The continuous deformation pattern does not allow to distinguish the numerous mostly strike slip faults in the area (Fig. 6.5). On the contrary, the interpolated movement show a very smooth decrease of northward movement going from south-east to north-west (Fig. 6.5b). Based on the available data set it is therefore not possible to define rigid blocks in the Tianshan based on active deformation.

6.4 Conclusion and Discussion

The recent and the present day deformations of the Tianshan continue to be rather complex. Based on a small set of Conozoic paleomagnetic data and a GPS velocity field consisting of around 700 data points does not unambiguously allow to define rigid blocks and to estimate their rotation rates. This situation is further complicated by the fact that the deformation has not been constant even through the late Cenozoic.This is exemplified by

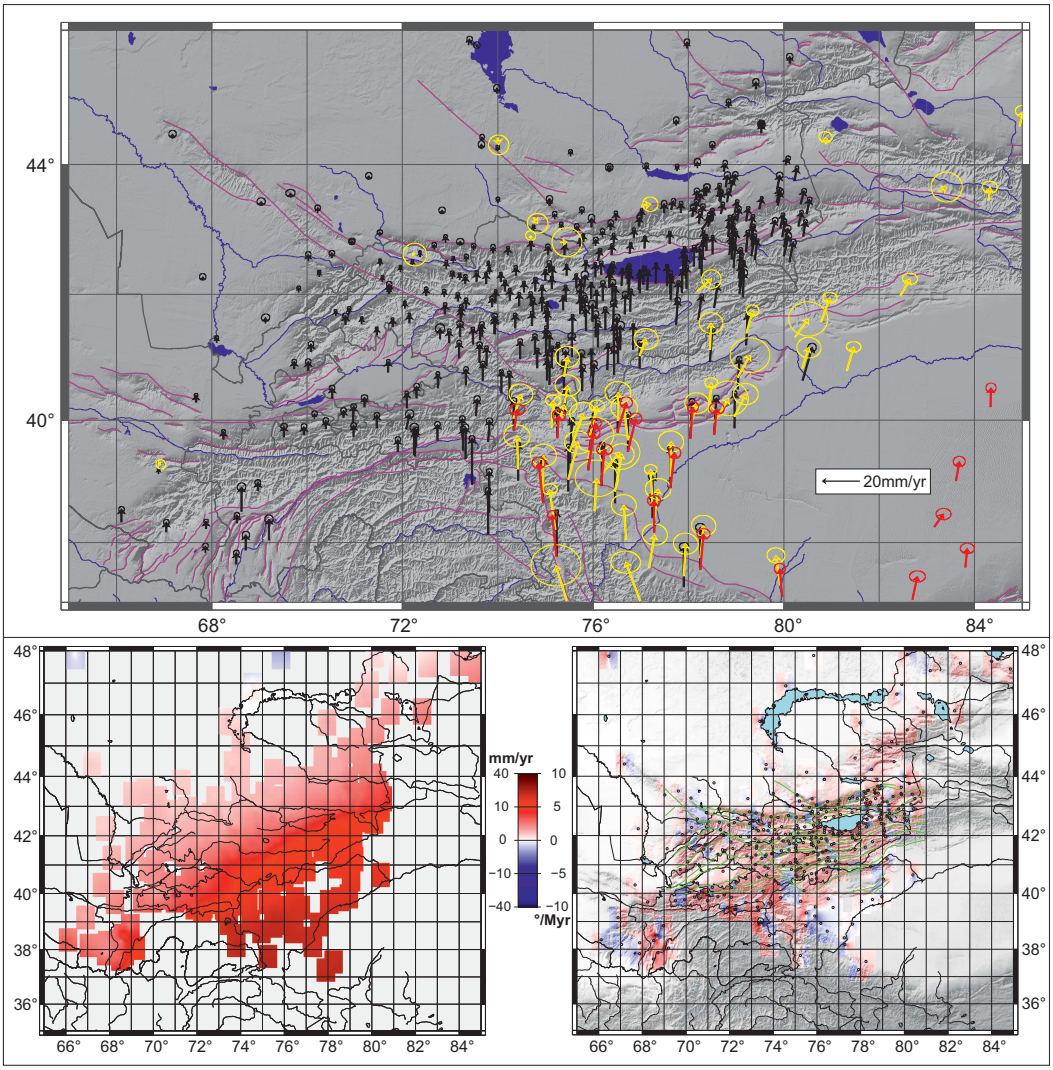

Figure 6.5: Top: GPS velocities with respect to Eurasia from Zubovich *et al.* (2010, black) and Zhang *et al.* (2004, yellow and red) with according error ellipses. Bottom left: Interpolation of the north component of the GPS velocities. Bottom right: Rotation strain rates calculated from the GPS velocities based on Hackl *et al.* (2009).

the TFF, which has evidently been active in the Holocene (with probable slip rates of up to $10\frac{mm}{yr}$) (Burtman *et al.*, 1996), but does not show a deformation signal in the GPS data (Zubovich *et al.*, 2010).

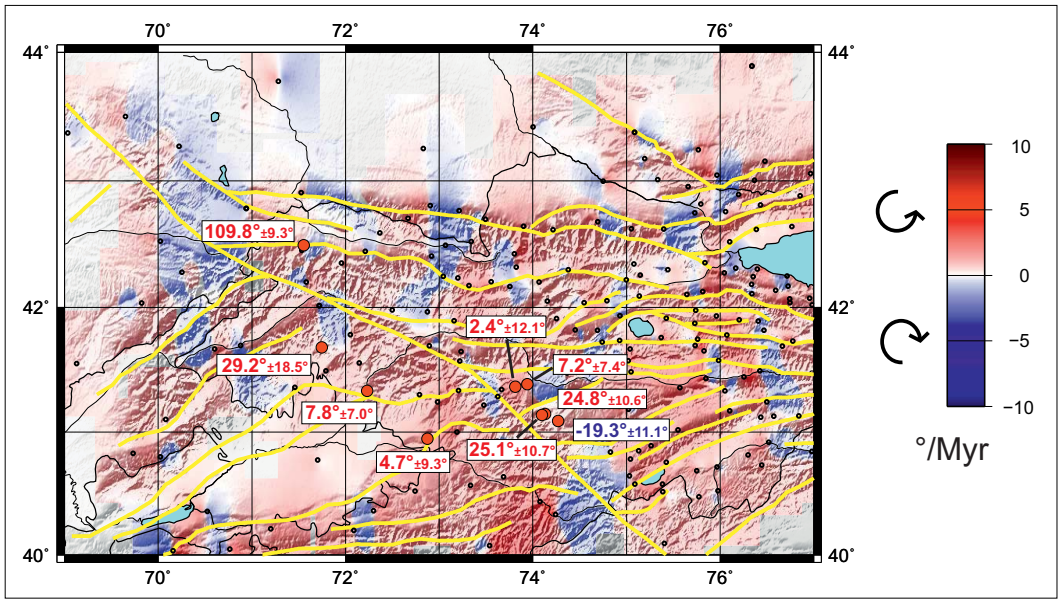

Figure 6.6: Results of comparison of GPS and paleoamgnetic data within Kyrgyzstan. Background colours indicate rotation strain rates in degrees per million year. Paleomagnetic sites are shown with the declination deviation of the ChRM and the expected mean Neogene declination for this area, where red (blue) indicates counterclockwise (clockwise) rotations. α_{95} error intervals of the mean directions are also shown. Grey outline suggests one block with similar rotational history of $\sim 5°$.

We might speculate that the proximity to large faults can increase the amount of rotation dramatically (TB in figure 6.6), and that with increasing distance to these faults the rotation amount decreases continuously (TAL4 and TAL3 in figure 6.6). These are concepts, which have already been described using paleomagnetic data (e.g., Nelson and Jones, 1987; Aubele *et al.*, 2012), but given the continuous deformation pattern in the region, much more data is needed to better evaluate this.

7

Conclusion and Outlook

Generally, we improved the paleogeographic picture of the Central Asian Orogenic Belt (CAOB) throughout the Paleozoic period. We added paleomagnetic constraints to the configuration of the CAOB and its paleodynamic evolution.

Foremost, we show in chapter 2 that the Karatau mountain ridge was subsequently bended in a counterclockwise sense starting between Devonian and Carboniferous times. The maximal amount of rotation of $\sim 65°$ found in Devonian rocks decreases monotonously towards $\sim 20°$ determined in Permian and Triassic rocks. Recognition of this this pattern is based on secondary magnetizations of syn-folding age in some of the areas studied. Comparing the resulting syn-folding paleolatitudes with expected paleolatitudes for this area allows us to assign an absolute age to this syn-folding mean direction. The correlation of the resulting ages with major deformational phases in the area provides confidence in this procedure. By this we emphasize the importance of remagnetization of magnetic signals in highly deformed areas like the Tianshan.

In chapter 3 the effect of post-depositional compaction on the inclination of the NRM was studied and it could be shown that the sediment from the North Tianshan (NTS)s have been affected by inclination. Although this phenomenon has been observed frequently in red sediments from all over Asia, studies applying modern tests are sparse from the Tianshan itself.

During this study we applied two of the most modern correction methods. We point out that probably all correction methods still contain unknown uncertainties depending on the exact mineral content, which got biased. The most important results is, however, the detection of this phenomena. We deduce a paleogeographical history of the NTS zone, which was probably more or less stable at about 30°N between the Devonian and late Carboniferous times.

In chapter 4 we show that paleomagnetic data suggest, supported by geological evidence, two collision-accretion events in the Tianshan during the Paleozoic. A first one in the Ordovician and the second one in the late Carboniferous (e.g. Variscan). Before the first collision event, we suggest that at least two separated terranes originated from different points of the Gondwana margin. Our main argument that these results are not affected by remagentization like the rocks from chapter 2 is that the resulting directions are not similar to any expected inclination of younger age. In addition, a regional fold test is positive lending further support to our interpretation that these results are of primary origin. The consistency of these results with published data show that early Paleozoic rocks can be used for paleogeographic studies even in highly deformed areas. Generally, it is very important to improve the global paleogeographic picture in this area by enlarging the available dataset with a careful separation of primary and secondary magnetic signals.

A compilation of all available paleomagnetic studies from Kyrgyzstan and Kazakhstan, based on a query of the Global Paleomagnetic Database (GPMDB), is presented in chapter 5. The paleolatitudinal evolution of the Kyrgyzs- Kazakh area seems to reflect the migration of one integral terrane assemblage since at least Ordovician times. Paleomagnetic evidence on its own, however, does not allow to determine when and how this area was separated from Siberian and/or Baltica. However, taken the results from Ordovician and Cambrian sequences from Kyrgyzstan (chapter 4) into account, it is likely that Kyrgyzstan and Kazakhstan acted as the origin of further accretion of arc and arc related rocks and were only amalgamated together with Siberia and Baltica in the Late Paleozoic. On the contrary, it was not possible to detect individual small blocks with a common rotational history. The paleopole distribution shows a rather uniform pattern indicating only counterclockwise rotational movements up to $\sim 120°$.

The previous chapter showed that the rotational pattern is very complex and does not indicate any continuous area with similar rotational history. It has been argued that the are especially east of the TFF has not

experienced large amounts of rotation after the amalgamation in the late Paleozoic. However, there are some studies, which indicate at least some amount of rotational variation in this area, which might have affected the Paleozoic paleomagnetic data se. Since it is known that large faults can cause huge amounts of vertical axis rotation in its surroundings, chapter 6 presents a preliminary study of paleomagnetic data of the last 40 Myr. Additionally, a comparison is presented to the active deformation field based on GPS measurements. By this we can compare if rotational movements of continuous areas are coherent in the recent past and today. The final goals of this approach would be to subtract the young rotational movements from the older Paleozoic one and therefore detect primary Paleozoic deformational pattern such as oroclinal bending. It has to be stressed that this is only a preliminary study, which has to be enlarged on rocks of Ceozoic and Mesozoic age. It turned out, however, that it is not possible to simplify the complicated picture from chapter 5 very much using relatively young rocks. Additionally, also young rocks occasionally indicate unexpectedly large vertical axis rotations. In contrast to these observations, the active tectonical deformation field does not allow to clearly identify any brittle block movement, but a continuous counterclockwise movement with respect to Eurasia of $\sim 1 - 2^{\circ}$/Myr.

Evidently, continuous rotational deformation is disrupted by episodical and distinct activation of faulting and maybe localized rotational movements. We speculate that faults might lead to large rotational movements up to $\sim 90^{\circ}$ in regions very close or within the fault zone, which might gradually decrease with increasing distance to the fault. To further constrain this conclusion much more paleomagnetic data of Cenozoic age is necessary, which is, however, out of the scope of this thesis.

Summarizing our different studies we fundamentally improve the paleogeographic picture of the south western part of the CAOB throughout the whole Paleozoic period using new paleomagnetic data:
The emerging picture is as follows: Several fragments were separated from Gondwana in the early Paleozoic. Some of these fragments collided in the middle Ordovician in a position slightly south of the paleo-equator leading to the formation of Kazahkstania. We speculate that this amalgamated microcontinents includes the Kokchetav massif and the Chingiz Range. This assemblage then crossed the equator and migrated towards a position at $\sim 30^{\circ}$ between the late Ordovician and the Devonian. Between the Devonian and the middle Carboniferous Kazakhstania occupied a stable position and was possibly the locus of further accretion. During this time move-

ments of the major cratons and Tarim caused a counterclockwise rotation of Kazakhstania. This movement continued and was enhanced during the final amalgamation of Eurasia incorporating Baltica, Siberia and Tarim with Kazakhstania. During the final amalgamation and the following Mesozoic and Cenozoic periods the area responded probably brittle to the mostly oblique stress field. By this the rotational history varies widely on a local scale and no original early Paleozoic terranes can be identified based on their rotational history.

Nevertheless, the fact that the maximum rotational deviation increases from the Karatau towards the Tianshan indicates that a general bending of an area which was originally elongated in the same sense as the Ural mountains can be assumed. In this respect we interpret our data to be in favour of a structural linkage of the Ural, Karatau and Tianshan Ranges.

Finally, taken together all these results a global paleogeographic picture similar to the south west Pacific since at least Middle Ordovician times, which was proposed by numerous authors (e.g. Filippova *et al.*, 2001; Windley *et al.*, 2007; Xiao *et al.*, 2010), seems very likely based on paleomagnetic data. On the contrary, we did not find good support for the still debated single arc, which connected Siberia and Baltica in the early Paleozoic Kröner and Rojas-Agramonte (2014); Şengör *et al.* (2014).

References

Abdulin, A., Chimbulatov, M., Azerbaev, N., Ergaliev, G., Kasymov, M., and (Eds.), B. T. (1986). Geology and Metallogeny of Karatau. *vol.1, Alma-Ata*, Seite 239. (in Russian). 2.2, 2.3.1, 2.3.2, 2.7

Abrajevitch, A., Van der Voo, R., Bazhenov, M., and Levashova, N. (2007). Paleomagnetic constraints on the paleogeography and oroclinal bending of the Devonian volcanic arc in Kazakhstan. *Tectonophysics*, **441**, 67–84. 2.1, 3.1, 3.9, 4.1, 4.10, 5.7, 5.9

Abrajevitch, A., Van der Voo, R., Bazhenov, M. L., Levashova, N. M., and McCausland, P. J. (2008). The role of the Kazakhstan orocline in the late Paleozoic amalgamation of Eurasia. *Tectonophysics*, **455**(1-4), 61–76. 2.1, 4.1, 5.4, 5.6

Alexeiev, D., Cook, H., Buvtyshkin, V., and Golub, L. (2009). Structural evolution of the Ural-Tien Shan junction: A view from Karatau ridge, South Kazakhstan. *Comptes Rendus Geoscience*, **341**, 287–297. 2.2, 2.3, 2.2, 2.3.1, 2.7, 2.11, 2.8, 3.2, 4.2

Alexeiev, D., Ryazantsev, A., Kröner, A., Tretyakov, A., Xia, X., and Liu, D. (2011). Geochemical data and zircon ages for rocks in a high-pressure belt of Chu-Yili Mountains, southern Kazakhstan: Implications for the earliest stages of accretion in Kazakhstan and the Tianshan. *Journal of Asian Earth Sciences*, **42**, 805–820. 4.5

Alexyutin, M., Bachtadse, V., Alexeiev, D., and Nikitina, O. (2005). Paleomagnetism of Ordovician and Silurian rocks from the Chu-Yili and Kendyktas mountains, south Kazakhstan. *Geophysical Journal International*, **162**, 321–331. 2.1, 3.6.3, 4.10, 5.1, 5.4, 5.6

Allen, M., Alsop, G., and Zhemchuzhnikov, V. (2001). Dome and basin refolding and transpressive inversion along the Karatau Fault System, southern Kazakstan. *Journal of the Geological Society, London*, **158**, 83–95. 2.2, 2.3.1, 2.3.2, 2.7

Amante, C. and Eakins, B. (2009). ETOPO1 1 Arc-Minute Global Relief Model: Procedures, Data Sources and Analysis. *NOAA Technical Memorandum NESDIS NGDC-24. National Geophysical Data Center, NOAA*. 3.1, 4.1, 5.2, 5.3

Aubele, K., Bachtadse, V., Muttoni, G., Ronchi, A., and Durand, M. (2012). A paleomagnetic study of Permian and Triassic rocks from the Toulon-Cuers Basin, SE France: Evidence for intra-Pangea block rotations in the Permian. *Tectonics*, **3**(3), TC3015. 6.1, 6.4

Bachmanov, D., Trifonov, V., Mikolaichuk, A., Vishnyakov, F., and Zarshchikov, A. (2008). The Ming-Kush-Kökömeren Zone of Recent Transpression in the Middle Tien Shan. *Geotectonics*, **42**(3), 186–205. 3.6.4

Bachtadse, V., Voo, R. V. D., Haynes, F., and Kesler, E. (1987). Late Paleozoic magnetization of mineralized and unmineralized Ordovician carbonates from east Tennessee: Evidence for a post-ore chemical event. *Journal of Geophysical*, **92**, 14,165–14,176. 2.5.4

Bakirov, A. and Mikolaichuk, A. (2009). International Excursion and Workshop: Tectonic Evolution and Crustal Structure of the Tien Shan Belt and Related Terrains in the Central Asian Orogenic Belt. *Guidebook. 8-17 June, Bishkek, Kyrgyzstan*, Seite 125pp. 3.2, 3.6.3, 3.7, 4.2, 6.1

Bakirov, A., Ghes, M., Maksumova, R., and Gusak, L. (2001). Geodynamic Map of Kyrgyzstan. Institute of Geology, National Academy of Science, Bishkek, Kyrgyz Republic. 6.1

Bazhenov, M. and Mikolaichuk, A. (2004). Structural Evolution of Central Asia to the North of Tibet: A Synthesis of Paleomagnetic and Geological Data. *Geotectonics*, **38**(5), 379–393. 5.1, 5.2, 6.1

Bazhenov, M., Klishevich, V., and Tselmovich, A. (1995). Palaeomagnetism of Permian red beds from south Kazakhstan: DRM inclination error or CRM shallowed directions? *Geophysical Journal International*, **120**, 445–452. 2.3.2, 2.6

Bazhenov, M., Burtman, V., and Dvorova, A. (1999). Permian paleomagnetism of the Tien Shan fold belt, Central Asia: post-collisional rotations and deformation. *Tectonophysics*, **312**, 303–329. 2.1, 3.1, 3.2, 3.9, 4.2, 5.1, 5.2

Bazhenov, M., Collins, A., Degtyarev, K., Levashova, N., Mikolaichuk, A., Pavlov, V., and der Voo, R. V. (2003). Paleozoic northward drift of the North Tien Shan (Central Asia) as revealed by Ordovician and Carboniferous paleomagnetism. *Tectonophysics*, **366**, 113–141. 2.1, 3.1, 3.3, 3.9, 3.6.3, 3.6.4, 4.1, 4.1, 4.2, 4.4.2, 4.9, 4.10, 4.5, 5.4, 5.6

Bazhenov, M., Levashova, N., Degtyarev, K., Van der Voo, R., Abrajevitch, A., and McCausland, P. (2012). Unraveling the early-midle Paleozoic paleogeography of Kazakhstan on the basis of Ordovician and Devonian paleomagnetic results. *Gondwana Research*, **22**, 974–991. 3.6.3, 4.11

Berzin, N. and Dobretsov, N. (1994). Geodynamic evolution of the Southern Siberia in Late Precambrian Early Paleozoic time. *In: Coleman, R.G. (Ed.), Reconstruction of the Paleo-Asian Ocean: Proceeding of the 29th International Geological Congress.*, **Part B.**, 53–70. VSP, Utrecht, The Netherlands. 2.1, 3.1, 5.2

Besse, J. and Courtillot, V. (2002). Apparent and true polar wander and the geometry of the geomagnetic field over the last 200 Myr. *Journal of Geophysical Research*, **107**. 6.2

Biggin, A., van Hinsbergen, D., Langereis, C., Straathof, G., and Deenen, M. (2008). Geomagnetic secular variation in the Cretaceous Normal Superchron and in the Jurassic. *Physics of the Earth and Planetary Interiors*, **169**, 3–19. 3.6.1

Bilardello, D. and Jackson, M. (2014). A comparative study of magnetic anisotropy measurement techniques in relation to rock-magnetic properties. *Tectonophysics*. in press. 3.5.3

Bilardello, D. and Kodama, K. (2009). Measuring remanence anisotropy of hematite in red beds: anisotropy of high-field isothermal remanence magnetization (hf-AIR). *Geophysical Journal International*, **178**(3), 1260–1272. 3.5.3

Bilardello, D. and Kodama, K. (2010). A new inclination shallowing correction of the Mauch Chunk Formation of Pennsylvania, based on high-field AIR results: Implications for the Carboniferous North American APW path and Pangea reconstructions. *Earth and Planetary Science Letters*, **299**, 218–227. 3.5.3

Bilardello, D., Jezek, J., and Kodama, K. (2011). Propagating and incorporating the error in anisotropy-based inclination corrections. *Geophysical Journal International*, **187**, 75–84. 3.5.3, 3.6.1

Biske, Y. and Seltmann, R. (2010). Paleozoic Tianshan as a transitional region between the Rheic and Urals-Turkestan oceans. *Gondwana Research*, **17**, 602–613. 3.2, 4.2

Borradaile, G. and Jackson, M. (2004). Anisotropy of magnetic susceptibility (AMS): magnetic petrofabrics of deformed rocks. In F. Martin-Hernndez, C. Lneburg, C. Aubourg, and M. Jackson, Herausgeber, *Magnetic Fabric: Methods and Applications*, Seiten 299–360. The Geological Society of London, London. 3.4

Brown, D., Juhlin, C., Ayala, C., Tryggvason, A., Bea, F., Alvarez-Marron, J., Carbonell, R., Seward, D., Glasmacher, U., Puchkov, V., and Perez-Estaun, A. (2008). Mountain building processes during continentcontinent collision in the Uralides. *Earth-Science Reviews*, **89**, 177–195. 2.2

Burakov, K. and Didenko, A. (1984). Evaluation of the geomagnetic field in the Middle Devonian by baked chert and gabbro in Southern Mugodzhary. *Izvestiya Akademii Nauk SSSR, Fizika Zemli*, **8**, 45–59. (in Russian). 5.5

Burg, J.-P. and Mikolaichuk, A. (2009). Digital Geological and Natural Hazard Maps of the Inner Tien-Shan (Kyrgyzstan). *SNSF, Project No IB7320-110694*. http://www.kyrgyzstan.ethz.ch. 4.2

Burg, J.-P., Mikolaichuk, A., and Apayarov, F. (2004). Digital Geological Map of the Kyrgyz Range and Chu Basin Transitional Zone. *SNSF, Project No 7KSPJ065518*. http://www.kyrgyzstan.ethz.ch (June, 2013). 3.2, 3.3

Burtman, B. (2006). The Tien Shan Early Paleozoic tectonics and geodynamics. *Russian Journal of Earth Sciences*, **8**, 1–23. 3.2

Burtman, V., Skobelev, S., and Molnar, P. (1996). Late Cenozoic slip on the Talas-Ferghana fault, the Tien Shan, central Asia. *Geological Society of America Bulletin*, **108**(8), 1004–1021. 6.4

Buslov, M. (2011). Tectonics and geodynamics of the Central Asian Foldbelt: the role of Late Paleozoic large-amplitude strike-slip faults. *Russian Geology and Geophysics*, **52**, 52–71. 3.1, 5.1, 5.2, 6.1

Buslov, M., Watanabe, T., Saphonova, I., Iwata, K., Travin, A., and Akiyama, M. (2002). A VendianCambrian arc system of the Siberian continent in Gorny Altai (Russia, central Asia). *Gondwana Research*, **5**, 781–800. 2.1, 3.1

Choulet, F., Chen, Y., Cogné, J.-P., Rabillard, A., Wang, B., Lin, W., Faure, M., and Cluzel, D. (2013). First Triassic palaeomagnetic constraints from Junggar (NW China) and their implications for the Mesozoic tectonics in Central Asia. *Journal of Asian Earth Sciences*, **78**, 371–394. 4.4.1

Cocks, L. and Torsvik, T. (2005). Baltica from the late Precambrian to mid-Palaeozoic times: The gain and loss of a terrane's identity. *Earth-Science Reviews*, **72**(1-2), 39–66. 4.1

Cocks, L. and Torsvik, T. (2007). Siberia, the wandering northern terrane, and its changing geography through the Palaeozoic. *Earth-Science Reviews*, **82**, 29–74. 2.11, 3.1, 3.9, 3.7, 4.1, 5.5, 5.6, 5.8

Cogné, J.-P., Besse, J., Chen, Y., and Hankard, F. (2013). A new Late Cretaceous to Present APWP for Asia and its implications for paleoamgnetic shallow inclinations in Central Asia and Cenozoic Eurasian plate deformation. *Geophysical Journal International*, **192**, 1000–1024. 3.2

Cook, H., Taylor, M., Zhemchuzhnikov, V., Apollonov, M., Ergaliev, G., Sargaskayev, Z., Dubinina, S., and Melnikova, L. (1991). Comparison of two Early Paleozoic carbonate submarine fans: West United States and South Kazakhstan, Soviet Union. In J. Cooper and C. Stevens, Herausgeber, *Paleozoic Paleogeography of the western United States II*, Ausgabe 67, Seiten 847–872. Pacific Sect. SEPM. 2.2

Cook, H., Zhemchuzhnikov, V., Buvtyshkin, V., L.Ya.Golub, Gatovskiy, Y., and Zorin, A. (1995). Devonian and Carboniferous

passive-margin carbonate platform of southern Kazakhstan: summary of depositional and stratigraphic models to assist in the exploration and production of coeval giant carbonate plat- form oil and gas fields in the North Caspian Basin, western Kazakhstan. In A. Embry, B. Beauchamp, and D. Glass, Herausgeber, *Pangea: Global Environments and Resources*, Ausgabe 17 von *Memoirs*, Seiten 363–381. Canadian Society of Petroleum Geologists. 2.2

Cook, H., Zhemchuzhnikov, V., Zempolich, W., Buvtyshkin, V., Zhaimina, V., Kotova, E., Golub, L., Zorin, A., Lehmann, P., Alexeiev, D., Giovanneli, A., Viaggi, M., Fretwell, N., Lapointe, P., Corboy, J., Bowman, M., and Coo, J. D. (2002). Devonian and Carboniferous carbonate platform facies in the Bolshoi Karatau, southern Kazakhstan: outcrop analogs for coeval carbonate oil and gas fields in the North Caspian basin, western Kazakhstan. In W. Zempolich and H. Cook, Herausgeber, *Paleozoic Carbonates of the Commonwealth of the Independent States (CIS): Subsurface Reservoirs and Outcrop Analogs*, Ausgabe 74, Seiten 81–122. SEPM Special Publication. 2.2, 2.3.1, 2.3.2

Şengör, A. and Natal'in, B. (1996). Paleotectonics of Asia: fragments of a synthesis. In: YIN, A. & HARRISON, M. (eds) The Tectonic Evolution of Asia. *Cambridge University Press, Cambridge*, Seiten 486–640. 3.1, 3.6.3

Şengör, A., Natal'in, B., and Burtman, V. (1993). Evolution of the Altaid tectonic collage and Paleozoic crustal growth in Eurasia. *Nature*, **364**, 299–307. 1, 2.1, 3.1, 4, 4.1, 5.1, 5.2

Şengör, A., Natal'in, B., Sunal, G., and Van der Voo, R. (2014). A new look at the Altaids: A superorogenic complex in Northern and Central Asia as a factory of continental crust. Part I: Geological data compilation (exclusive of palaeomagnetic observations). *Austrian Journal of Earth Sciences*, **107/1**, 168–232. 5.1, 7

de Boer, C. and Dekkers, M. (1996). Grain-size dependence of the rock magnetic properties for a natural maghemite. *Geophysical Research Letters*, **23**(20), 2815–2818. 4.4.1

Dewey, J., Cande, S., and Pitman, W. (1989). Tectonic evolution of the India/Eurasia Collision Zone. *Eclogae geol.Helv.*, **82**(3), 717–734. 5.2

Didenko, A., Mossakovsky, A., Pechersky, D., Ruzhentsev, S., Samygin, S., and Kheraskova, T. (1994). Geodynamics of paleozoic oceans of central asia. *Geol. Geofiz.*, **35**(7-8), 59–75. in Russian. 3.1, 3.9, 3.6.3

Djenchuraeva, A. (1997). Paleozoic stratigraphy of the Kyrgyz Range eastern part. *The report of the Paleontologic-Stratigraphic Department based on labors during 1994-1997. Bishkek.* Archives of The Kyrgyz State Geological Agency. 3.3, 4.2

Dunlop, D. (1972). Magnetic Mineralogy of Unheated and Heated Red Sediments by Coercivity Spectrum Analysis. *Geophysical Journal of the Royal Astronomical Society*, **27**(1), 37–55. 3.5.2

Dupont-Nivet, G., Guo, Z., Butler, R., and Jia, C. (2002). Discordant paleomagnetic direction in Miocene rocks from the central Tarim Basin: evidence for local deformation and inclination shallowing. *Earth and Planetary Science Letters*, **199**, 473–482. 3.5.3

Echtler, H. and Hetzel, R. (1998). Main Uralian Thrust and Main Uralian Normal Fault: Non-extensional Paleozoic high-P Rock Exhumation, Oblique Collision, and Normal Faulting in the Southern Urals. *Terra Nova*, **9**, 158–162. 2.8

Echtler, H., Stiller, M., Steinhoff, F., Krawczyk, C., Berzin, R., Suleimanov, A., Spiridonov, V., Knapp, J., Yunusov, N., Menshikov, Y., and Alvarez-Marron, J. (1996). Preserved collisional crustal structure of the Southern Urals revealed by vibroseis profiling. *Science*, **274**, 224–226. 2.2

Echtler, H., Ivanov, K., Ronkin, Y., Karsten, L., Hetzel, R., and Noskov, A. (1997). The Paleozoic tectono-metamorphic evolution of gneiss complexes in the Middle Urals, Russia: A reappraisal. *Tectonophysics*, **276**, 229–251. 2.2

Enkin, R. (2003). The direction-correction tilt test: an all-purpose tilt/fold test for paleomagnetic studies. *Earth and Planetary Science Letters*, **212**, 151–166. 3.6.2, 4.5

Filippova, I., Bush, V., and Didenko, A. (2001). Middle Paleozoic subduction belts: The leading factor in the formation of the Asian fold-

and-thrust belt. *Russian Journal of Earth Sciences*, **3**(6), 105–426. 3.1, 3.2, 3.6.3, 3.7, 4.1, 4.5, 5.2, 5.9, 7

Fisher, R. (1953). Dispersion on a sphere. *Proceedings of the Royal Society London*, **A217**, 295–305. 2.1, 2.5.2, 2.5, 2.5.4, 3.2, 3.3, 4.3, 4.2, 4.3, 4.4, 4.5, 5.6

Flinn, D. (1962). On folding during three-dimensional progressive deformation. *Quarternary Journal of the Geological Society of London*, **118**, 385–428. 3.5.2

Galitskaya, A. and Korolev, V. (1961). The Carboniferous in Northen Kyrgyzstav. *Materials on the geology of the Tien Shan., Vol. 1, Publishing house AN Kyrg.SSR*, Seiten 43–75. (in Russian). 3.3

Gilder, S., Chen, Y., and Sen, S. (2001). Oligo-Miocene magnetostratigraphy and rock magnetism of the Xishuigou section, Subei (Gansu Province, western China) and implications for shallow inclinations in central Asia. *Journal of Geophysical Research*, **106**, 30,505–30,521. 3.1, 3.5.3

Gilder, S., Chen, Y., Cogné, J., Tan, X., Courtillot, V., Sun, D., and Li, Y. (2003). Paleomagnetism of Upper Jurassic to Lower Cretaceous volcanic and sedimentary rocks from the western Tarim Basin and implications for inclination shallowing and absolute dating of the M-O (ISEA?) chron. *Earth and Planetary Science Letters*, **206**, 587–600. 3.5.3

Gordon, R. (1998). THE PLATE TECTONIC APPROXIMATION: Plate Nonrigidity, Diffuse Plate Boundaries, and Global Plate Reconstructions. *Annual Review of Earth and Planetary Sciences*, **26**, 615–642. 5.3

Grishchenko, V. (1967). Geological structure and minerals of terrain of sheets -43-52; -43-53 Scale 1:50000. *Archives of The Kyrgyz State Geological Agency*. 3.3

Hackl, M., Malservisi, R., and Wdowinski, S. (2009). Strain rate patterns from dense GPS networks. *Natural Hazards and Earth System Science*, **9**(4), 1177–1187. 6.3, 6.3, 6.5

Haldan, M., Langereis, C., Biggin, A., Dekkers, M., and Evans, M. (2009). A comparison of detailed equatorial red bed records of secular variation during the Permo-Carboniferous Reversed Superchron. *Geophysical Journal International*, **177**, 834–848. 3.6.1

Hall, R. (2009). The Eurasian SE Asian margin as a modern example of an accretionary orogen. *In: Cawood, P.A., Kröner, A. (Eds.) Accretionary Orogens in Space and Time, Geological Society of London Special Publications*, **318**, 351–372. 1, 3.1, 4.1

Heslop, D., Dekkers, M., Kruiver, P., and van Oorschot, I. (2002). Analysis of isothermal remanent magnetization acquisition curves using the expectation-maximization algorithm. *Geophysical Journal International*, **148**, 58–64. 3.4

Heslop, D., Roberts, A., and Hawkins, R. (2014). A statistical simulation of magnetic particle alignment in sediments. *Geophysical Journal International*, **197**, 828–837. 3.5.2

Iosifidi, A., Niocaill, C. M., Khramov, A., Dekkers, M., and Popov, V. (2010). Palaeogeographic implications of differential inclination shallowing in permo-carboniferous sediments from the donets basin, Ukraine. *Tectonophysics*, **490**, 229–240. 3.1

Jelinek, V. (1977). The statistical theory of measuring anisotropy of magnetic susceptibility of rocks and its application. *Geophyzika, Brno*, Seite 88 pp. 3.4

Jenchuraeva, A. (1997). Paleozoic stratigraphy of the Kyrgyz Range eastern part. The report of the Paleontologic-Stratigraphic Department based on labors during 1994-1997. Technical report, Archives of The Kirghiz State Geological Agency, Bishkek. (in Russian). 3.2

Kheraskova, T., Didenko, A., Bush, V., and Volozh, Y. (2003). The Vendian-Early Paleozoic history of the Continental margin of Eastern Paleogondwana, Paleoasian Ocean, and Central Asian Foldbelt. *Russian Journal of Earth Sciences*, **5**, 165–184. 3.2, 5.2

Khristov, E. (1970). Middle Paleozoic transitional sections of the northern slope of the Moldotoo range and there position in the regional structure of the Tien Shan. *Tectonics Pre-Paleozoic and Paleozoic rock mass of Tien Shan. Frunze, Ilim*, Seiten 125–142. (in Russian). 3.3, 3.2, 3.3

Khristov, E. (1971). Structural-facial correlations of Middle and Upper Paleozoic in a zone of 'the most important structural line of the Tien-Shan' in

the Moldo-Tau ridge. *Thesis of candidate of geological-mineralogical sciences (04.120-geology). Lvov*, Seite 210. Archives of the State Geological Agency of the Kyrgyz Republic. 3.3, 3.2, 3.3

Kirscher, U., Zwing, A., Alexeiev, D., Echtler, H., and Bachtadse, V. (2013). Paleomagnetism of Paleozoic sedimentary rocks from the Karatau Range, Southern Kazakhstan: Multiple remagnetization events correlate with phases of deformation. *Journal of Geophysical Research: Solid Earth*, **118**, 3871–3885. 3.6.4, 3.7, 4.1, 4.4.2, 4.5, 5.3.2, 5.4

Kirscher, U., Bilardello, D., Mikolaichuk, A., and Bachtadse, V. (2014). Correcting for inclination shallowing of early Carboniferous sedimentary rocks from Kyrgyzstan–indication of stable subtropical position of the North Tianshan Zone in the mid-late Palaeozoic. *Geophysical Journal International*, **198**(2), 1000–1015. 4.1, 4.2, 4.10, 6.2

Kirschvink, J. (1980). The least squares lines and plane analysis of paleomagnetic data. *Geophysical Journal of the Royal Astronomical Society*, (62), 699–718. 2.3, 3.4, 4.3

Klishevich, V. and Kolobova, I. (1990). To the substantiation of the Toluk Group age (Northern Tien-Shan). *Yearbook of All-Union Paleontologic Society. Volume XXXIII. Leningrad. Nauka, Leningrad Department*, Seiten 219–232. (in Russian). 4.2

Kodama, K. (2012). *Paleomagnetism of Sedimentary Rocks: Process and Interpretation*. Wiley, West Sussex, UK. 3.7

Konopelko, D., Kullerud, K., Apayarov, F., Sakiev, K., Baruleva, O., Ravna, E., and Lepekhina, E. (2012). SHRIMP zircon chronology of HP-UHP rocks of the Makbal metamorphic complex in the Northern Tien Shan, Kyrgyzstan. *Gondwana Research*, **22**, 300–309. 4.1

Krasa, D., Petersen, K., and Petersen, N. (2007). Variable field translation balance. *Encyclopedia of Earth Sciences Series.*, Seiten 977–979. In: Gubbins, D., Herrero-Bervera, E. (Eds.), Encyclopedia of Geomagnetism and Paleomagnetism. 2.3, 2.4, 3.4

Kröner, A. and Rojas-Agramonte, Y. (2014). The Altaids as seen by Eduard Suess, and present thinking on the Late Mesoproterozoic to Palaeozoic evolution of Central Asia. *Austrian Journal of Earth Sciences*, **107/1**, 156–168. 5.1, 7

Kröner, A., Alexeiev, D., Hegner, E., Rojas-Agramonte, Y., Corsini, M., Chao, Y., Wong, J., Windley, B., Liu, D., and Tretyakov, A. (2012). Zircon and muscovite ages, geochemistry, and NdHf isotopes for the Aktyuz metamorphic terrane: Evidence for an Early Ordovician collisional belt in the northern Tianshan of Kyrgyzstan. *Gondwana Research*, **21**(4), 901–927. 4.2, 4.2

Kröner, A., Alexeiev, D., Rojas-Agramonte, Y., Hegner, E., Wong, J., Xia, X., Belousova, E., Mikolaichuk, A., Seltmann, R., Liu, D., and Kiselev, V. (2013). Mesoproterozoic (Grenville-age) terranes in the Kyrgyz North Tianshan: Zircon ages and Nd-Hf isotopic constraints on the origin and evolution of basement blocks in the southern Central Asian Orogen. *Gondwana Research*, **23**, 272–295. 4.2

Kröner, A., Kovach, V., Belousova, E., Hegner, E., Armstrong, R., Dolgopolova, A., Seltmann, R., Alexeiev, D., Hoffmann, J., Wong, J., Sun, M., Cai, K., Wang, T., Tong, Y., Wilde, S., Degtyarev, K., and Rytsk, E. (2014). Reassessment of continental growth during the accretionary history of the Central Asian Orogenic Belt. *Gondwana Research*, **25**, 103–125. 1, 4.1

Kruiver, P., Dekkers, M., and Heslop, D. (2001). Quantification of magnetic coercivity components by the analysis of acquisition curves of isothermal remanent magnetisation. *Earth and Planetary Science Letters*, **189**, 269–276. 3.4, 3.6, 3.5.2

Levashova, N., Mikolaichuk, A., McCausland, P., Bazhenov, M., and der Voo, R. V. (2007). Devonian paleomagnetism of the North Tien Shan: Implications for the middle-Late Paleozoic paleogeography of Eurasia. *Earth and Planetary Science Letters*, **257**, 104–120. 2.1, 4.1, 4.10, 5.1, 5.7

Li, Y. (1990). An Apparent polar wander path from the Tarim Block, China. *Tectonophysics*, **181**, 31–41. 4.11

Lowrie, W. (1990). Identification of ferromagnetic minerals in a rock by coercivity and unblocking temperature properties. *Geophysical Research Letters*, **17**(2), 159–162. 2.3, 2.4, 4.3, 4.4.1, 4.3

Lowrie, W. and Heller, F. (1982). Magnetic Properties of Marine Limestones. *Reviews of Geophysics and Space Physics*, **20**(2), 171–192. 3.4

Mandl, G. (1987). Tectonic deformation by rotating parallel faults: the 'bookshelf' mechanism. *Tectonophysics*, **141**, 277–316. 5.3.2, 5.9

McCabe, C. and Elmore, R. (1989). The occurrence and origin of late Paleozoic remagnetization in the sedimentary rocks of North America. *Reviews of Geophysics*, **27**(4), 471–494. 2.6

McFadden, P. and McElhinny, M. (1988a). The combined analysis of remagnetization circles and direct observations in palaeomagnetism. *Earth and Planetary Science Letters*, **87**, 161–172. 2.5.2, 2.5, 4.4

McFadden, P. and McElhinny, M. (1988b). The combined analysis of remagnetization circles and direct observations in palaeomagnetism. *Earth and Planetary Science Letters*, **87**, 161–172. 4.4.2

McFadden, P. and McElhinny, M. (1990). Classification of the reversal test in paleomagnetism. *Geophysical Journal International*, **103**, 725–729. 2.8, 2.5.2, 2.5.3, 2.5, 2.5.4

M.E. Beck, J. (1991). Coastwise transport reconsidered: lateral displacements in oblique subduction zones, and tectonic consequences. *Physics of the Earth and Planetary Interiors*, **68**, 1–8. 5.3.1

Meert, J. and Torsvik, T. (2003). The making and unmaking of a supercontinent: Rodinia revisited. *Tectonophysics*, **375**(1-4), 261–288. 4.1

Mikolaichuk, A. and Djenchuraeva, A. (2000). Middle-Paleozoic complexes of Turkestan and Kazakh basins in the territory of Central Asia. General tectonic questions. *Tectonics of Russia. Materials of XXXIII Tectonic Meeting. Moscow: GEOS publishing house.*, Seiten 318–321. (In Russian). 3.2, 3.6.3, 3.7

Mikolaichuk, A. and Mambetov, A. (1998). Lower Paleozoic deposits in the structure of the Kapka-Tash Ridge (Northern Tien Shan). *Russian Geology and Geophysics*, **39**(5), 581–590. 4.2, 4.2

Mikolaichuk, A., Kurenkov, S., Dagtyarev, K., and Rubtsov, V. (1997). Northern Tien Shan: Main stages of geodynamic evolution in the late Precambrian - early Paleozoic. *Geotectonics*, **31**(6), 445–462. 4.2, 4.2

Molnar, P. and Tapponnier, P. (1975). Cenozoic tectonics of Asia; effects of a continental collision. *Science*, **189**, 419–426. 6.1

Morozov, V. (1993). Geological structures and minerals of Aktuz-Boordu ore area. Report of Kemin party on results of geological studying in 1:50000 scale. *Bishkek. Archives of the State Geological Agency of the Kyrgyz Republic.* (in Russian). 4.2

Mossakovsky, A., Ruzhentsev, S., Samygin, S., and Kheraskova, T. (1993). Central Asian fold belt: geodynamic evolution and history of formation. *Geotectonics*, **6**, 3–33. 2.1, 3.1, 5.2

Natal'in, B. A. and Şengör, A. C. (2005). Late Palaeozoic to Triassic evolution of the Turan and Scythian platforms: The pre-history of the Palaeo-Tethyan closure. *Tectonophysics*, **404**(3-4), 175–202. 3.2, 3.7, 5.3.1, 5.4, 5.9

Nelson, M. and Jones, C. (1987). Paleomagnetism and crustal rotations along a shear zone, Las Vegas Range, southern Nevada. *Tectonics*, **6**(1), 13–33. 5.4, 5.3.2, 5.9, 6.1, 6.4

Neyevin, A. (2008). Paleozoic stratotypes of the Middle Tien-Shan. *Report of the Paleontologic-stratigraphic Party on the works held in 2004-2008. Bishkek. Archives of the State Geological Agency of the Kyrgyz Republic.* (in Russian). 3.3

Oliver, J. (1986). Fluids expelled tectonically from orogenic belts: Their role in hydrocarbon migration and other geologic phenomena. *Geology*, **14**(February), 99–102. 2.6

Peacock, D. C. P., Anderson, M. W., Morris, A., and Randall, D. E. (1998). Evidence for the importance of small faults on block rotation. *Earth*, **299**, 1–13. 5.3.2, 5.9

Pechersky, D. and Didenko, A. (1995). Palaeoasian ocean: Petromagnetic and Paleomagnetic Information of Its Lithosphere. *OIFZ RAN, Moscow*, Seite 298 pp. (in Russian). 5.5

Popov, L., Ebbestad, J., Mambetov, A., and Apayarov, F. (2007). A low diversity shallow water lingulid brachiopod-gastropod association from the Upper Ordovician of North Kyrgyzstan. *Acta Palaeontologica Polonica*, **52**(4), 27–40. 4.1, 4.2, 5.9

Press, W., Flannery, B., Teukolsky, S., and Vetterling, W. (1986). *Numerical Recipes: The Art of Scientific Computing.* Cambridge University Press, Cambridge. 3.4

Puchkov, V. (1997). Structure and geodynamics of the Uralian orogen. In: Burg, J.P. & Ford, M. (eds) Orogeny through Time. *Geological Society, London, Special Publications*, **121**, 201–236. 3.2, 4.2

Puchkov, V. (2000). Paleogeodynamics of the Southern and Middle Urals. *Pauria, Ufa*, Seite 145 pp. (in Russian). 3.2, 4.2

Rolland, Y., Alexeiev, D., Kröner, A., Corsini, M., Loury, C., and Monié, P. (2013). Late Palaeozoic to Mesozoic kinematic history of the Talas-Ferghana strike-slip Fault (Kyrgyz West Tianshan) as revealed by $^{40}Ar/^{39}Ar$ dating of syn-kinematic white mica. *Journal of Asian Earth Sciences*, **67-68**, 76–92. 2.2, 2.2, 2.8

Samygin, S. and Burtman, V. (2009). Tectonics of the Ural Paleozoides in Comparison with the Tien Shan. *Geotectonics*, **43**(2), 133–151. 1, 3.1, 3.6.3, 3.7, 4.1, 5.1, 5.2

Schwartz, S. Y. and Van der Voo, R. (1983). Paleomagnetic evaluation of the orocline hypothesis in the central and southern Appalachians. *Geophysical Research Letters*, **10**, 505–508. 5.7

Slautsitais, I. (1971). Palaeomagnetic directions and pole positions. *Data for the USSR - Issue 1, Soviet Geophysical Committee: World Data Center-B (Moscow).* (in Russian). 5.5

Smethurst, M., Khramov, A., and Pisarevsky, S. (1998). Palaeomagnetism of the Lower Ordovician Orthoceras Limestone, St. Petersburg, and a revised drift history for Baltica in the early Palaeozoic. *Geophys.J.Int.*, **133**, 44–56. 2.5.4, 2.7, 2.10, 2.11, 2.8

Stamatakos, J. and Kodama, K. (1991). Flexural flow folding and the paleomagnetic fold test: An example of strain reorientation of remanence in the Mauch Chunk Formation. *Tectonics*, **10**, 807–819. 3.5.2

Stampfli, G. M., Borel, G. D., Machant, R., and Mosar, J. (2002). Western Alps geological constraints on western Tethyan reconstructions. *Journal of the Virtual Explorer*, **8**, 77–106. 5.2

Stephenson, A., Sadikun, S., and Potter, D. (1986). A theoretical and experimental comparison of the anisotropies of magnetic susceptibility and remanence in rocks and minerals. *Geophysical Journal of the Royal Astronomical Society*, **84**, 185–200. 3.4

Svyazhina, I. (1971). Palaeomagnetic directions and pole positions. *Data for the USSR - Issue 7, Soviet Geophysical Committee: World Data Center-B (Moscow)*. (in Russian). 5.5

Tan, X., Kodama, K., Chen, H., Fang, D., Sun, D., and Li, Y. (2003). Paleomagnetism and magnetic anisotropy of Cretaceous red beds from the Tarim basin northwest China: Evidence for a rock magnetic cause of anomalously shallow paleomagnetic inclinations from central Asia. *Journal of Geophysical Research*, **108**, 1–20. 3.5.3, 3.7, 3.4

Tauxe, L. (1998). *Paleomagnetic Principles and Practice*, chapter 2, Seite 299. Kluwer Academic Publishers, Dordrecht, The Netherlands. 3.4

Tauxe, L. and Kent, D. (1984). Properties of a detrital remanence carried by hematite from study of modern river deposits and laboratory redeposition experiments. *Geophys.J.R.Astron.Soc.*, **77**, 543–561. 3.5.3

Tauxe, L. and Kent, D. (2004). A simplified statistical model for the geomagnetic field and the detection of shallow bias in paleomagnetic inclinations: was the ancient magnetic field dipolar? *In: Channell, J.E.T. e.a. (Ed.), Timescales of the Paleomagnetic Field*, **145**, 101–116. American Geophysical Union,Washington, DC. 2.6, 3.1, 3.5.1, 3.5.3, 3.8, 3.6.2, 3.7, 3.4

Tauxe, L., Constable, C., Stokking, L., and Badgley, C. (1990). Use of anisotropy to determine the origin of characteristic remanence in the Siwalik red beds of northern Pakistan. *Journal of Geophysical Research*, **95**(B4), 4391–4404. 3.5.2

Tauxe, L., Mullender, T., and Pick, T. (1996). Potbellies, wasp-waists, and superparamagnetism in magnetic hysteresis. *Journal of Geophysical Research*, **101**, 571–583. 2.4

Tauxe, L., , Kodama, K., and Kent, D. (2008). Testing corrections for paleomagnetic inclination error in sedimentary rocks: A comparative approach. *Physics of the Earth and Planetary Interiors*, **169**, 152–165. 3.5.3

Taylor, T. R., Dewey, J. F., and Monastero, F. C. (2008). Transtensional Deformation of the Brittle Crust: Field Observations and Theoretical Applications in the Coso-China Lake Region, Eastern Margin of the

Sierra Nevada Microplate, Southeastern California. *International Geology Review*, **50**(3), 218–244. 5.3.2

Thatcher, W. (2009). How the Continents Deform: The Evidence From Tectonic Geodesy *. *Annual Review of Earth and Planetary Sciences*, **37**(1), 237–262. 5.3

Thomas, J.-C., Perroud, H., Cobbold, P. R., Bazhenov, M. L., Burtman, V. S., Chauvin, a., and Sadybakasov, E. (1993). A paleomagnetic study of Tertiary formations from the Kyrgyz Tien-Shan and its tectonic implications. *Journal of Geophysical Research*, **98**(B6), 9571. 6.1, 6.2

Torsvik, T., , Smethurst, M., Meert, J., der Voo, R. V., McKerrow, W., Brasier, M., Sturt, B., and Walderhaug, H. (1996). Continental break-up and collision in the Neoproterozoic and Palaeozoic A tale of Baltica and Laurentia. *Earth-Science Reviews*, **40**(3-4), 229–258. 3.1

Torsvik, T., Van der Voo, R., Preeden, U., Mac Niocaill, C., Steinberger, B., Doubrovine, P., van Hinsbergen, D., Domeier, M., Gaina, C., Tohver, E., Meert, J., McCausland, P., and Cocks, L. (2012). Phanerozoic polar wander, palaeogeography and dynamics. *Earth-Science Reviews*, **114**(3-4), 325–368. 3.1, 3.9, 3.7, 4.10, 4.5, 4.11, 5.1, 5.5, 5.6, 5.8

Van der Voo, R. (1990). The reliability of paleomagnetic data. *Tectonophysics*, **184**, 1–9. 5.5, 5.5

Van der Voo, R. (2004). 2004 Presidential Address: Paleomagnetism, Oroclines, and Growth of the Continental Crust. *GSA Today*, **14**(12), 4. 5.3.2

Van der Voo, R., Levashova, N., Skrinnik, L., Kara, T., and Bazhenov, M. (2006). Late orogenic, large-scale rotations in the Tien Shan and adjacent mobile belts in Kyrgyzstan and Kazakhstan. *Tectonophysics*, **426**, 335–360. 1, 2.1, 2.7, 2.8, 3.7, 4.1, 4.4.3, 5.4

Vasilev, D. (1991). *Volcanic formations in history of geologic development of caledonides of the Northern Tien Shan.* Dissertation, Leningrad. (in Russian). 4.2

Wack, M. and Gilder, S. (2012). The SushiBar: An automated system for paleomagnetic investigations. *Geochemistry, Geophysics, Geosystems*, **13**(12), 1–24. 4.3

Wack, M., Gilder, S., Macaulay, E., Sobel, E., Charreau, J., and Mikolaichuk, A. (2014). Cenozoic magnetostratigraphy and magnetic properties of the southern Issyk-Kul basin, Kyrgyzstan. *Tectonophysics*, **629**, 14–26. 6.1

Wang, B., Chen, Y., Zhan, S., Shu, L., Faure, M., Cluzel, D., Charvet, J., and Laurent-Charvet, S. (2007). Primary Carboniferous and Permian paleomagnetic results from the Yili Block (NW China) and their implications on the geodynamic evolution of Chinese Tianshan. *Earth and Planetary Science Letters*, **263**(3-4), 288–308. 3.9

Watson, G. and Enkin, R. (1993). The fold test in paleomagnetism as a parameter estimation problem. *Geophysical Research Letters*, **20**(19), 2135–2137. 2.7, 2.5.1, 2.8, 2.5.2, 2.5.2, 2.5.3, 2.5, 2.7, 2.8, 4.5, 4.4.2

Wessel, P. and Smith, W. (1998). New, improved version of the Generic Mapping Tools released. *EOS Trans. AGU*, **79**(579). 3.1, 4.1, 5.2, 5.3

Windley, B., Alexeiev, D., Xiao, W., Kroener, A., and Badarch, G. (2007). Tectonic models for accretion of the Central Asian Orogenic Belt. *Journal of the Geological Society, London*, **164**, 31–47. 1, 2.1, 3.1, 3.6.3, 4.1, 4.5, 5.1, 5.2, 5.1, 5.7, 7

Xiao, W., Chunming, H., Chao, Y., Min, S., Shoufa, L., Hanlin, C., Zilong, L., Jiliang, L., and Shu, S. (2008). Middle Cambrian to Permian subduction-related accretionary orogenesis of Northern Xinjiang, NW China: Implications for the tectonic evolution of central Asia. *Journal of Asian Earth Sciences*, **32**, 102–117. 2.1, 3.1

Xiao, W., Huang, B., Han, C., Sun, S., and Li, J. (2010). A review of the western part of the Altaids: A key to understanding the architecture of accretionary orogens. *Gondwana Research*, **18**, 253–273. 2.1, 3.1, 3.6.3, 5.1, 5.2, 7

Yakubchuk, A., Shatov, R. S. V., and Cole, A. (2001). The Altaids: tectonic evolution and metallogeny. *Society of Economical Geologists Newsletters*, **46**, 7–14. 2.1, 3.1

Yanshin, A. (1965). Tectonic structure of Eurasia. *Geotektonika*, **5**, 7–35. (in Russian). 1, 4.1, 5.1

Zegers, T., Dekkers, M., and Bailly, S. (2003). Late Carboniferous to Permian remagnetization of Devonian limestones in the Ardennes: Role of temperature, Fluids, and deformation. *Journal of Geophysical Research*, **108**(B7), 2357. 2.6

Zhang, P., Shen, Z., Wang, M., Gan, W., Bürgmann, R., Molnar, P., Wang, Q., Niu, Z., Sun, J., Wu, J., Hanrong, S., and Xinzhao, Y. (2004). Continuous deformation of the Tibetan Plateau from global positioning system data. *Geology*, **32**(9), 809–812. 6.1, 6.3, 6.5

Zhao, P., Chen, Y., Zhan, S., Xu, B., and Faure, M. (2014). The Apparent Polar Wander Path of the Tarim block (NW China) since the Neoproterozoic and its implications for a long-term TarimAustralia connection. *Precambrian Research*, **242**, 39–57. 4.1

Zijderveld, J. (1967). A. C. demagnetization of rocks: Analysis of results. In D. W. Collinson, K. M. Creer, and S. K. Runcorn, Herausgeber, *Methods in Paleomagnetism*, Seiten 254–286. Elsevier, Amsterdam. 2.6, 3.3, 4.4, 4.6, 6.2

Zonenshain, L., Kuzmin, M., Natapov, L., and Page, B. (1990). *Geology of the USSR: A Plate-Tectonic Synthesis*, Ausgabe 21 von *Geodynamics series*. American Geophysical Union. 2.1, 3.1, 5.1, 5.2

Zubovich, A. V., Wang, X.-q., Scherba, Y. G., Schelochkov, G. G., Reilinger, R., Reigber, C., Mosienko, O. I., Molnar, P., Michajljow, W., Makarov, V. I., Li, J., Kuzikov, S. I., Herring, T. a., Hamburger, M. W., Hager, B. H., Dang, Y.-m., Bragin, V. D., and Beisenbaev, R. T. (2010). GPS velocity field for the Tien Shan and surrounding regions. *Tectonics*, **29**(6). 6.1, 6.3, 6.3, 6.5, 6.4

Acknowledgments

First and foremost I thank my advisor Valerian Bachtadse. He accompanied me during all these years not only by providing the projects, support in the field, and assistance in the scientific process, but also in a general way. I am very thankful that I got the opportunity to do this thesis with him including fieldwork in a remarkable region, which had a great influence on my life. Then, of course, I thank all my co-authors, who significantly improved the scientific content of this thesis. First of all, Alexander Mikolaichuk is thanked for providing the geological background and organizing two field trips. It was a pleasure to do fieldwork with such a high standard of professionalism. Alexander Zwing, Dario Bilardello, Helmut Echtler, Dima Alexeiev and Alfred Kröner for their huge scientific input in the respective study. It was a honour for me to work with them. Additionally, all other people are thanked who in one way or the other participated in the scientific content of this thesis, especially Matthias Hackl and Alejandro Bande. On the other hand I thank all the people who helped performing the field trips and the measurement procedures. In Kyrgyzstan especially Elmira and Jura were very helpful. Yvonne Koch did her Bachelors thesis with me by helping me in the second field trip and doing the thesis on rotations in Central Asia.

The magnetism group of Professor Stuart Gilder is thanked for providing all the laboratory infrastructure, which got renewed during the time of the thesis and provided me with most of the newest instruments available for paleomagnetism. In this respect the two people, which are responsible for the labs, Manuela Weiss and Michael Wack are especially thanked for their help and support. Then I would like to thank my office mates, Matthias Hackl, Katharina Aubele and Edoardo Dallanave for a very nice time not only during office hours. Also the whole Tuesday's group was very important for me to discuss science and life in general, especially Jo, Jürgen, Christoph, Felix and Hacki, are thanked therefore. The Deutsche Forschungsgemeinschaft (DFG) is thanked for funding these studies. The

Chair of Geophysics is thanked for providing the place of work and the IT infrastructure.

Finally, I would like to thank the non-scientific people around me. Without them doing this thesis would not have been possible. My mother, father and brother supported me throughout all these years. It was very important for me to refill the batteries at home and in Hohenroth with the family of my girlfriend.

A special thank goes to Stjerna, who had to cope with me in every state of exhaustion. She helped me in many ways and has a large part that I stayed more or less relaxed during all this time and that I enjoyed the years of my PhD very much.